THE UNIVERSITY OF SUSSEX

Phenomenological aspects of dark energy dominated cosmologies

Pier Stefano Corasaniti

Centre for Theoretical Physics

Submitted for the degree of Doctor of Philosophy

July 2003

Declaration

The work presented in this thesis is the result of a number of collaborations with my supervisor Ed Copeland and Bruce Bassett and Carlo Ungarelli at the Institute of Cosmology of Portsmouth University. Some of the work has already been published in [110], [137], [161], [162].

I hereby declare that this thesis describes my own original work, except where explicitly stated. No part of this work has previously been submitted, either in the same or different form, to this or any other University in connection with a higher degree or qualification.

Signed..... Date.....

Pier Stefano Corasaniti

Acknowledgements

This thesis is the final result of almost three years of hard work and God only knows how much this has coasted me in terms of personal affections and sacrifices, but I would do it again. It has been a really great experience and has given me the opportunity to realise myself as the theoretical cosmologist that I always wanted to be. Living in UK was not easy at the beginning, but now I am perfectly integrated with this country that I consider my second home. I have learned not to complain about the weather and the food since there are other things that make life worth living. At the end of this adventure I have discovered that all the joys and sorrows I went through have made me a much better person. I really have to thank my supervisor Ed Copeland who gave me this chance without knowing me, a chance that my home country refused to offer to me. I am particularly thankful to him for allowing me to develop my own ideas about research projects, ideas that we improved together through open minded discussions. I also thank the Institute of Cosmology of Portsmouth for their welcoming hospitality during these many years. It has been a pleasure to start a fruitful collaboration with Bruce Bassett and Carlo Ungarelli and if this has been possible I have to thank my dear friend Cristiano Germani with whom I established a strong brotherhood. I thank Luca Amendola for the hospitality during my visit at the Astronomical Observatory of Rome and the Physics Department of Dartmouth College (New Hampshire) where a large part of this thesis was written. In particular it is a pleasure to thank Marcelo Gleiser, Robert Caldwell and Michael Doran for the welcoming atmosphere I found in Dartmouth, for the useful and interesting physics discussions and for bearing the visit of a crazy roman. I am particularly grateful to Andrew Liddle, Nelson Nunes, Nicola Bartolo, Martin Kunz and Michael Malquarti for the many cosmological discussions and all the members of the physics and astronomy group, in particular Mark Hindmarsh, Andre Lukas, Peter Schroder, Beatriz de Carlos and David Bailin, for the pleasant and friendly environment of the Sussex group. I am glad to have met and mention an enormous number of friends: first of all my friend Gonzalo Alvarez, also Lys Geherls, Jane Hunter, Gemma Dalton, Electra Lambiri, Isaac Neumann, Asher Weinberg, my flat mates Stephen Morris and particularly Neil McNair for booking concert tickets so many

times , Matteo and Chiara Santin for their kind and nice friendship, Fernando Santoro, James Gray, Malcom Fairbairn, Seung-Joo Lee, Maria Angulo, Liam O'Connell for is effort to explain to me the rules of cricket during the world cup football matches, James Fisher, Jon Roberts, Neil Bevis and in particular Yaiza Schmohe. I will never forget the amazing Sweet Charity Band and its conductor Chloe Nicholson who gave me the opportunity to play my clarinet on the stage again. They made me remember who I truly am deep in my soul, simply a clarinet player. A particularly express my thanks to my parents for their moral support and for paying the flight tickets to Italy. This thesis is dedicated to the memory of Franco Occhionero, he was an extraordinary scientist and one of the most lovely people I have ever met. Always generous in helping and guiding his students he paid attention to teaching and researching as much as to the popularization of science. I will never forget his public lectures, his kindness and the strength and genuine humility of his personality. My approach to Cosmology is the result of the daily interaction with such a great man and I am proud of being one of his many pupils. Finally I would like to conclude with a little bit of the sarcasm that plays a fundamental role in my life. It may be that all this work is entirely wrong, I do not think it is since I am responsible for it, but in the remote eventuality I would like to remind the reader of Francis Bacon's words: *'The truth arises more from the errors rather than from the confusion'.*

THE UNIVERSITY OF SUSSEX

Phenomenological aspects of dark energy dominated cosmologies

Pier Stefano Corasaniti

Submitted for the degree of Doctor of Philosophy

July 2003

Abstract

Cosmological observations suggest that the Universe is undergoing an accelerated phase of expansion driven by an unknown form of matter called dark energy. In the minimal standard cosmological model that best fits the observational data the dark energy is provided by a cosmological constant term. However there is currently no convincing theoretical explanation for the origin and the nature of such an exotic component. In an attempt to justify the existence of the dark energy within the framework of particle physics theories, several scenarios have been considered. In this thesis we present and discuss the phenomenological aspects of some of these dark energy models. We start by reviewing the cosmological measurements that give direct and indirect evidence for the dark energy. Then we focus on a class of theoretical models where the role of the dark energy is played by a minimally coupled scalar field called quintessence. For the sake of simplicity we place special emphasis on two of these models, the Inverse Power Law times an Exponential potential and the Two Exponential potential. We then consider the effect of scalar field fluctuations on the structure formation process in these two models. By making use of the cosmological distance measurements such as the supernova luminosity distance and the position of the acoustic peaks in the CMB power spectrum, we constrain the shape of a general parameterized quintessence potential. We find that by the present time the scalar field is evolving in a very flat region or close to a minimum of its potential. In such a situation we are still unable to distinguish between a dynamical model of dark energy and the cosmological constant scenario. Going beyond constraining specific classes of models, we develop a model independent approach that allows us to determine the physical properties of the dark energy without the need to refer to a particular model. We introduce a parameterization of the dark energy equation of state that can account

for most of the proposed quintessence models and for more general cases as well. Then we study the imprint that dark energy leaves on the CMB anisotropy power spectrum. We find that dynamical models of dark energy produce a distinctive signature by means of the integrated Sachs-Wolfe effect. However only models characterized by a rapid transition of their equation of state can most likely be distinguished from the cosmological constant case. By using a formalism to model localized non-Gaussian CMB anisotropies, we compute analytical formulae for the spectrum and the bispectrum. The use of these formulae in specific cases such as the SZ signature of clusters of galaxies provide an alternative cosmological test.

To the memory of

Prof. Franco Occhionero

Contents

Declaration i

Acknowledgements ii

Abstract iv

Contents vii

Introduction 1

1 The dark side of the Universe 3

1.1 A historical introduction 4

1.2 Standard cosmology 5

1.3 Observational evidence 7

1.3.1 CMB anisotropies 7

1.3.2 Clustering of matter 9

1.3.3 Age of the Universe 10

1.3.4 Supernovae Ia and luminosity distance measurements 10

1.4 Cosmic complementarity 12

2 An explanation for the dark energy? 14

2.1 Vacuum energy 14

2.2 Anthropic solutions 16

2.3 Quintessence 17

2.3.1 Scalar field dynamics 18

2.3.2 Quintessential problems 19

2.4 Supergravity inspired models 23
2.4.1 Exponential Times Inverse Power Law potential 23
2.4.2 Two Exponential potential 24

3 Quintessence field fluctuations 26
3.1 Quintessence perturbations in Newtonian gauge 26
3.2 Evolution of perturbations 28
3.2.1 Analytical solution in the tracker regime 28
3.2.2 Numerical analysis 30

4 Constraining the quintessence potential 34
4.1 Upper bounds on the cosmic equation of state 34
4.2 Parameterized quintessence potential 37
4.3 CMB peaks 38
4.4 Likelihood analysis and results 40
4.4.1 Constraints from supernovae 40
4.4.2 Constraints from Doppler peaks and Sn Ia 41
4.5 Discussion 45

5 A model independent approach to the dark energy equation of state 47
5.1 The effective equation of state 47
5.2 Cosmological distance fitting functions 49
5.3 *Statefinder* method 51
5.4 Low redshift parameterization 52
5.5 An exact parameterization for the dark energy equation of state 54

6 Dark energy effects in the Cosmic Microwave Background Radiation 61
6.1 A beginner's guide to CMB physics 62
6.1.1 Basic equations 62
6.1.2 CMB anisotropies 65
6.2 Dark energy and the Integrated Sachs-Wolfe effect 69
6.3 Differentiating dark energy models with CMB measurements 72
6.4 Testing dark energy with ideal CMB experiments 76

7 Alternative cosmological test with higher order statistics 79

7.1 Higher order statistics 80

7.2 Frequentist approach and estimation of higher moments 81

7.3 Modelling localized non-Gaussian anisotropies 85

7.4 Discussion 88

Conclusion and prospects 90

Bibliography 93

Introduction

The set of astrophysical observations collected in the past decades and the theoretical and experimental developments in high energy physics have provided the natural framework that defines Cosmology as a scientific discipline. The identification of the 'Hot Big-Bang' scenario as a paradigm has been of crucial importance for the beginning of Cosmology as a modern science. In fact it has allowed us to address a number of questions about the nature and the evolution of the Universe that otherwise would have been the subject of investigation of philosophers and theologians. Since this paradigm has been accepted by the majority of the scientific community, more specific and detailed studies have been undertaken in order to extend the validity of the paradigm to a wider class of phenomena such as the formation of the structures we observe in the Universe. As result of this intense activity, that the philosopher of science T.S. Kuhn would define as *normal science investigation* [1], the initial paradigm of Cosmology has been extended in order to include the inflationary mechanism and dark matter, two necessary ingredients to explain a number of issues that arise within the 'Hot Big-Bang' scenario. This extended paradigm is extremely successful and recent measurements in observational cosmology have widely confirmed its prediction. It is very remarkable that long before the recent developments of the cosmological science, T.S. Kuhn identified the basic steps that a scientific discipline follows in its evolution, steps that applies to modern Cosmology too. In particular he has pointed out that there are phenomena which evading an explanation of the paradigm are the subject of 'extraordinary' investigations, in opposition to the 'ordinary' normal science activity. Most of the time these studies lead to a crisis of the underlying paradigm and trigger what he has called a 'scientific revolution'. In this light the discovery that the Universe is dominated by a dark energy component that accounts for 70% of the total matter budget belongs to this class of phenomena. This is the subject of this thesis. In Chapter 1 we will

describe the observational evidence of dark energy and in Chapter 2 we will review some of proposed explanations. From Kuhn's point of view these explanations would represent the attempt to force Nature to fit within the 'Hot Big-Bang' paradigm. In fact these models fail to succeed since they manifest inconsistencies with the expectations of particle physics theories that are included in the standard cosmological paradigm. The solution to this difficulty most probably will need a new paradigm. This necessity will be more urgent if the observational data will indicate a time dependence of the dark energy properties. In this perspective the aim of this thesis is to investigate some of the phenomenological aspects of minimally coupled quintessence scalar field scenarios. In Chapter 3 we describe the evolution of fluctuations in the quintessence field. In Chapter 4 we discuss the constraints on a general class of quintessence potentials obtained from the analysis of the position of the acoustic peaks in the Cosmic Microwave Background (CMB) anisotropy power spectrum and the Sn Ia data. In Chapter 5 we describe some of the methods used to constrain the dark energy. We then introduce a model independent approach that allows us to study the full impact a general dark energy fluid has had in Cosmology. In fact this fluid description, based on a very general parameterization of the dark energy equation of state, allows us to infer the dark energy properties from cosmological observations, instead of constraining specific classes of dark energy models. In Chapter 6 we study the effects dark energy produces in the CMB anisotropy power spectrum and show that clustering of dark energy leaves a distinguishable signature only for a specific class of models. In Chapter 7 we present the results of preliminary work that aims to develop alternative cosmological tests using the non-gaussianity produced by localized sources of CMB anisotropies. We hope that the work reviewed in this thesis will provide the basis for those 'extraordinary' investigations that will help us in developing the new paradigm that modern Cosmology needs.

Chapter 1

The dark side of the Universe

The recent results obtained in different areas of observational cosmology provide an astonishing picture about the present matter content of the Universe. The accurate measurements of the Cosmic Microwave Background radiation (CMB) give strong evidence that the curvature of the space-time is nearly flat. On the other hand the analysis of large scale structure surveys shows that the amount of clustered matter in baryonic and non-baryonic form can account only for thirty per cent of the critical energy density of the Universe. In order to be consistent these two independent analyses require the existence of an exotic form of matter, that we call *dark energy*. More direct evidence is provided by the Hubble diagram of type Ia supernova (Sn Ia) at high redshifts. It suggests that the Universe is undergoing an accelerated expansion sourced by this dark energy component that is characterized by a negative value of its equation of state. A lot of criticism has been levelled to these measurements. In fact the physics of Sn Ia is still a matter of debate and consequently their use as standard candles has not yet convinced the whole astronomical community. In spite of such an important issue it is worth underlining that the combination of CMB and supernova data constrains the amount of clustered matter in the Universe to a value that is consistent with the large scale structure observations. As we shall review in this chapter, indirect evidence for a dominant dark energy contribution comes mainly from the combination of CMB results and the constraints on the density of baryons and cold dark matter. The simplest explanation for the dark energy would be the presence for all time of a cosmological constant term Λ in Einstein's equations of General Relativity. However evidence for a non vanishing value of Λ raises a fundamental

problem for theoretical physics, (for a review of the subject [2–7]). In fact, as we shall see later, it is rather difficult to explain the small observed value of Λ from the particle physics point of view. In this chapter we will briefly review some historical developments of the dark energy problem. We will introduce the standard cosmological model and the equations describing the expansion of the Universe. Then we will discuss the build up of observational evidence for dark energy.

1.1 A historical introduction

The cosmological constant was initially introduced by Einstein in the equations of General Relativity (GR) as a term that could provide static cosmological solutions [8]. Motivated by the observed low velocities of the stars, he assumed that the large scale structure of the Universe is static. We should remind ourselves that the notion of the existence of other galaxies had been established only a few years later. Besides, Einstein believed that the GR equations had to be compatible with the Mach's principle, which in a few words states that the metric of the space-time is uniquely fixed by the energy momentum tensor describing the matter in the Universe. For this reason he thought the Universe had to be closed. These two assumptions were, however, not compatible with the original form of the GR equations. In fact a matter dominated closed Universe is not static, therefore he needed to introduce a term leading to a repulsive force that could counterbalance the gravity. In such a case he found a static and closed solution that preserved Mach's principle. But in the same year, 1917, de Sitter discovered an apparent static solution that incorporated the cosmological constant but contained no matter [9]. As pointed out by Weyl, it was an *anti-Machian* model with an interesting feature: test bodies are not at rest and an emitting source would manifest a linear redshift distance relation. Such an argument was used by Eddington to interpret Slipher's observations of the redshift of spiral nebula (galaxies). Subsequently expanding matter dominated cosmological solutions without a cosmological constant were found by Friedman [10,11] and Hubble's discovery of the linear redshift distance relation [12] made these models the standard cosmological framework. The cosmological constant was then abandoned. For some time a non vanishing Λ was proposed to solve an '*age problem*'. Eddington pointed out the Hubble time scale obtained by using the measured Hubble constant was only 2 billion years in contrast with the estimated age of the Earth, stars and stellar systems. In the 1950s the revised values of

the Hubble parameter and the improved constraints on the age of stellar objects resolved the controversy and the cosmological constant became unnecessary. However in 1967 it was again invoked to explain a peak in the number count of quasars at redshift $z = 2$. It was argued that the quasars were born during a hesitation era , at the transition between the matter and the Λ dominated era. More observational data confirmed the existence of this peak and allowed for a correct interpretation as simply an evolutionary effect of active galactic nuclei, with no necessity for Λ. We shall discuss the theoretical implications of the cosmological constant in Chapter 2, here we would like to stress that in the past few decades the Λ term has played the role of a fitting parameter necessary to reconcile theory and observations which has been discarded every time systematic effects were considered. It is therefore natural to ask the question if today we are facing a similar situation. In what follows we will try to show that this turns not to be the case and the dark energy is indeed most likely to be present in our Universe.

1.2 Standard cosmology

The Einstein field equations are:

$$R_{\mu\nu} - \frac{1}{2} g_{\mu\nu} R = g_{\mu\nu}\Lambda + \frac{8\pi G}{3} T_{\mu\nu}, \tag{1.1}$$

where $R_{\mu\nu}$ is the Ricci tensor, R is the Ricci scalar, Λ is the cosmological constant term and $T_{\mu\nu}$ is the matter energy momentum tensor which determines the dynamics of the Universe. When different non interacting sources are present the energy momentum tensor is the sum of the energy momentum tensor of each of the sources. Assuming an isotropic and homogeneous space-time the large scale geometry can be described by the Friedman-Robertoson-Walker metric:

$$ds^2 = dt^2 - a^2(t) \left(\frac{dr^2}{1 - kr^2} + r^2 d\theta^2 + r^2 sin^2\theta d\phi^2 \right), \tag{1.2}$$

where $a(t)$ is a function of time (called the *scale factor*) and $k = 0, \pm 1$ sets a flat, open (-1) or close (+1) geometry. Spatial homogeneity and isotropy implies that the energy momentum tensor of each component is diagonal:

$$T^i_{\mu\nu} = diag(\rho_i(t), p_i(t), p_i(t), p_i(t)), \tag{1.3}$$

where $\rho_i(t)$ is the energy density and $p_i(t)$ is the pressure of the i-th matter component (radiation, baryons, cold dark matter, etc..). In the FRW metric the Einstein equations (1.1) with a mixture of different matter components are the Friedman equations:

$$H^2 = \left(\frac{\dot{a}}{a}\right)^2 = \frac{8\pi G}{3}\sum_i \rho_i + \frac{\Lambda}{3} - \frac{k}{a^2}, \tag{1.4}$$

$$\frac{\ddot{a}}{a} = -\frac{4\pi G}{3}\sum_i (\rho_i + 3p_i) + \frac{\Lambda}{3}. \tag{1.5}$$

We define the density parameters $\Omega_i = \rho_i/\rho_c$, $\Omega_\Lambda = \Lambda/3\rho_c$ and $\Omega_k = -k/H^2a^2$ where $\rho_c = 3H^2/8\pi G$ is the critical energy density. Then the Friedman equation Eq. (1.4) can be rewritten as:

$$1 - \Omega_k = \sum_i \Omega_i = \Omega_{tot}, \tag{1.6}$$

showing that the spatial curvature is fixed by the total matter content. Since the different components do not interact with each other, their energy momentum tensor must satisfy the energy conservation equation $T^\nu_{\mu;\nu} = 0$. Hence in addition to the Friedman equations the evolution of the energy density of each matter component is given by:

$$\dot{\rho}_i = -3H(\rho_i + p_i). \tag{1.7}$$

It is worth remarking that, as has been stressed by T. Padmanabhan [16], *'absolutely no progress in cosmology can be made until a relationship between ρ_i and p_i is provided in the form of the functions $w_i(a)$'*. In fact once these relations are known, we can solve the dynamical equations and make predictions about the evolution of the Universe, that can be tested by cosmological observations. If the matter components consist of normal laboratory matter, then the knowledge of how the matter equation of state w evolves at different energy scales is provided by particle physics. At present the behaviour of matter has been tested up to about 100 GeV, in this domain the relation between energy density and pressure can be taken to be that of an ideal fluid, $p_i = w_i\rho_i$, with $w = 0$ for non relativistic matter and $w = 1/3$ for relativistic matter and radiation. However if a cosmological model based on conventional matter components fails to account for cosmological observations, we could interpret this fact as a failure of the cosmological model or as a signal for the existence of a source not seen in laboratories. For instance the cosmological constant term behaves as a perfect fluid with negative pressure. This

can be seen rewriting the Λ term in Eq. (1.4) and Eq. (1.5) as an energy density and a pressure term. Then one finds $p_\Lambda = -\rho_\Lambda = -\Lambda/(8\pi G)$. The effect of such a component on the expansion of the Universe can be seen from Eq. (1.5), and the value of deceleration parameter today is

$$q_0 \equiv -H_0^{-2}\left(\frac{\ddot{a}}{a}\right)_0 = \frac{\Omega_m}{2} - \Omega_\Lambda, \tag{1.8}$$

and we have neglected the radiation. For $\Omega_\Lambda > \Omega_m/2$ the expansion of the Universe is accelerated since $q_0 < 0$. Hence in a Universe dominated by the cosmological constant the expansion is eternally accelerating. In summary the dynamics of our Universe is observationally determined by two geometrical quantities, the Hubble parameter H_0, which provides us with a measure of the observable size of the Universe and its age, and the deceleration parameter q_0 which probes the equation of state of matter and the cosmological density parameter.

1.3 Observational evidence

Different cosmological tests can be used to constrain the geometry and the matter content of the Universe. We shall briefly review the latest limits on Ω_m and Ω_Λ obtained by recent experiments in cosmology.

1.3.1 CMB anisotropies

During the last few years an avalanche of balloon and ground experiments, together with the most recent WMAP satellite observatory have measured the small angular temperature fluctuations of the Cosmic Microwave Background Radiation. Such measurements have detected a series of acoustic peaks in the anisotropy power spectrum and confirmed early predictions about the evolution of pressure waves in the primordial photon-baryon plasma [17,18]. The specific features of such peaks are sensitive to the value of the cosmological parameters, in particular to Ω_{tot}, Ω_b and the scalar spectral index n. The sensitivity to the curvature of the Universe however does not allow us to constrain independently Ω_m and Ω_Λ, that are consequently degenerates. The earlier analysis of the Boomerang experiment [19–21] found $\Omega_k \sim 0$ and the latest data released constrain the total energy density to be $\Omega_{tot} = 1.04\pm^{0.06}_{0.04}$ [22]. Such a result is consistent with the ones found by other CMB experiments. For instance, the data from MAXIMA-1, another balloon

experiment, when combined with the COBE-DMR data suggest $\Omega_{tot} = 1.00\pm^{0.15}_{0.30}$ [23]. Similarly the two ground experiments, DASI and CBI provide $\Omega_{tot} = 1.04 \pm 0.06$ [24] and $\Omega_{tot} = 0.99 \pm 0.12$ [25] respectively. Recently three more groups, ARCHEOPS [26], VSA [27] and ACBAR [28] have released their data finding similar results. The constraints on the baryon density are in good agreement with the prediction of the Big-Bang Nucleosynthesis (BBN) and the scalar spectral index is found to be of order unity, as predicted by generic inflationary paradigms. However CMB alone poorly determines Ω_Λ and a vanishing cosmological constant cannot be excluded at 2σ. Nonetheless due to the strong constraint on the curvature of the Universe, it is reasonable to restrict the data analysis to the flat cosmological models ($\Omega_{tot} = 1$). In this case, assuming the so called 'HST prior' on the value of the Hubble constant, $h = 0.71 \pm 0.076$ [29], then all the CMB data constrain the cosmological constant density parameter to be $\Omega_\Lambda = 0.69\pm^{0.03}_{0.06}$ [25]. The WMAP satellite provided CMB data with such an high level of accuracy that is worth mentioning a part. The experiment has measured CMB anisotropies in different frequency bands, allowing for an efficient removal of the foreground emissions. The measurements mapped the full sky in the unpolarized and polarized components providing an accurate determination of the temperature power spectrum (TT) and the temperature-polarization cross-correlation spectrum (TE) [30]. The position of the first peak in the TT spectrum constrain the curvature to be $\Omega_k = 0.030\pm^{0.026}_{0.025}$ [31]. The combination of WMAP data with ACBAR and CBI, 2dF measurements and Lyman α forest data find the best fit cosmological parameters: $h = 0.71\pm^{0.04}_{0.03}$, the baryon density $\Omega_b h^2 = 0.0224 \pm 0.0009$, the dark matter density $\Omega_m h^2 = 0.0135\pm^{0.008}_{0.009}$, the optical depth $\tau = 0.17 \pm 0.04$, the scalar spectral index $n = 0.93\pm0.03$ and the amplitude of the fluctuations $\sigma_8 = 0.84\pm0.04$ [32]. The value of τ comes from an excess of power on the large angular scales of the TE spectrum [33]. This signal cannot be explained by systematic effects or foreground emissions and has a natural interpretation as the signature of early reionization, most probably occurred at redshift $z \approx 20$. This conflicts with the measurements of the Gunn-Peterson absorption trough in spectra, which indicate the presence of neutral hydrogen at redshift $z \approx 6$ [34]. Therefore we have evidence for a complex ionization history of the Universe, which most probably underwent two reionization phases, an early and a late one. Of particular interest is the running of the scalar spectral index that provides a better fit to the data when WMAP is combined with small angular scale measurements such as ACBAR, CBI, 2dF galaxy survey and Lyman α. Another interesting finding of the WMAP TT spectrum is

the lack of power at low multipole. In particular the quadrupole and the octupole are suppressed compared to the expectation of the best fit ΛCDM model. It has been claimed that such suppression could be the signature of new physics [35, 36].

1.3.2 Clustering of matter

The cosmological structures we observe today have been formed by the gravitational amplification of small density perturbations. The amount of such inhomogeneities at different cosmological scales is measured by the matter power spectrum. This is estimated from the statistical analysis of a large sample of galaxies and provides a measurement of the amount of clustered matter in the Universe. Recently two large galaxy surveys, the 2dF Galaxy Redshift Survey [37] and the Sloan Digital Sky Survey [38], have probed intermediate scales ($10 - 100$ Mpc). The fit to the power spectrum data of the 2dF yields $\Omega_m h = 0.20 \pm 0.03$ and the baryon fraction $\Omega_b/\Omega_m = 0.15 \pm 0.07$ [37]. Such a low value of Ω_m gives indirect evidence for a large non vanishing cosmological constant contribution when this LSS data is combined with the CMB. A joint analysis of the CMB and 2dF data indicates $0.65 \lesssim \Omega_\Lambda \lesssim 0.85$ at 2σ [39]. An independent estimate of Ω_m is provided by the peculiar velocities of galaxies. In fact mass density fluctuations cause galaxy motion with respect to the Hubble flow. Such a motion reflect the matter distribution and therefore is sensitive to Ω_m. The analysis of the Mark III and SFI catalogs constrain $\Omega_m = 0.3 \pm 0.06$ [40]. Low values of Ω_m are also indicated by the studies of cluster of galaxies, where it is assumed the amount of matter in rich clusters provides a fair sample of the matter content of the Universe. Recent surveys have precisely determined the local X-ray luminosity function. Using the observed mass-luminosity relation, the cluster mass function has been compared with the prediction from numerical simulations. This analysis constrains $\Omega_m < 0.36$ at 1σ [41] (see also [42]). This result is in agreement with the limits found by an alternative study from which, $0.1 < \Omega_m < 0.5$ at 2σ [43]. Another way of estimating the amount of dark matter is to measure the baryon fraction f_b from X-ray cluster observations. In fact the ratio of the baryonic to total mass in cluster should closely match the ratio Ω_b/Ω_m. Therefore a measurement of f_b combined with accurate determination of Ω_b from BBN calculation can be used to determine Ω_m. Using such a method it was found $\Omega_m \approx 0.32$ for $h \sim 0.7$ [44]. This is in agreement also with the value obtained by a study of the redshift dependence of the baryon fraction, that indicates $\Omega_m = 0.3 \pm^{0.04}_{0.03}$ [45]. Similarly a different analysis based on gravitational lens statistics

provides $\Omega_m = 0.31 \pm^{0.39}_{0.24}$ [46].

1.3.3 Age of the Universe

The Friedman equation Eq. (1.4) can be integrated to obtain the age of a given cosmological model:

$$H_0 t_0 = \int_0^1 \frac{da}{a\sqrt{(1-\Omega_m-\Omega_\Lambda)/a^2 + \Omega_m/a^3 + \Omega_\Lambda}}. \tag{1.9}$$

The numerical solutions are shown in figure 1.1. The solid lines correspond to increasing value of $H_0 t_0$ in the $\Omega_m - \Omega_\Lambda$ plane. It is easy to see that for fixed values of Ω_m the age of the Universe increases for larger values of Ω_Λ. Since matter dominated cosmological models are younger than globular clusters, in the past few decades the possibility of an 'age problem' has been a matter of debate. The presence of a cosmological constant can alleviate such a problem. However a key role is played by the Hubble parameter, in fact low values of H_0 increase t_0. The age of globular clusters is estimated to be about 11.5 ± 1.5 Gyr [47], therefore a purely matter dominated Universe ($\Omega_m = 1$ and $\Omega_\Lambda = 0$) cannot be excluded if $h < 0.54$. However such a low value of h seems to be inconsistent with the accepted value of $h \approx 0.71 \pm 0.07$ [29]. It is worth mentioning that the determination of the age of high redshift objects can be used to constrain Ω_Λ by studying the redshift evolution of the age of the Universe [48].

1.3.4 Supernovae Ia and luminosity distance measurements

Supernovae type Ia are violent stellar explosions, their luminosity at the peak becomes comparable with the luminosity of the whole hosting galaxy. For such a reason they are visible to cosmic distances. These supernovae appear to be standard candles and therefore are used to measure cosmological distances by means of the magnitude-redshift relation:

$$m - M = 5 \log_{10} \frac{d_L}{Mpc} + 25, \tag{1.10}$$

where m is the apparent magnitude, M is absolute magnitude and d_L is the luminosity distance which depends upon the geometry of the space and its matter content. In the standard scenario a white dwarf accretes mass from a companion star. Once the Chandrasekhar mass limit is reached, the burning of carbon is ignited in the interior of the white dwarf. This process propagates to the exterior layers leading to a complete destruction of the star. The physics of these objects is not completely understood yet. It requires the

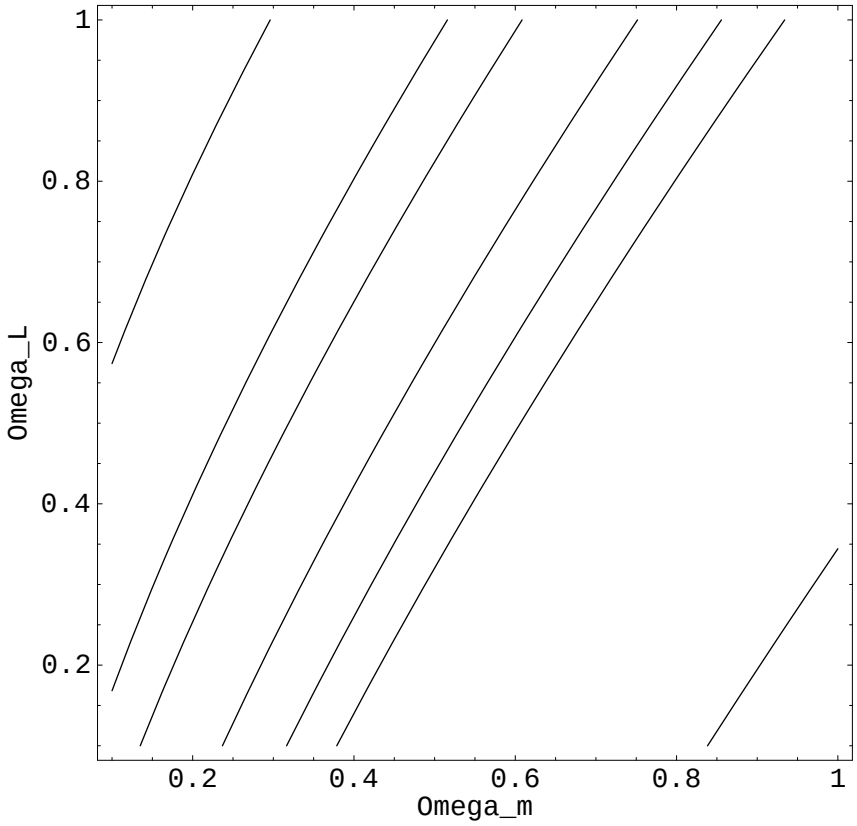

Figure 1.1: Lines of constant $H_0 t_0$ in the $\Omega_m - \Omega_\Lambda$ plane. From top left to bottom right $H_0 t_0 = (1.08, 0.94, 0.9, 0.85, 0.82, 0.8, 0.67)$.

use of numerical simulations from which it appears that the thermonuclear combustion is highly turbulent. Such theoretical uncertainties prevent us from having reliable predictions of possible evolutionary effects. It is also matter of debate as to whether the history of the supernova progenitors can have important effects in the final explosion (see [49] for a general review). For these reasons it is a rather unreliable assumption that supernova Ia are perfect standard candles. However the observations show the existence of an empirical relation between the absolute peak luminosity and the light curve shapes. There are also correlations with the spectral properties. Using such relations it is possible to reduce the dispersion on magnitude of each supernova to within 0.17 magnitudes allowing them to be used for cosmological distance measurements (see [50] and references therein). The Supernova Cosmology Project [51] and the High-Z Supernova Research Team [52] have observed and calibrated a large sample of supernovae at low and high redshifts. The result of their analysis [52, 53] shows that distant supernovae are on the average about 0.20

magnitudes fainter than would be expected in a Milne universe (empty). The likelihood analysis, due to the degeneracy of the luminosity distance with the values of Ω_Λ and Ω_m, constrains these parameters in a region approximated by $0.8\Omega_m - 0.6\Omega_\Lambda \approx -0.2 \pm 0.1$. The data give evidence for a non vanishing cosmological constant. Including the farthest supernova Sn 1997f with $z \approx 1.7$ [54], the data analysis shows that at redshift $z \sim 1.2$ the Universe was in a decelerating phase. However the presence of possible systematic uncertainties has attracted some criticism. In particular there could be a dimming of the light coming from the supernovae due to intergalactic dust. Moreover the Sn Ia might have an evolution over the cosmic time, due to changes in characteristics of the progenitors so as to make their use as standard candles unreliable. The argument against the extinction is that high-redshift supernovae suffer little reddening. While the fact that their spectra appear similar to those at low-redshift seems to exclude the possibility of evolutionary effects in the data. For instance in [55], the Hubble diagram of distant type Ia supernovae segregated according to the type of host galaxy has been analysed. The results shows that host galaxy extinction is unlikely to systematically affect the luminosity of Sn Ia in a manner that would produce a spurious cosmological constant. In reality only a theoretical prediction, not available at the present time, would convince the entire community. Nevertheless none of these systematic errors can reconcile the data with a vanishing Λ.

1.4 Cosmic complementarity

Figure 1.2 shows the region of the $\Omega_m - \Omega_\Lambda$ constrained by different cosmological observations. It appears evident that the joint analysis of the recent CMB, large scale structure and Sn Ia observations, previously reviewed, indicate a region of the parameter space where they are consistent [56–58]. In particular the likelihood contours of Sn Ia and CMB are orthogonal and therefore their combination breaks the geometric degeneracy between Ω_m and Ω_Λ. Such consistency tells us that the Universe is nearly flat, the structures we observe today are the result of the growth of initial density fluctuations characterized by a nearly scale invariant spectrum as predicted by inflationary scenarios. The matter content of the Universe consist of baryons (3%), while most of the clustered matter consists of cold dark particles that account for only 30% of the total energy density. About 67% of the matter is in a 'dark energy' form and is responsible for the present accelerated expansion. In spite of any astronomical uncertainties, the limits on Ω_Λ impose that $\Lambda \lesssim 10^{-47}$

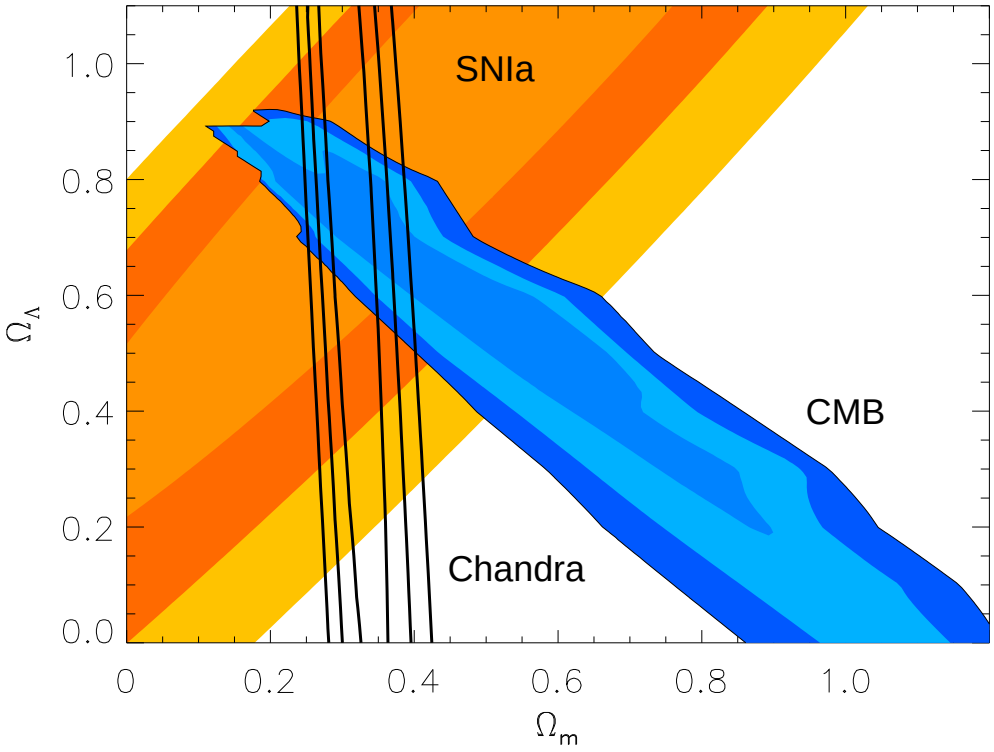

Figure 1.2: 1, 2 and 3 σ confidence contours on $\Omega_m - \Omega_\Lambda$ plane determined from Sn Ia, CMB and Chandra $f_{\rm gas}$(z) data (from [45])

GeV^4. Understanding the origin and the smallness of this term is the challenge of modern theoretical physics. In principle nothing prevents the existence of a Λ-term in the Einstein equations. However if Λ appears on the left hand side, the gravitational part of the Einstein-Hilbert action will depend on two fundamental constants, G and Λ, which differ widely in scale. For instance the dimensionless combination of fundamental constants $(G\hbar/c^3)^2\Lambda \lesssim 10^{-124}$. On the other hand we know that several independent phenomena can contribute as an effective Λ term on the right hand side of the Einstein equations [2]. However, as we shall see in the next chapter, in order to reproduce the small observed value, these terms have to be fine tuned with bizarre accuracy. Therefore the solution to such an enigma may well lead us to the discovery of new physics.

Chapter 2

An explanation for the dark energy?

The cosmological constant can be naturally interpreted as the energy contribution of the vacuum. However its measured value turns out to be extremely small compared to the particle physics expectations. Therefore alternative candidates for the dark energy component have been considered. In particular a light scalar field rolling down its self-interacting potential can provide the missing energy in the Universe and drive a late time phase of accelerated expansion. A lot of effort has gone into justifying the existence of this field, called *quintessence*, within the context of particle theories beyond the Standard Model. Different versions of this original idea have been developed in the literature. In this Chapter we will review the vacuum energy problem. Then we will discuss the application of the anthropic principle to the solution of the 'coincidence problem'. We will describe the main characteristic of a minimally coupled quintessence scenario. At the end we will analyse the dynamics of two specific scalar field models.

2.1 Vacuum energy

It was initially pointed out by Y.B. Zeldovich [59] that in Minkowski space-time, Lorentz invariance constrains the energy momentum tensor of zero point vacuum fluctuations to be proportional to the Minkowski metric, *i.e.* $T^{vac}_{\mu\nu} = const. \times diag(1, -1, -1, -1)$. This relation can be generalized to the case of a curved space-time with metric $g_{\mu\nu}$. The principle of general covariance requires that $T^{vac}_{\mu\nu} \propto g_{\mu\nu}$, which has the form of a cosmological

constant. This implies that in General Relativity, since the gravitational field couples through the Einstein equations with all kinds of energy, the vacuum energy contributes to the total curvature of space-time. The vacuum state of a collection of quantum fields, that describes the known forces and particles, is defined to be the lowest energy density state. If we think of the fields as a set of harmonic oscillators the total zero point energy is given by:

$$\rho_{vac} = \frac{1}{2}\sum_{\mathbf{k}} = \frac{1}{4\pi^2}\int_0^\infty \sqrt{k^2+m^2}k^2 dk, \tag{2.1}$$

that diverges as k^4 (ultraviolet divergence). However any quantum field theory is valid up to a limiting cut-off scale, beyond which it is necessary to formulate a more fundamental description. Consequently the integral Eq. (2.1) can be regularized imposing a cut-off k_{max}, and we obtain

$$\rho_{vac} = \frac{k_{max}^4}{16\pi^2}. \tag{2.2}$$

If we set the cut-off k_{max} at the Planck scale, the energy density of the vacuum is $\rho_{vac} \approx (10^{19}\ \text{GeV})^4$ which is about 120 orders of magnitude larger than the observed value of ρ_Λ. Fixing the cut-off scale at the QCD phase transition, $k_{max} = \Lambda_{QCD}$, we find $\rho_{vac}^{QCD} \approx 10^{-3}$ GeV^4 which is still 44 orders of magnitude above the expected one. On the other hand if Supersymmetry is realized in nature, the cosmological constant vanishes because the vacuum energy contribution of the bosonic degree of freedom exactly cancels that of the fermionic ones. However, because we do not observe super-particles, Supersymmetry must be broken at low energy. This implies that the cosmological constant vanishes in the early Universe and reappears later after SUSY breaking. Assuming that Supersymmetry is broken at $M_{SUSY} \approx 1TeV$ the resulting ρ_{vac} is about 60 orders of magnitude larger then the observational upper bounds. Hence any cancellation mechanism will require a bizarre fine tuning in order to explain the huge discrepancy between ρ_{vac} and ρ_Λ. By the present time we do not have any theoretical explanation for this cosmological constant problem. Moreover such a tiny value presents an other intriguing aspect. In fact we could ask why Λ has been fixed at very early time with such an extraordinary accuracy that today it becomes the dominant component of the Universe. In other words we should explain why the time when Λ starts dominating nearly coincides with the epoch of galaxy formation. This is the so called coincidence or 'why now' problem. The solution to the cosmological constant problem will provide an explanation also for this cosmic coincidence. On the

other hand it could be easier to justify a vanishing cosmological constant assuming the existence of some unknown symmetry coming from quantum gravity or string theory [60]. As we shall see in the following sections, alternative scenarios of dark energy formulate the initial condition problem and the coincidence problem in a different way.

2.2 Anthropic solutions

The use of anthropic arguments in cosmology has been often seen as an anti-scientific approach. However a different use of the 'Anthropic Principle' has been recently proposed in the literature and for a review of the subject we refer to [61]. We should always have in mind that at the speculative level our Universe can be one particular realization of possible universes. Therefore the fact that we live in this Universe makes us privileged observers, since under other circumstances we would not be here. For instance several authors pointed out that not all values of Λ are consistent with the existence of conscious observers [62–64]. The reason is that in a flat space-time the gravitational collapse of structure stops at the time $t \sim t_\Lambda$, as consequence universes with large values of Λ will not have galaxies formed at all. This argument can be used to put an anthropic bound on ρ_Λ by requiring that it does not dominate before the redshift z_{max} when the earliest galaxy formed. In [64] assuming $z_{max} = 4$ it was found $\rho_\Lambda \lesssim \rho_m^0$. However it was suggested in [65, 66] that observers are in galaxies and therefore there is a conditional probability to observe a given value of Λ. In particular this value will be the one that maximizes the number of galaxies. In such a case the probability distribution can be written as

$$d\mathscr{P}(\rho_\Lambda) = \mathscr{P}_*(\rho_\Lambda)\nu(\rho_\Lambda)d\rho_\Lambda, \tag{2.3}$$

where $\mathscr{P}_*(\rho_\Lambda)$ is the *a priori* probability density distribution and $\nu(\rho_\Lambda)$ is the average number of galaxies that form per unit volume with a given value of ρ_Λ. The calculation of $\nu(\rho_\Lambda)$ can be done using the Press-Schechter formalism. Assuming a flat *a priori* probability density distribution the authors of [67] found that the peak of $\mathscr{P}(\rho_\Lambda)$ is close to the observed value of Λ. This anthropic solution to the cosmological constant problem would be incomplete without an underlying theory that allows Λ to take different values and predicts a flat $\mathscr{P}_*(\rho_\Lambda)$. The recent developments in string/M theory seems to provide a natural framework where such issues can be addressed (see [68]).

2.3 Quintessence

A non-anthropic solution to the cosmic coincidence problem would be an exotic form of matter playing the role of dark energy. The existence of such a component should be the prediction of some fundamental theory of particle physics. For instance it was initially suggested that a network of topological defects could provide such a form of energy [69–71]. In fact topological defects are characterized by a negative value of the equation of state $w_X \lesssim -1/3$ and lead to an accelerated expansion if they dominate the energy budget of the Universe. However these models are ruled out by current cosmological observations. On the other hand, long before the time of Sn Ia measurements, it was considered that an evolving scalar field, called quintessence, could take into account for the missing energy of the Universe [72–78]. In this scenario the cosmic coincidence problem is formulated in a different way. In fact the evolution of the quintessence is determined by the initial conditions and by the scalar field potential. Consequently there would be no coincidence problem only if the quintessence becomes the dominant component today independently of the initial conditions, that have been set at very early time. It was pointed out by Zlatev, Wang and Steinhardt [79, 80] that viable quintessence potentials are those manifesting 'tracking' properties. In these cases, for a wide range of initial conditions, the scalar field evolves towards an attractor solution such that at late time it dominates over the other matter components. However such a time will depend on the energy scale of the potential and is fixed in way such that ρ_Q reproduces the observed amount of dark energy. In other words the tracker quintessence solves the initial conditions problem, but the 'why now' problem is related to the energy scale of the model. If such a scale is consistent with the high energy physics scales there is no fine tunning and the fact that the acceleration starts only by the present time does not have any particular meaning. On the contrary the coincidence problem would result if such a scale is much smaller than any particle physics scale, because this will require a fine tuning similar to the cosmological constant case. As we shall see consistent quintessence model building is a difficult challenge [81]. Cosmic coincidence is absent in quintessence models where the scalar field is non-minimally coupled to the cold dark matter [82–85]. Coupling with baryons is strongly constrained by tests of the equivalence principle, however a coupling with cold dark matter cannot be excluded. In this case the coupling will naturally produce the gravitational collapsing time scale of the order of the time when the Q field starts dominating, $t_G \sim t_Q$. Moreover in

these models structure formation can occur even during the accelerated phase of expansion and consequently no coincidence have to be explained [86]. It may be argued that for this class of models to fully succeed what has to be explained is the strength of the couplings. However the non universality of the couplings may arise in the context of brane models, where dark energy and dark matter belong to an hidden sector.

2.3.1 Scalar field dynamics

A multiple fluid system consisting of a scalar field, pressureless matter and radiation interacting through the gravitational field is described by the action:

$$S = -\frac{1}{16\pi G}\int d^4x\sqrt{-g}R + \int d^4x\sqrt{-g}(\mathscr{L}_Q + \mathscr{L}_m), \tag{2.4}$$

where R is the Ricci scalar and $\mathscr{L}_m$ Lagrangian density of the matter and radiation and $\mathscr{L}_Q$ is the Lagrangian density of the quintessence field which is given by:

$$\mathscr{L}_Q = \frac{1}{2}\partial^\mu Q\partial_\mu Q - V(Q). \tag{2.5}$$

The scalar field energy-momentum tensor then reads as

$$T_{Q\,\mu\nu} = \partial_\mu Q\partial_\nu Q - g_{\mu\nu}\left(\frac{1}{2}\partial^\alpha Q\partial_\alpha Q - V(Q)\right). \tag{2.6}$$

In a FRW flat Universe for a nearly homogeneous scalar field, the quintessence pressure and energy density are $p_Q = \dot{Q}^2/2 - V$ and $\rho_Q = \dot{Q}^2/2 + V$. The quintessence behaves as perfect fluid with a time dependent equation of state which is given by:

$$w = \frac{\dot{Q}^2/2 - V(Q)}{\dot{Q}^2/2 + V(Q)}. \tag{2.7}$$

The scalar field evolution is described by the Klein-Gordon equation,

$$\ddot{Q} + 3H\dot{Q} + \frac{dV}{dQ} = 0, \tag{2.8}$$

with

$$H^2 = \frac{8\pi G}{3}\left[\rho_m + \rho_r + \frac{\dot{Q}^2}{2} + V(Q)\right], \tag{2.9}$$

where ρ_m and ρ_r are the matter and radiation energy densities and evolve according to the energy conservation equation Eq. (1.7). As an example we analyse the dynamics of this system in the case of an Inverse Power Law potential [73, 79]:

$$V(Q) = \frac{\Lambda^{\alpha+4}}{Q^\alpha}, \tag{2.10}$$

where $\alpha = 6$ and we set Λ such that $\Omega_Q = 0.7$. We solve numerically the equations of motion. In figure 2.1 we show the evolution with redshift of the energy density of radiation (blue dash line), matter (green dot line) and quintessence (red solid line). Different red lines correspond to different initial conditions, we may distinguish two distinct behaviours. For initial values of the quintessence energy density larger than matter energy density, $\rho_Q^{in} > \rho_m^{in}$, ρ_Q rapidly decreases. This regime is called *kination*. In fact, as we can see in figure 2.2a, the kinetic energy rapidly falls off while the potential energy remains nearly constant. The overshooting is then followed by the *frozen field* phase, where the energy density is dominated by the potential. During this period ρ_Q remains constant until the kinetic energy becomes comparable with the potential one and the field reaches the *tracker regime*. In the tracker solution the kinetic and potential energies scale with a constant ratio, therefore the equation of state is constant or slowly varying. For a given potential the existence of a period of tracking is guaranteed by the condition $\Gamma = V''V/(V')^2 > 1$ [80]. Moreover during this phase the value of the quintessence equation of state mimics the value w_B of the background component according to the relation:

$$w_Q \approx \frac{w_B - 2(\Gamma - 1)}{1 + 2(\Gamma - 1)}. \tag{2.11}$$

For inverse power law potentials $\Gamma = 1 + \alpha^{-1}$. At late time the field leaves the tracker solution, the potential energy starts dominating over the kinetic one (figure 2.2b) and the equation of state tends to negative values. During this final phase the field becomes the dominant component of the Universe and drives the accelerated expansion. The same arguments hold for initial conditions corresponding to $\rho_Q^{in} < \rho_m^{in}$. In such a case the quintessence starts its evolution in the frozen regime. Such a behavior occurs over a range of initial conditions that covers more then 100 orders of magnitude, consequently the quintessence dominated period is obtained with no need of fine tunning of the initial conditions. For tracker models the final value of the equation of state depends on the parameter Λ or equivalently on Ω_Q and on the slope of the potential. In general for large values of Ω_Q or flat potential $w_Q \to -1$, in the case of the Inverse Power Law potential small values of α corresponds to large negative value of w_Q^0 (figure 2.3).

2.3.2 Quintessential problems

The existence of the tracker phase cancels any knowledge of the initial condition of the scalar field providing an elegant way of solving the coincidence problem. Nevertheless it is

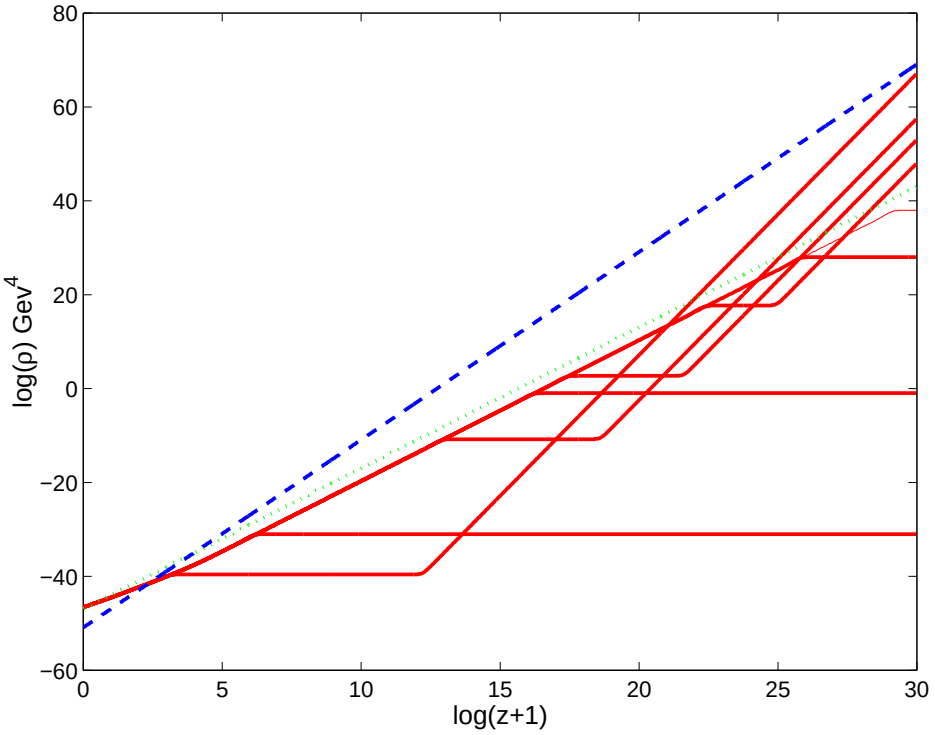

Figure 2.1: Energy density versus redshift for radiation (blue dash line), matter (green dot line) and quintessence (red solid line). As we may notice for a large range of initial conditions the quintessence energy density converges to the tracker solution.

a rather difficult task to build consistent particle physics models of quintessence. One of the reasons it that for a given tracker potential, $V(Q) = \Lambda f(Q)$, the cosmic coincidence is fully solved only if the scale Λ is consistent with the energy scale of the underlying particle physics theory that predicts the shape $f(Q)$ of the quintessence potential. For example let us consider the Inverse Power Law model. It was shown in [87, 88] that it can be derived from a Supersymmetric extension of QCD. By the present time the condition $|V'/V| < 1$ has to hold in order to guarantee the Universe is accelerating, this implies that today the scalar field $Q \sim M_{Pl}$. Since the observations suggest $\rho_Q \approx \rho_c$, for values of the slope $\alpha \geq 6$ we find that $\Lambda \approx 4.8 \times 10^6$ GeV, a very reasonable scale from the particle theory point of view. On the other hand for tracker models the slope of the potential is constrained by measurements of the present value of the quintessence equation of state w_Q^o that indicate a low value of α. But, as we can see in figure 2.4 for values of $\alpha < 6$ the energy scale is much smaller than any known particle physics scale. Therefore the Inverse Power Law seems not to be a viable quintessence model. Alternative models have been proposed in the literature, they can be distinguished into two categories, dilatonic and supersymmetric

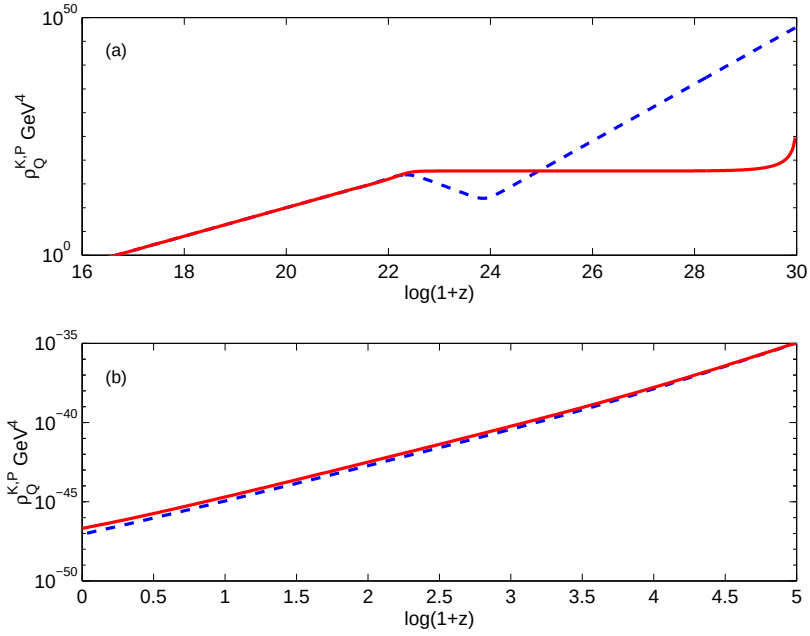

Figure 2.2: Evolution of the kinetic (blue dash line) and potential energy density (red solid line) at early times (a) and after matter-radiation equality (b).

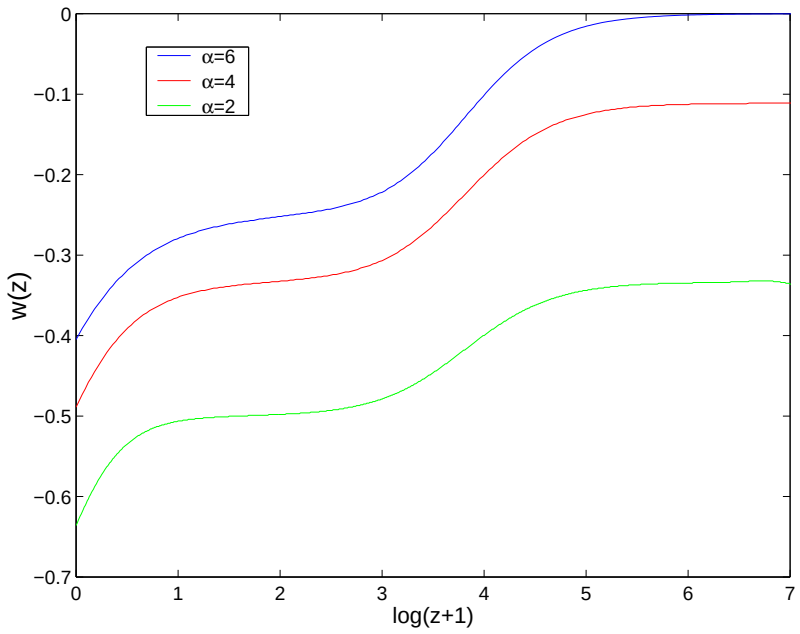

Figure 2.3: Equation of state versus redshift for an Inverse Power Law potential with $\alpha = 6$ (blue solid line) $\alpha = 4$ (red solid line) and $\alpha = 2$ (green solid line).

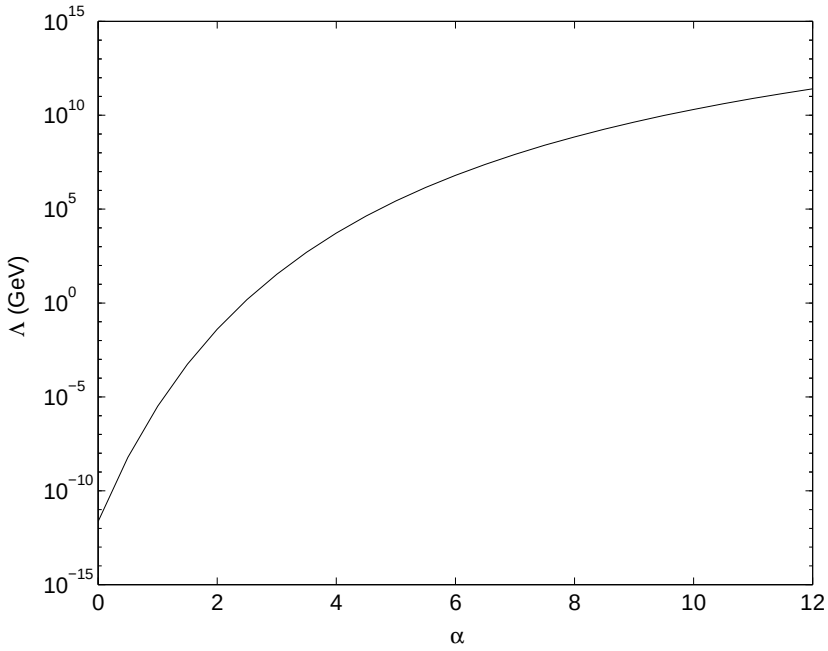

Figure 2.4: Energy scale versus α for the quintessence Inverse Power Law potential.

quintessence. The former class of models assume that the quintessence field is the dilaton, this possibility has been studied in [89, 90]. The dilaton is predicted by all string theory models and it couples to all the fields including gravity [91]. Therefore it could be a good candidate for dark energy. However it predicts a running of the different coupling constants, that are strongly constrained by present observations and the violation of the equivalence principle. Nevertheless these models deserve more investigation and some of these issues have been recently addressed in [92, 93]. It is worth mentioning that the non-minimally coupled scalar field models which solve the coincidence problem belong to this category [82–85, 94, 95]. In the second class of models the quintessence is one of the scalar fields predicted by Supersymmetric extensions of the Standard Model of particle physics. In particular a lot of effort has been recently devoted to the formulation of viable quintessence models in the context of Supergravity theory. In fact it was noticed that Inverse Power Law potentials generated by Supersymmetric gauge theories are stable against quantum and curvature corrections, but not against K*ä*hlerian corrections [96–98]. Since $Q_0 \approx M_{Pl}$, Supergravity (SUGRA) corrections cannot be neglected and therefore any realistic model of quintessence must be based on SUGRA. It is argued that also this class of models lead to violation of the equivalence principle, the quintessence field can in fact mediate a long range fifth force that we do not observe. However we want to stress

that in the context of Supersymmetric theories this is not the main problem. The reason is that the quintessence can belong to a hidden sector of the theory that couples only gravitationally to the visible sector. It was pointed out in [81] that any supersymmetric inspired model has to address two specific issues. The first one concerns the case of Supersymmetry breaking quintessence, if the quintessence field belongs to a sector of the theory that breaks Supersymmetry, because of the shape of the potential it turns out it cannot be the main source of breaking. In such a case SUSY can be broken by the presence of an F-term that leads to an intolerably large vacuum energy contribution that completely spoils the nice properties of the quintessence potential. The other difficulty arises from the coupling of quintessence to the field responsible for the supersymmetry breaking. Such a coupling leads to corrections of the scalar field potential such that the quintessence acquires a large mass. Some alternatives have been recently investigated, for instance a way of avoiding such problems has been considered in [99], where a Goldstone-type quintessence model in heterotic M-theory has been proposed.

2.4 Supergravity inspired models

We now review some of the properties of two models proposed in the context of Supergravity theories: the Exponential Times Inverse Power Law potential and the Two Exponential potential.

2.4.1 Exponential Times Inverse Power Law potential

The authors of [96] have shown that taking into account Supergravity corrections to the Inverse Power Law potential, the quintessence potential takes the form:

$$V(Q) = \frac{\Lambda^{4+\alpha}}{Q^{\alpha}} e^{\frac{\kappa}{2}Q^2}, \tag{2.12}$$

where $\kappa = 1/M_{Pl}^2$. This potential is an improvement the Inverse Power Law. In fact the dynamic remains unchanged during the radiation and the matter dominated era, while the presence of the exponential term flatten the shape of the potential in the region corresponding to the late time evolution of the scalar field. This allows for more negative values of the equation of state today independently of the slope of the inverse power law. Consequently we can have a reasonable particle physics energy scale even for large values of α. For instance for $\alpha = 11$ and $\Omega_Q = 0.7$ we have $\Lambda \approx 10^{11}$ GeV and the present value of the equation of state is $w_Q^0 = -0.82$, in better agreement with observational constraints.

2.4.2 Two Exponential potential

The dynamics of cosmologically relevant scalar fields with a single exponential potential has been largely studied in the literature and within a variety of contexts (see for instance [77]). The existence of scalar field dominated attractor solutions is well known, however for this class of models an accelerated phase of expansion can be obtained with an extreme fine tunning of the initial conditions [102]. It has been shown in [100,101] that quintessence Supergravity inspired models predict the scalar field potential to be of the form:

$$V(Q) = M_{Pl}^4 \left(e^{\alpha\sqrt{\kappa}(Q-A)} + e^{\beta\sqrt{\kappa}(Q-B)} \right), \tag{2.13}$$

where A is a free parameter, while B has to be fixed such that $M_{Pl}^4 e^{-\beta B} \sim \rho_Q^0$. This potential has a number of interesting features. As it has been pointed out by the authors of [100] in the form given by the Eq. (2.13) all the parameters are of the order of the Planck scale. Only B has to be adjusted so that $M_{Pl} e^{-\beta B} \approx \rho_Q$, it turns out to be $B = \mathscr{L}(100) M_{Pl}$. For a large range of initial conditions the quintessence field reaches the tracker regime during which it exactly mimics the evolution of the barotropic fluid and at some recent epoch it evolves into a quintessence dominated regime. It is useful to rewrite the two exponential potential as:

$$V(Q) = M^4 \left(e^{-\alpha Q/M_{Pl}} + e^{-\beta Q/M_{Pl}} \right), \tag{2.14}$$

where M is the usual energy scale parameter. For a given value of Ω_Q the slopes α, β fix the final value of the equation of state. The sign of the slopes distinguish this class of potentials into two categories: $\alpha > \beta > 0$ and $\alpha > 0$, $\beta < 0$. For both the cases the Q-field initially assumes negative values and rolls down the region of the potential dominated by the exponential of α. When it reaches the tracker regime its equation of state exactly reproduces the value of the background dominant component, $w_Q = w_B$ and the energy density is given by

$$\Omega_Q = 3(w_B + 1)/\alpha^2. \tag{2.15}$$

The late time evolution is determined by the value of β that fixes the present value of the equation of state. In the case of slopes with the same sign $w_Q^0 \to -1$ for small value of β, while for α and β with opposite sign the scalar field reaches by the present time the minimum of potential at $Q_{min}/M_{Pl} = ln(-\alpha/\beta)/(\alpha - \beta)$. Consequently $w_Q^0 \approx -1$ after a series of small damped oscillations. This can be seen in figure 2.5 where we plot

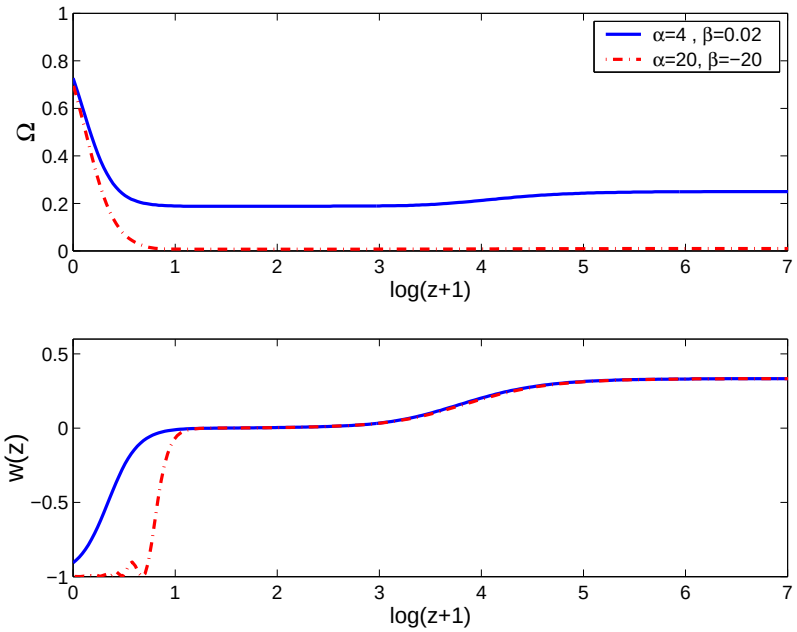

Figure 2.5: Evolution of the quintessence energy density and equation of state for parameters (α,β): blue solide line (20,0.5); red dashed line (-20,-20) and $\Omega_Q = 0.7$.

the evolution of the quintessence energy density parameter Ω_Q and the equation of state w_Q for $\alpha = 4$, $\beta = 0.02$ and $\alpha = 20$, $\beta = -20$. In the latter model the equation of rapidly drops to -1 after few damped oscillations, while the former shows a more smooth behaviour. It is worth remarking that for the two exponential potential with same sign of the slopes the accelerated phase can be a transient regime. This can occurs for large value of β, in such a case after a short period dominated by the potential energy the scalar field acquires kinetic energy so that the equation of state can be $w_Q > -1/3$. As we may note in figure 2.5, because Eq. (2.15) holds during the tracker regime, for small values of α the quintessence energy density assumes non-negligible values at early times. Such an early contribution during the radiation dominated era is constrained by nucleosynthesis bound to be $\Omega_Q(1\ \mathrm{MeV}) < 0.13$. This implies that $\alpha > 5.5$. Such a limit has pushed toward larger value by a new analysis of the Big-Bang nucleosynthesis [103] that constrains $\Omega_Q(1$ MeV$) < 0.045$ at 2σ. In principle this bound can be avoided if the tracker regime starts after Big-Bang nucleosynthesis. However this can be obtained only by tuning the scalar field initial conditions in a restricted range of values. Moreover a recent analysis of the large scale structure data and CMB measurements strongly constrain the value of Ω_Q during the matter dominated era [104].

Chapter 3

Quintessence field fluctuations

The cosmological constant is a smooth component and therefore does not play any active role during the period of structure formation. On the contrary a peculiar feature of the quintessence field is that it is spatially inhomogeneous just as any other scalar field. Therefore it is possible that the clustering properties of the dark energy can play a determinant role in revealing the nature of this exotic fluid. In this Chapter we introduce the scalar field fluctuation equations in the Newtonian gauge. We derive an analytical solution of the quintessence perturbation in the tracking regime and describe the behaviour during different cosmological epochs. We then present the numerical analysis of the perturbations in a multiple fluids system in the particular cases of an Inverse Power law potential and the two exponential potential.

3.1 Quintessence perturbations in Newtonian gauge

The evolution of minimally coupled scalar field perturbations has been studied in a number of papers. For instance in [73, 77, 105, 106] the analysis has been done in the synchronous gauge, while in [107–109] the authors have used the Newtonian gauge. In what follows we use the Newtonian gauge. When compared to the synchronous one it has a number of advantages. In fact since the gauge freedom is fully fixed there are no gauge modes that can lead to misleading conclusions about the evolution of superhorizon modes. Besides, the metric perturbations play the role of the gravitational potential in the Newtonian

limit. The equations we need to linearize are the Einstein's equations

$$R_{\mu\nu} - \frac{1}{2}g_{\mu\nu}R = 8\pi G T_{\mu\nu}, \tag{3.1}$$

the Klein-Gordon equation

$$\frac{1}{\sqrt{-g}}\partial_\mu(\sqrt{-g}g^{\mu\nu}\partial_\nu Q) + \frac{dV}{dQ} = 0 \tag{3.2}$$

and the conservation equation of the stress energy tensor of the different matter components

$$T^{\nu}_{\mu;\nu} = 0, \tag{3.3}$$

In the Newtonian gauge the line element in a spatially flat FRW background reads as

$$ds^2 = (1+2\Phi)dt^2 - a^2(t)(1-2\Phi)dx^i dx_i, \tag{3.4}$$

where Φ is the metric perturbation and t is the real time. We consider a multiple fluid system composed of a scalar field, cold dark matter and radiation. Expanding the fluid variables at first order around the homogeneous value we have:

$$\rho_i^e = \rho_i(1+\delta_i), \tag{3.5}$$

where δ_i is the density perturbation of the i-th component,

$$Q^e = Q + \delta Q, \tag{3.6}$$

where δQ is the scalar field fluctuation and Q is the homogenous part of the quintessence field. The linearized Eq. (3.1), Eq. (3.2) and Eq. (3.3) provide a set of differential equations for the metric, scalar field, radiation and cold dark matter perturbations. In Fourier space the equations are:

$$\dot{\Phi} + \Phi + \frac{k^2}{3H^2a^2}\Phi = \frac{4\pi G}{3H^2}(\delta\rho_Q + \rho_r\delta_r + \rho_c\delta_c), \tag{3.7}$$

$$\delta\ddot{Q} + 3H\delta\dot{Q} + \frac{k^2}{a^2}\delta Q + \frac{d^2V}{dQ^2}\delta Q = 4\dot{Q}\dot{\Phi} - 2\frac{dV}{dQ}\Phi, \tag{3.8}$$

$$\dot{\delta_c} = \frac{k}{a}V_c + 3\dot{\Phi}, \tag{3.9}$$

$$\dot{V_c} = -\frac{k}{a}\Phi, \tag{3.10}$$

$$\dot{\delta_r} = \frac{4k}{3a}V_r + 4\dot{\Phi}, \tag{3.11}$$

$$\dot{V_r} = -\frac{k}{4a}\delta_r - \frac{k}{a}\Phi, \tag{3.12}$$

where δ_c and δ_r are the density perturbations of cold dark matter and radiation, while V_c and V_r are the corresponding velocity perturbations. The perturbed quintessence energy density and pressure are,

$$\delta\rho_Q \equiv \rho_Q\delta_Q = \dot{Q}\delta\dot{Q} - \dot{Q}^2\Phi + \frac{dV}{dQ}\delta Q, \tag{3.13}$$

$$\delta p_Q = \dot{Q}\delta\dot{Q} - \dot{Q}^2\Phi - \frac{dV}{dQ}\delta Q. \tag{3.14}$$

3.2 Evolution of perturbations

3.2.1 Analytical solution in the tracker regime

From Eq. (3.8) we note that the perturbations of the other fluids feed back onto the scalar field perturbations through the gravitational potential Φ. Deep during the radiation and the matter dominated eras the gravitational potential is constant and therefore the first term on the right-hand-side can be neglected. As a first approximation we ignore the second term as well, hence Eq. (3.8) becomes

$$\delta\ddot{Q} + 3H\delta\dot{Q} + \left(\frac{k^2}{a^2} + \frac{d^2V}{dQ^2}\right)\delta Q = 0. \tag{3.15}$$

We can find an analytical solution during the tracker regime when

$$\frac{d^2V}{dQ^2} \sim A_Q^B H^2, \tag{3.16}$$

with A_Q^B a constant that depends on the specifics of the potential and on the equation of state of the background dominant component. This can be obtained as follows. Consider the adiabatic definition of the sound speed associated with the quintessence field:

$$\begin{aligned} c_Q^2 &\equiv \frac{\dot{p}_Q}{\dot{\rho}_Q} = w_Q - \frac{\dot{w}_Q}{3H(1+w_Q)} \\ &= 1 + \frac{2V_{,Q}}{3H\dot{Q}}. \end{aligned} \tag{3.17}$$

During the tracker regime the quintessence equation of state is nearly constant implying that $c_Q^2 \approx w_Q = const.$ Hence by differentiating Eq. (3.17) with respect to time and dividing by H we have

$$\frac{\dot{c_Q^2}}{H} = \frac{2V_{,QQ}}{3H^2} + (1-c_Q^2)\left[1 + \frac{\dot{H}}{H^2} - \frac{1}{2}(3c_Q^2+5)\right], \tag{3.18}$$

From Eq. (3.18) using the second of the Hubble equations $\dot{H}/H^2 = -3(1+w_B)/2$, with w_B being the equation of state of the background dominant fluid, we finally obtain:

$$\frac{V_{,QQ}}{H^2} = \frac{9}{4}(1-c_Q^2)\left(w_B + c_Q^2 + 2\right) \equiv A_Q^B. \tag{3.19}$$

It is useful to rewrite Eq. (3.15) in conformal time, which is defined as $d/d\tau \equiv a(t)d/dt$,

$$\delta Q'' + 2\mathscr{H}\delta Q' + \left(k^2 + a^2H^2A_Q^B\right)\delta Q = 0, \tag{3.20}$$

where a prime denotes the derivative with respect to τ. In the radiation dominated era the scale factor evolves as $a = \tau/2$, while the Hubble rate is given by $H = 2/\tau$, hence Eq. (3.20) becomes:

$$\delta Q'' + 2\delta Q' + (k^2 + 4A_Q^r)\delta Q = 0, \tag{3.21}$$

with A_Q^r being the value of A_Q^B in radiation dominated era. During the tracker regime $c_Q^2 \approx w_r = 1/3$ and $A_Q^r \approx 4$. In such a case the characteristic roots of Eq. (3.21) are complex and the solutions are of the form:

$$\delta Q = e^{-2\tau}\left(C_1\cos\nu_r\tau + C_2\sin\nu_r\tau\right), \tag{3.22}$$

where C_1 and C_2 are integration constants and

$$\nu_r = \sqrt{k^2 + 4A_Q^r - 1}. \tag{3.23}$$

Eq. (3.22) is a damped oscillatory solution with frequency ν_r, On large scales ($k < 1$ Mpc^{-1}) the frequency of these oscillations is scale independent and is set by the tracker properties (A_Q^r). On the other hand if $A_Q^r = 0$, Eq. (3.21) has real roots and the solutions contain a constant mode and a decaying one. Similar solutions can be found in the matter dominated era. The addition of the source term Φ on the right-hand-side of Eq. (3.8) leads to an attractor solution for the quintessence perturbations in the long-wavelength limit, $\delta Q(t) \to \delta Q_c$. In fact from Eq. (3.8) we obtain:

$$\delta Q_c \approx -2\frac{V_{,Q}}{V_{,QQ}}\Phi_c, \tag{3.24}$$

that is constant as long as the quintessence is in the tracker regime. As a consequence this solution does not hold in the kinetic and particularly in the potential phase when the quintessence exits away from the tracker.

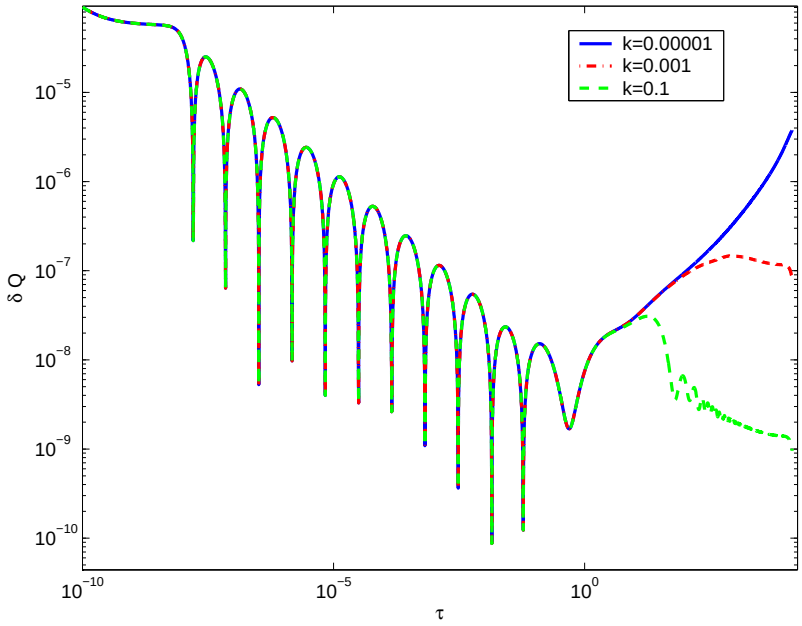

Figure 3.1: Evolution of the scalar field perturbation δQ_k for $k = 0.00001$ (blue solid line), $k = 0.001$ (red dash line) and $k = 0.1$ (green dash line).

3.2.2 Numerical analysis

In this section we present the analysis of the numerical solution of the system of equations Eq. (3.7-3.12), where we have imposed adiabatic initial conditions. We consider a quintessence SUGRA inspired model described in Chapter 2. The scalar field potential is specified by Eq. (2.12) where we set the slope $\alpha = 6$ and the parameter M such that today $\Omega_Q = 0.7$. The initial conditions for the homogeneous part of the scalar field Q have been set such that the tracker solution is reached deep in the radiation dominated era. In figure 3.1 we plot the behaviour of δQ against the conformal time for three different wavenumbers. We can see that as the system enters the tracker regime, decaying oscillations are set for all the three modes with a constant frequency given by Eq. (3.23). Since k^2 is negligible in Eq. (3.23) the frequency of these oscillations is the same for all modes. When the second term in the right-hand-side of Eq. (3.8) becomes comparable to the term $V_{,QQ}$ the fluctuations evolves onto the attractor solution given by Eq. (3.24). In the specific case we consider there is not an exact tracking and consequently the ratio $V_{,Q}/V_{,QQ}$ scales linearly and not steadily as in the exact tracking case. This explains why δQ increases with time in the long wavelength mode. As different scales cross the horizon they leave this attractor solution. For instance the shortest wavelengths ($k = 0.1$) enter

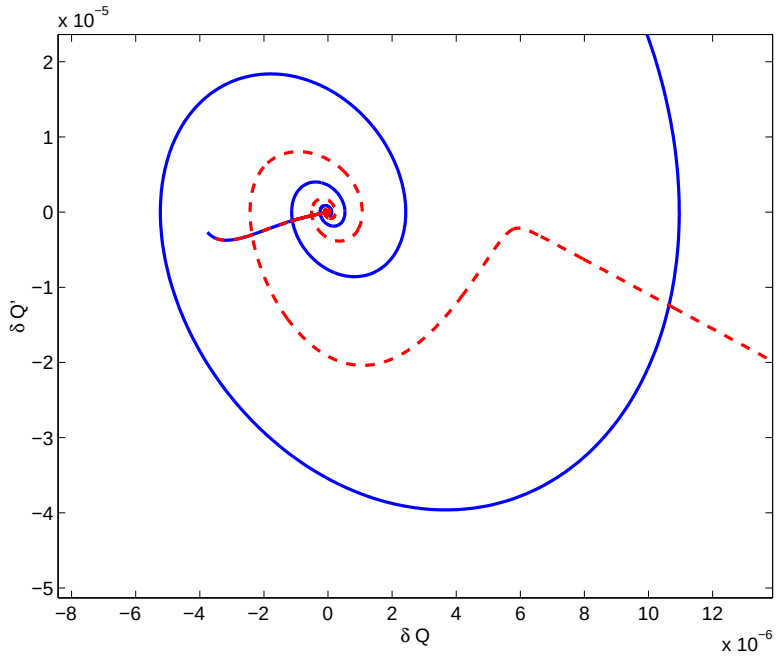

Figure 3.2: Phase diagram for long wavelength quintessence fluctuations with two different initial conditions. The attractor point δQ_c (Eq. 3.24) is a transient attractor.

the horizon after matter radiation equality. Due to the decay of the gravitational potential the first term on the right-hand-side of Eq. (3.8) becomes large leading to a decaying solution with small damped oscillations whose frequency is set by the effective mass term k on the left-hand-side of Eq. (3.8). The presence of an attractor solution for the scalar field perturbations is evident in figure 3.2, where we plot the phase space $\delta Q - \delta\dot{Q}$. As the system evolves in the tracker regime, δQ and $\delta\dot{Q}$ spiral toward the attractor point δQ_c. As soon as the tracker terminates the long wavelength fluctuations have converged to the same values and their evolution is indistinguishable. In minimally coupled quintessence models the effects of the scalar field perturbations on the structure formation process are negligible. This is because the quintessence interacts only gravitationally with the other fluid components and it is usually a subdominant component during the epochs that are relevant for the formation of the early structures. Therefore the clustering of the dark energy can have detectable effects only at late times through the time evolution of the gravitational potentials. As we shall see in Chapter 6 this produces a characteristic imprint in the CMB anisotropy power spectrum. In figure 3.3 we plot the behaviour of the gravitational potential Φ normalized to the cosmological constant case for $k = 0.0004$ (upper panel) and $k = 0.04$ for three different quintessence models whose dynamics have been

described in Chapter 2: (model A) the SUGRA potential Eq. (2.12) with slope $\alpha = 6$ (blue solid line); (model B) the two exponential potential Eq. (2.13) with $\alpha = 20$ and $\beta = -20$ (red dash line) and (model C) $\alpha = 4$ and $\beta = 0.02$ (blue dash dot line). We may note a number of features that arises from the presence of dark energy perturbations and a different expansion rate of the Universe compared to the ΛCDM model. Let us consider the mode $k = 0.0004$ that crosses the horizon during the matter era. For model B (red dash line) the quintessence energy density is always negligible during the matter era and consequently there are no effects due to the perturbations in the evolution of the gravitational potential. On the other hand because of the scalar field dynamics the late time expansion rate of the Universe is different compared to the Λ case, hence Φ/Φ_Λ diverges from the unity. In contrast in models A and C the quintessence energy density dominates earlier, especially in model C where Ω_Q is a large fraction of the total energy density (see figure 2.5). In this case we can distinguish two different evolutionary regimes of the gravitational potential. At redshift $z > 10$ the Universe is matter dominated and the quintessence is in the tracker solution with an equation of state very close to the matter value. Therefore during this period the expansion rate is the same as in the Λ model and we would expect $\Phi/\Phi_\Lambda \approx 1$. The fact this ratio deviates from unity is due to the presence of the dark energy perturbations. On the other hand the evolution of the gravitational potential at $z << 10$ is caused by the accelerated phase of expansion. This can be seen by the change of the slope of Φ/Φ_Λ at a redshift $z \approx 2$ when the acceleration starts. The late time decay of the gravitational potential sources the formation of CMB anisotropy through the late Integrated Sachs-Wolfe effect (ISW). The same arguments hold for the mode $k = 0.04$ that enters the horizon soon after matter-radiation equality. However it is worth noticing that in the case of model C, the early contribution of dark energy causes the scalar field perturbations to produce a bigger effect on the decay of Φ, leading to a larger early ISW effect. From this analysis we conclude that different dark energy models will lead to a characteristic signature in the CMB power spectrum and will prove this point in a more general way in Chapter 6.

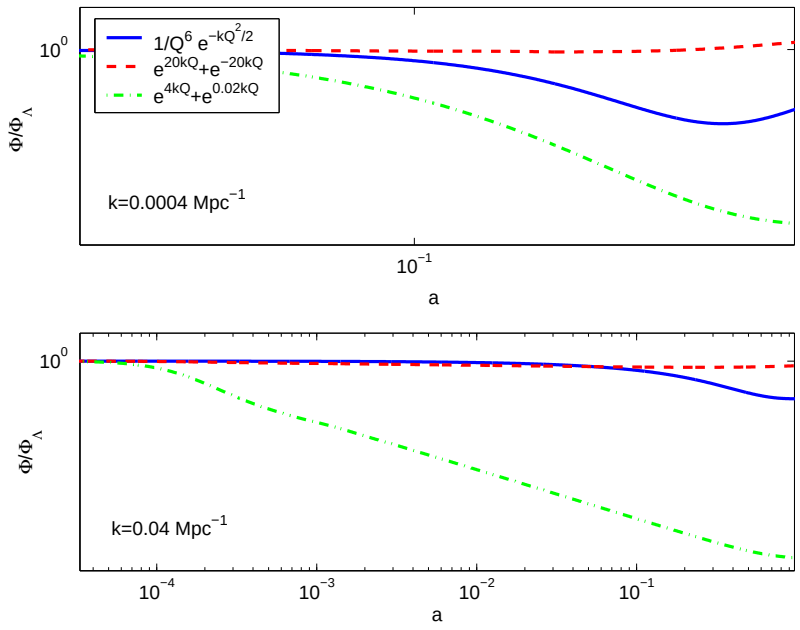

Figure 3.3: Evolution of the gravitational potential Φ normalized to the cosmological constant case for a SUGRA model (blue solid line), two exponential potentials with slopes $(-20, 20)$ (red dash line) and $(4, 0.02)$ (green dash line) respectively. The top panel shows the mode with $k = 0.0004$ and the lower panel shows $k = 0.04$.

Chapter 4

Constraining the quintessence potential

Cosmological distance measurements test the expansion rate of the Universe at different redshifts. Therefore they can be used to constrain the dark energy properties and eventually disprove the ΛCDM model. A lot of effort has gone into constraining the value of the dark energy equation of state with the current available data. In this Chapter we will review some of the constraints obtained in previous works. Then we will describe the analysis of the Sn Ia data and the measured position of the CMB peaks that we performed to constrain the shape of a general quintessence potential [110]. We will comment on our results and compare them to those obtained in other related work.

4.1 Upper bounds on the cosmic equation of state

Different dark energy models are usually constrained assuming that the dark energy behaves as a perfect fluid with a constant equation of state $w_X = p_X/\rho_X \leq -1$. This can take into account for models such as a network of topological defects with $w_X = -n/3$ (n is the dimension of the defect) [111] and as first approximation time dependent tracker quintessence models with $w_Q > -1$. Different values of w_X will lead to a different expansion rate and consequently to a different cosmological distance. In particular for larger negative values of w_X the phase of acceleration starts at earlier times and therefore cosmological distance indicators will appear farther than in models with smaller negative values of w_X. This can be seen in figure 4.1, we plot in the solid line the redshifts z_{acc} when the

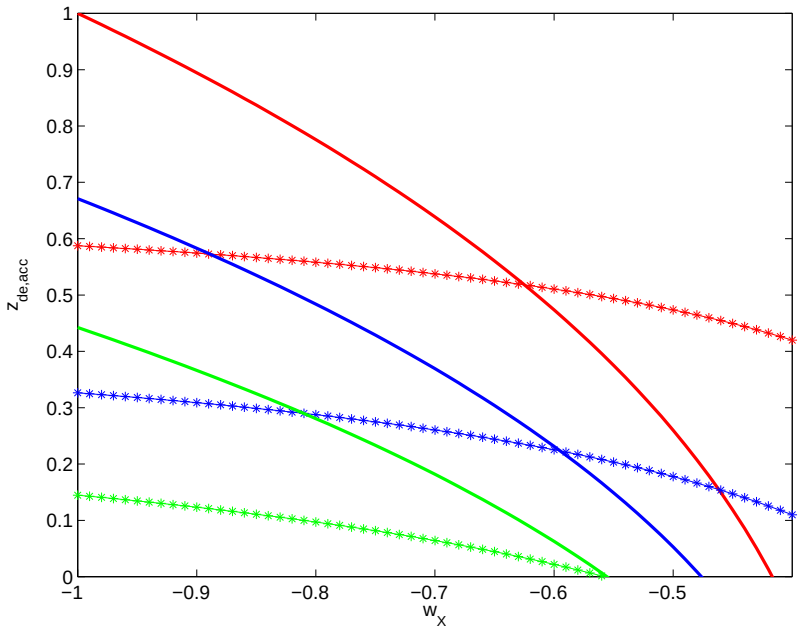

Figure 4.1: Redshifts z_{acc} (solid line) and z_{eq} (starred line) corresponding to the start of the accelerated phase and the dark energy dominated epoch versus a constant w_X for $\Omega_X = 0.6, 0.7, 0.8$ (in *blue, red* and *green* lines respectively).

Universe starts accelerating and in a starred line the redshift z_{de} when the dark energy starts dominating as a function of w_X for different values of Ω_X. For a flat Universe The redshift z_{acc} is given by

$$(1 + z_{acc})^3 = -(1 + 3w_X)\frac{\Omega_X}{1 - \Omega_X}, \tag{4.1}$$

and the redshift z_{de} is

$$(1 + z_{de})^3 = \frac{\Omega_X^{-1/w_X}}{1 - \Omega_X}. \tag{4.2}$$

Note for $w_X < -0.6$ we have $z_{acc} > z_{de}$. For a flat Universe the effect on cosmological distances produced by varying w_X is degenerate with $\Omega_m = 1 - \Omega_X$ and with the Hubble parameter H_0. By making use of the Sn Ia data the authors of [53,112] find the constraint $w_X < -0.55$ (2σ) for $\Omega_m > 0.1$. We will comment in the next Chapter about the bias effect introduced in the analysis of data by assuming a constant equation of state. The position of the Doppler peaks in the CMB anisotropy power spectrum is another indicator of the cosmological distance to the last scattering surface and hence can be used to constrain w_X. In [113] a constant effective equation of state

$$w_{eff} = \frac{\int w_X(a)\Omega_X(a)da}{\int \Omega_X(a)da}, \tag{4.3}$$

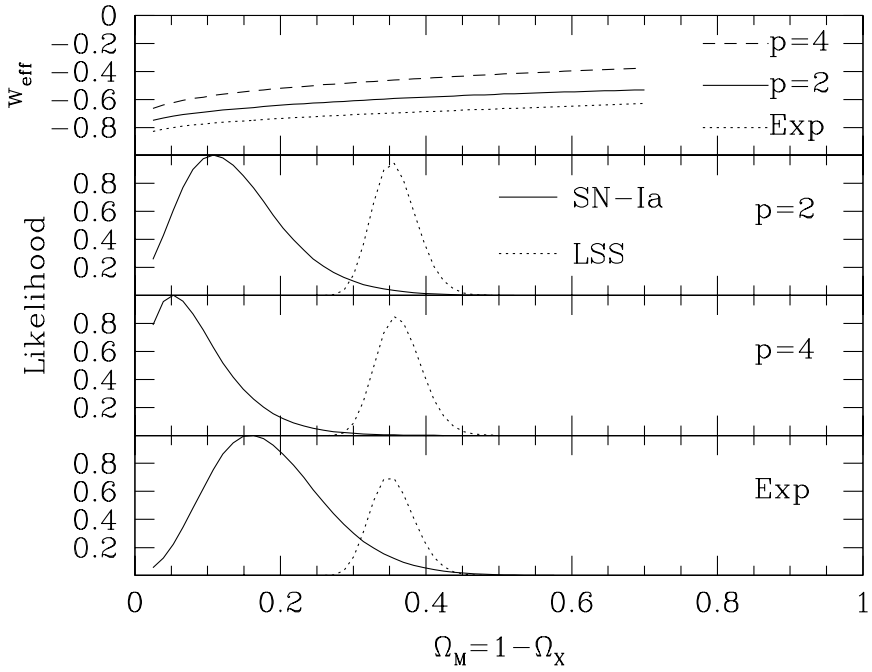

Figure 4.2: Upper panel: relation between w_{eff} and Ω_m for an Inverse Power Law potential with slope p and an Exponential potential $V \propto \exp(m_{Pl}/\mathrm{Q})$. Lower panels: One dimensional likelihoods as a function of Ω_m for CMB+LSS (dot) and Sn Ia (solid) data (from [113]).

has been constrained with the Sn Ia, CMB and the LSS data. The authors find $w_{eff} < -0.65$ (2σ) with $w_{eff} = -1$ being best fit. They comment that tracker models can marginally accommodate the Sn Ia and LSS constraints at the same time (see figure 4.2). Such an inconsistency can be explained as follows. The supernova luminosity distance is sensitive to the value of w_{eff}, while large scale structure data are more sensitive to the amount of clustered matter Ω_m through the matter power spectrum. This implies that dark energy models with different values of w_{eff} will not change the likelihood in Ω_m of the large scale structure data. In fact assuming the value of the effective equation of state to be $w_{eff} > -1$, this shifts the Sn Ia likelihood towards smaller values of Ω_m (*i.e.* larger values of Ω_X). As we will show later, extending the likelihood analysis to the slope of the tracker potential enables us to find models that simultaneously fit the whole data. Similar constraints from Sn Ia and CMB data have been found by Efstathiou [114], namely $w_X \lesssim -0.6$ (2σ). In a different approach Saini et al. [115] have parameterized the luminosity distance and by constraining their parameter space with the Sn Ia data

they have been able to reconstruct the redshift dependence of the dark energy equation of state. They find a time dependence with $-1 \leq w_X \leq -0.86$ today and $-1 \leq w_X \leq -0.6$ at $z = 0.83$. Waga and Frieman have constrained the slope of the Inverse Power Law potential α (see Eq. (2.10)) by making use of the Sn Ia and lensing statistic data [116]. Imposing $\Omega_m > 0.3$ they obtain an upper limit on the present value of the equation of state $w_Q^0 < -0.67$ that implies $\alpha < 1.8$. The combined analysis of the CMB power spectrum measured by the Boomerang and MAXIMA experiments with Sn Ia and large scale structure, limits a constant equation of state to be $w_X < -0.7$ with $w_X = -1$ being the favoured value [117].

4.2 Parameterized quintessence potential

We have seen in Chapter 2 that for tracker models the present value of the equation of state depends of the shape of the scalar field potential. In particular for SUGRA inspired models [96, 100, 101, 118] the equation of state parameter varies in the range $-1 \leq w_Q^0 < -0.8$, while Inverse Power Law potentials require larger values. A general potential which can accommodate for these classes of scenarios is:

$$V(Q) = \frac{M^{4+\alpha}}{Q^\alpha} e^{\frac{1}{2}(\kappa Q)^\beta}, \tag{4.4}$$

where $\kappa = \sqrt{8\pi G}$ and M is fixed in such a way that today $\rho_Q = \rho_c \Omega_Q$, where ρ_c is the critical energy density. For $\beta = 0$ Eq.(4.4) becomes an inverse power law, while for $\beta = 2$ we have the SUGRA potential proposed by [96]. For $\alpha = 0$, $\beta = 1$ and starting with a large value of Q, the Quintessence field evolves in a pure exponential potential [77]. We do not consider this case further since it is possible to have a dark energy dominated universe, but at the expense of fine tuning for the initial conditions of the scalar field. Larger values of β mimic the late time evolution of the model studied in [101]. For $\alpha, \beta \neq 0$ the potential has a minimum, the dynamics can be summarized as follows: for small values of β and for a large range of initial conditions, the field does not reach the minimum by the present time and hence $w_Q^0 > -1$. For example, if the Quintessence energy density initially dominates over the radiation, the Q field quickly rolls down the inverse power law part of the potential eventually resting in the minimum with $w_Q \sim -1$ after a series of damped oscillations [119]. This behaviour however requires fine tuning the initial value of Q to be small. On the other hand, this can be avoided if we consider large values of α

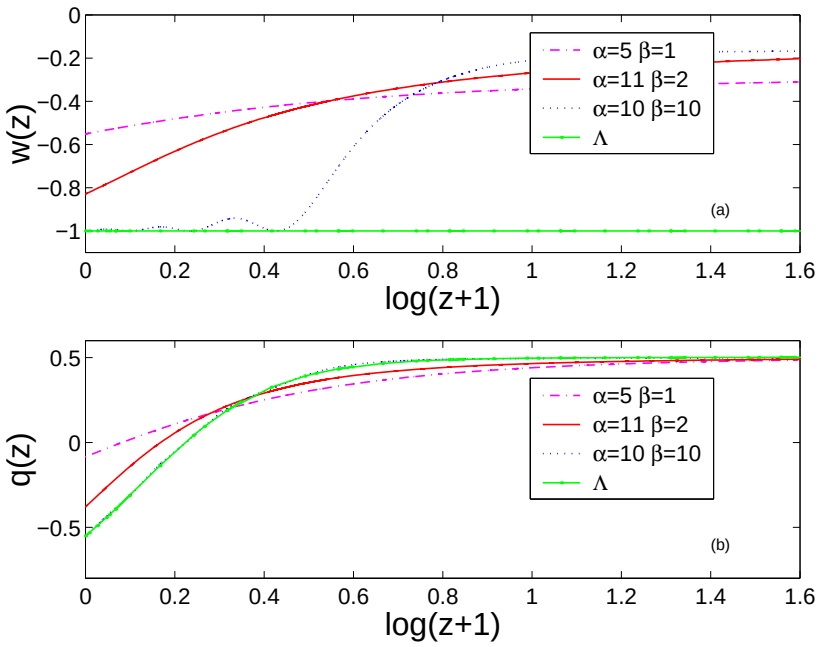

Figure 4.3: In (a) the evolution of w_Q against the red-shift is plotted for different values of α and β. In (b) the behaviour of the deceleration parameter, q, is plotted against the red-shift. The acceleration starts ($q < 0$) earlier for models with an equation of state close to that of a true cosmological constant.

and β (figure 4.3a). In these models the fractional energy density of the quintessence field, Ω_Q, is always negligible during both radiation and matter dominated eras. In fact, for small initial values of Q, $V(Q)$ acts like an inverse power law potential, hence as Q enters the scaling regime its energy density is subdominant compared to that of the background component. Therefore nucleosynthesis constraints [103] are always satisfied and there are no physical effects on the evolution of the density perturbations. The main consequence is that for a different value of w_Q^0 the Universe starts to accelerate at a different redshift (figure 4.3b). This implies that different values of α and β lead to a different luminosity distance and angular diameter distance. Consequently by making use of the observed distances we may in principle determine an upper limit on w_Q^0, potentially constraining the allowed shape of the quintessence potential [120].

4.3 CMB peaks

The CMB power spectrum provides information on combinations of fundamental cosmological parameters. The physical processes responsible for the anisotropy are well under-

stood allowing us to accurately predict the shape of the anisotropy power spectrum for a given cosmological model. The presence of acoustic oscillations of the photon-baryon plasma before the recombination epoch establishes a multiple peaks pattern in the power spectrum. For a review of the subject we refer to [121]. During the radiation dominated era the equation describing the effective temperature fluctuation ΔT of the CMB is of the form [122]:

$$\Delta T'' + c_s^2 \Delta T = 2\Psi'', \tag{4.5}$$

where Ψ is the gravitational potential sourced by the energy density perturbations in the different matter components, $c_s^2 = 1/3(1 + 3\rho_b/\rho_r)$ is the sound speed of the barotropic fluid and the primes are derivatives with respect to $k\tau$, τ being the conformal time and k the comoving wavenumber. Eq. (4.5) has the form of a perturbed harmonic oscillator, therefore when the photons decouple from the baryons their energy carries an imprint of such oscillations. The characteristic frequency of these oscillations is fixed by the size of the sound horizon at the decoupling $r_{sh} = \int c_s d\tau$. Therefore we have a series of compressions and rarefactions at scales $k_m r_{sh} = m\pi$. Today such scales appear at angles that are multiple integers of the angular size of the sound horizon at the decoupling $\theta_{sh} = r_{sh}/D_\kappa(\tau_{ls})$, where $D_\kappa(\tau_{ls})$ is the distance to the last scattering surface for a space-time with curvature κ. As a consequence of these the position of the 'Doppler' peaks in the power spectrum depends on the geometry of the Universe. For a flat Universe the peaks will appear at the multipoles

$$l_m = m l_{sh} = m \frac{\pi}{\bar{c}_s} \left(\frac{\tau_0}{\tau_{ls}} - 1 \right), \tag{4.6}$$

where $\bar{c}_s$ is the mean sound speed and τ_0, τ_{ls} are the conformal time today and at last scattering respectively. However the acoustic oscillations are perturbed by the evolution of the gravitational potential Ψ on the right-hand-side of Eq. (4.5), which shifts the position of the peaks by an amount that depends on the cosmological parameters that are relevant before the recombination. This results in a better estimate for the peak positions being given by:

$$l_m = l_{sh}(m - \delta l - \delta l_m), \tag{4.7}$$

where δl is an overall shift [122] and δl_m is the shift of the m-th peak. These corrections depend on the amount of baryons $\Omega_b h^2$, on the fractional quintessence energy density at last scattering (Ω_Q^{ls}) and today (Ω_Q^0), as well as on the scalar spectral index n. Analytic

formulae, valid over a large range of the cosmological parameters, have been provided to good accuracy for δl and δl_m [123]. Of crucial importance is the observation that the position of the third peak appears to remain insensitive to other cosmological quantities. This is because at small scales, well inside the horizon, Ψ is usually negligible, hence we recover the unperturbed harmonic oscillator equation for Eq. (4.5) that describes oscillations with zero point offset. Hence we can make use of this fact to test dark energy models [124, 125]. As we shall discuss in more detail in Chapter 6, the quintessence field can leave a distinctive signature on the shape of the CMB power spectrum through both the early integrated Sachs-Wolfe effect (ISW) and the late one [126]. The former is important if the dark energy contribution at the last scattering surface is not negligible [100,118] or in non-minimally coupled models [82, 127, 128], whereas the late ISW is the only effect in models with $\Omega_Q^{ls} \sim 0$ such as those described by our parameterized quintessence potential [129]. However the late ISW produces an imprint on the CMB power spectrum of the order of 10% and therefore is not detectable with the pre-WMAP measurements. In such a case an accurate determination of the position of the Doppler peaks is more sensitive to the actual amount of dark energy.

4.4 Likelihood analysis and results

4.4.1 Constraints from supernovae

We want to constrain the set of parameters α, β and Ω_Q confined in the range: $\alpha \in (1, 10)$, $\beta \in (0, 10)$ and $\Omega_Q \in (0, 1)$, subject to the assumption of a flat universe. This choice of the parameters allows us to account for a large number of models. We use the Sn Ia data fit C of Perlmutter *et al.* (1999) [53], that excludes 4 high redshift data points, which are very likely reddened by their host galaxies. The magnitude-redshift relation is given by:

$$m(z) = 5 \log D_L(z, \alpha, \beta, \Omega_Q) + \mathscr{M}, \tag{4.8}$$

where $\mathscr{M}$ is the 'Hubble constant free' absolute magnitude and $D_L(z) = H_0 d_L(z)$ is the free-Hubble constant luminosity distance. In a flat universe

$$d_L(z) = (\tau_0 - \tau(z))(1 + z), \tag{4.9}$$

where τ_0 is the conformal time today and $\tau(z)$ is the conformal time at the red-shift z of the observed supernova. Both of these quantities are calculated solving numerically

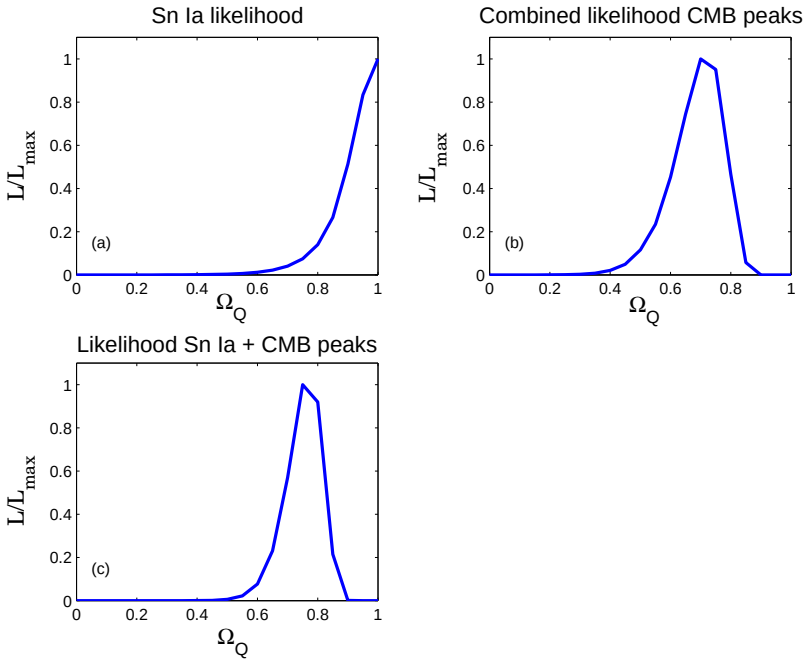

Figure 4.4: Fractional Quintessence energy density likelihoods, (a) for Sn Ia, (b) for the combined CMB peaks and (c) for the combined data sets.

Eq. (2.8) and Eq. (2.9) for each value of α, β and Ω_Q. In $\mathscr{M}$ we neglect the dependence on a fifth parameter (α in [53]) and assume it to be 0.6, the best fit value in [53]. We then obtain a gaussian likelihood function $\mathscr{L}^{Sn}(\alpha, \beta, \Omega_Q)$, by marginalizing over $\mathscr{M}$. In figure 4.4a we present the one-dimensional likelihood function normalized to its maximum value for Ω_Q. When considering only Sn Ia data, there is a maximum at $\Omega_Q = 1$, such a high value of Ω_Q is required if we impose the constraint $\Omega_k = 0$ and it is in agreement with the analysis in [130]. In figure 4.5a we present the likelihood contours in the $\alpha - \beta$ parameter space, obtained after marginalizing over Ω_Q. Note that all values are allowed at the 2σ level. The confidence regions for the Sn Ia data correspond to Quintessence models with $w_Q^0 < -0.4$ for $\Omega_Q = 0.6$, an upper limit that agrees with those found in [53, 114].

4.4.2 Constraints from Doppler peaks and Sn Ia

We now compute the position of the three Doppler peaks l_1, l_2 and l_3 using Eq. (4.7). In addition to the parameter space used in the supernovae analysis we consider the physical baryon density and the scalar spectral index varying respectively in the range $\Omega_b h^2 \in (0.018, 0.026)$ and $n \in (0.9, 1.1)$. The Hubble constant is set to $h = 0.70$ in agreement with the recent HST observations [29]. It is worth remarking that the baryons density and

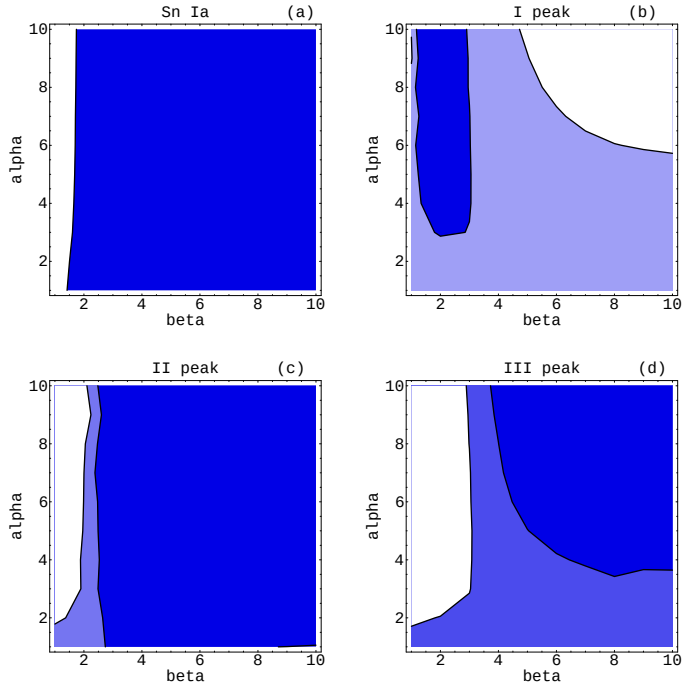

Figure 4.5: Likelihood contour plots for Sn Ia, I, II and III acoustic peaks. The blue region is the 68% confidence region while the 90% is the light blue one. For the Sn Ia the white region correspond to 2σ. The position of the third CMB acoustic peak strongly constrains the acceptable parameter space.

H_0 are degenerate with the quintessence parameters. In fact increasing $\Omega_b h^2$ reduces the value of c_s causing a shift of the CMB peaks towards large multipoles. The same effect occurs for low values of the Hubble constant, therefore the results of this analysis will depend on the HST prior. The predicted peak multipoles are then compared with those measured in the Boomerang and DASI spectra [131]. Note, that the third peak has been detected in the Boomerang data but not in the DASI data. In table 4.1 we report the position of the peaks with 1σ errors estimated from the Boomerang, DASI and WMAP data with a model independent analysis. Since the errors are non Gaussian (see also [132]), to be conservative we take our 1σ errors on the data to be larger than those reported in [131], so that our analysis is significant up to 2σ. We then evaluate a gaussian likelihood function $\mathscr{L}^{Peaks}(\alpha, \beta, \Omega_Q, \Omega_b h^2, n)$. The combined one-dimensional likelihood function for the peaks is shown in figure 4.4b, where we find $\Omega_Q = 0.69 \pm^{0.13}_{0.10}$. The likelihood for all the data sets combined is shown in figure 4.4c, where we find $\Omega_Q = 0.75 \pm^{0.09}_{0.08}$. These results are in agreement with the analysis in [21, 133, 148]. The likelihood functions,

Peak	Boomerang	DASI	WMAP
l_1	213^{+10}_{-13}	202 ± 15	220.1 ± 0.8
l_2	541^{+20}_{-32}	548 ± 10	546 ± 10
l_3	845^{+12}_{-25}	-	-

Table 4.1: Location of the CMB peaks inferred from the power spectrum of Boomerang and MAXIMA data using a model independent procedure (from [131]).

combining all the CMB peaks data, for the scalar spectral index and the physical baryon density are shown in figure 4.6. Since the dependence of the peak multipoles on $\Omega_b h^2$ and n is weak, it is not possible to obtain some significant constraints on these cosmological parameters. In figure 4.5b-4.5d we plot the two-dimensional likelihood function in the plane $\alpha - \beta$ for each peak, obtained after having marginalized over Ω_Q, $\Omega_b h^2$ and n. Their shape reflects the accuracy in the estimation of the position of the peaks. Actually the first one is very well resolved, while we are less confident with the location of the second and third peak. Therefore their likelihoods are more spread and flat in the $\alpha - \beta$ plane. The 1σ confidence contour (figure 4.5b) for the first acoustic peak constrains the slopes of our potential in the range: $3 \leq \alpha \leq 10$ and $1 \leq \beta \leq 3$. In particular the likelihood has a maximum at $\alpha = 9$ and $\beta = 2$, corresponding to an equation of state $w_Q^0 = -0.8$ for $\Omega_Q = 0.7$, in agreement with the recent analysis in [133]. However, the second and third peaks constrain a complementary region where the equation of state is compatible with the cosmological constant value. Therefore the effect of including all the data in the likelihood analysis is to move the constraint from models with $w_Q^0 \sim -0.8$ to models with an equation of state $w_Q^0 \sim -1$. The constraints on the slopes of the quintessence potential allows us to infer an upper limit on the present value of the equation of state only after having fixed the value of Ω_Q. In fact the scalar field potential Eq. (4.4) is fully specified by three numbers that are M, α, β. However the map $(M, \alpha, \beta) \rightarrow w_Q^0$ is not one-to-one and therefore it is not possible to transform the likelihood $\mathscr{L}(\alpha, \beta, \Omega_Q) \rightarrow \mathscr{L}(w_Q^0, \Omega_Q)$. Therefore there is a substantial difference between inferring the bounds on the dark energy equation of state by directly constraining its present value and constraining the scalar field potential. As we can see in figure 4.8 the values of α and β, allowed by the likelihood

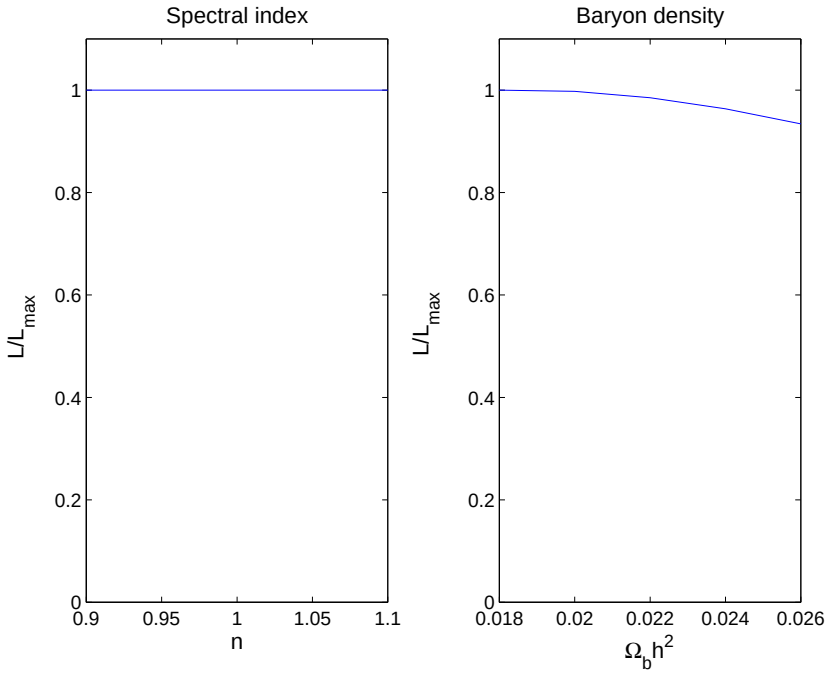

Figure 4.6: One-dimensional likelihood for n and $\Omega_b h^2$.

including all the data (figure 4.7), correspond to our models with values of w_Q^0 in the range $-1 \leq w_Q^0 \leq 0.93$ at 2σ for our prior probability $\Omega_Q = 0.75$. Assuming smaller values of Ω_Q relaxes the constraints on w_Q^0, for instance for $\Omega_Q = 0.5$ we have $-1 \leq w_Q^0 \leq -0.6$ at 2σ. The results of our analysis can be interpreted as follows. At the 1σ level the position of the first peak is inconsistent with the position of the other two. A possible explanation of this discrepancy is that the multipoles l_2 and l_3 are less sensitive to small shifts induced by the dependence on $\Omega_b h^2$ and n. Therefore we can obtain a different constraint on the dark energy equation of state if we consider the peaks individually. It is worth remarking that the position of the first peak in the Boomerang data prefers slightly spatially closed models. Having assumed a flat geometry affects our upper bounds on the slope of the potential in a region corresponding to $w_Q^0 > -1$. On the other hand the location of the third peak inferred in [131], is at $l_3 = 845 \pm^{12}_{23}$, for which values of $w_Q^0 \sim -1$ fit this multipole better than models with $w_Q^0 > -1$. In fact the peaks are shifted toward larger multipoles as w_Q^0 approaches the cosmological constant value. This is because, in models with $w_Q^0 \sim -1$ the Universe starts to accelerate earlier than in those with $w_Q^0 > -1$, consequently the distance to the last scattering surface is farther and hence the sound horizon at the decoupling is projected onto smaller angular scales. A possible source of bias in our analysis is due to the prior on the value of H_0, in fact assuming $h = 0.70$

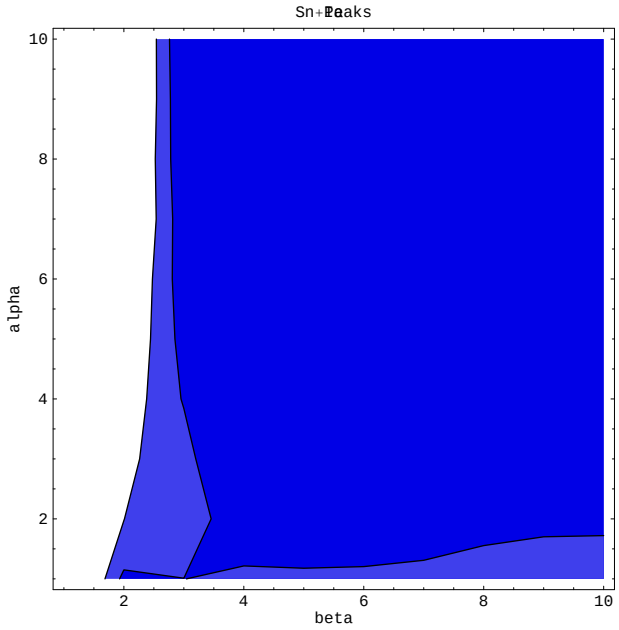

Figure 4.7: Two-dimensional likelihood for Sn Ia and CMB with 1 (dark blue) and 2σ (light blue) contours.

implies that models with a large negative equation of state and large value of Ω_Q are preferred. However our results are consistent with other studies which assume similar priors. For instance in [133], using the complete set of available CMB measurements the slope of the Inverse Power Law potential has been constrained to be $\alpha = 0.8 \pm^{0.6}_{0.5}$ under the prior $h = 0.65$, corresponding to $w_Q^0 = -0.82 \pm^{0.14}_{0.11}$. Similarly in [134], by making use of the CMB, Sn Ia and large scale structure data, it has been found $w_Q \leq -0.85$ for a constant equation of state. A time dependent dark energy equation of state, characterized by a late time transition, has been constrained using all cosmological data in [135], where it has been found $w_Q^0 = -1^{+0.2}$.

4.5 Discussion

The analysis of Sn Ia data and the location of the CMB peaks in Boomerang and DASI data constrain the slope of a general quintessence potential in a range of values such that the quintessence field is undergoing small damped oscillations around a minimum of the potential (see figure 4.3). Such a situation implies that the value of the quintessence equation of state has to be very close to -1. However this does not imply that the dark energy is the cosmological constant. What our result means is that the quintessence

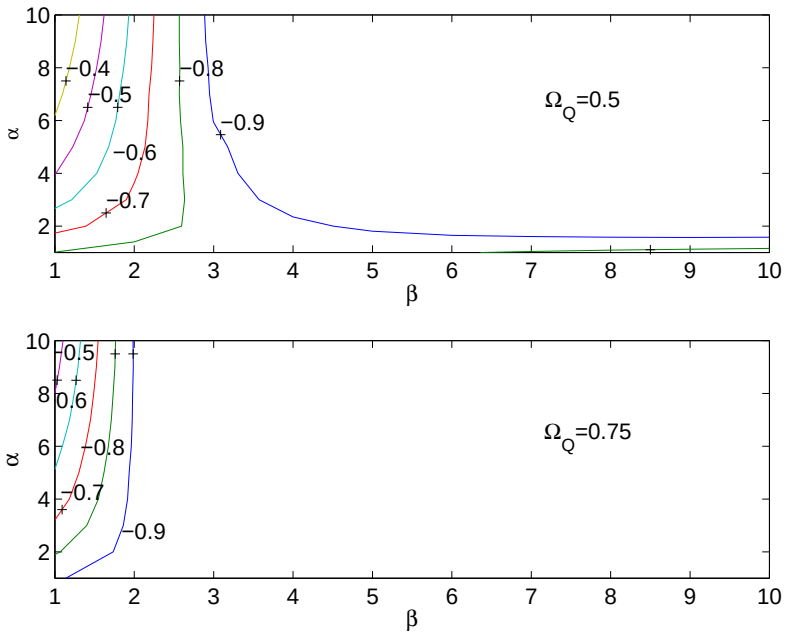

Figure 4.8: Contour values of w_Q^0 in the $\alpha - \beta$ plane for $\Omega_Q = 0.5$ (upper panel) and $\Omega_Q = 0.75$ (upper panel).

field today is evolving in a nearly vacuum state. In fact models where the scalar field is rolling down a very flat region of the potential can fit the data and pass the constraints even though they are not included in our analysis. Another important caveat is that this study does not take into account quintessence scenarios where the contribution of the dark energy is not negligible. In such a case we would have to take into account physical effects not only on distance measurements, but on the structure formation process itself (see for instance [104, 136]). These effects however are not detectable with the level of accuracy provided by the recent balloon and ground CMB experiments. A revised analysis of the Boomerang data has been recently published in [22], the position of the peaks has been determined with a better accuracy, in particular the third peak is shifted at a smaller multipole than previously detected. This slightly changes our results, relaxing the lower bounds on the slope β. Here we want to stress the fact that it seems likely the present value of the dark energy equation of state is close to -1. However the possibility that the equation of state was largely different from -1 cannot be excluded, as it is shown by the class of models that best fit the Sn Ia data and the CMB peaks. The new generation of satellite experiments we will probably be able to detect the specific effects produced by a time varying dark energy component.

Chapter 5

A model independent approach to the dark energy equation of state

The detection of time variation in the dark energy equation of state can be considered as the 'smoking gun' for the cosmological constant scenario. The new generation of experiments in cosmology will provide high precision measurements that in principle can discriminate between different dark energy candidates. On the other hand it is unrealistic to assume we can infer some general information constraining some particular quintessence model. In fact a plethora of scalar field potentials have been proposed, all leading to similar late time behaviour of the universe, hence to a lack of predictability. In this Chapter, we first review some of the methods that have been proposed in the literature to constrain the time features of a general quintessence component. We then introduce a model independent approach which simply involves parameterizing the dark energy equation of state in terms of known observables [137]. This allows us to analyse the impact dark energy has had on cosmology without the need to refer to particular scalar field models and opens up the possibility that future experiments will be able to constrain the dark energy equation of state in a model independent manner.

5.1 The effective equation of state

Measuring the present value of the dark energy equation of state can distinguish between a cosmological constant scenario and a quintessential component if $w_Q^0 > -1$. Using the tracker properties of the quintessence field, the most reliable method to infer a bound

$\Lambda^{4+\alpha}/Q^{\alpha}$	[73]	$\Lambda^4 e^{-\lambda Q}$	[77]
$(\Lambda^{4+\alpha}/Q^{\alpha})e^{\frac{\kappa}{2}Q^2}$	[96]	$\Lambda^4(\cosh\lambda Q-1)^p$	[138]
$\Lambda^4(e^{\alpha\kappa Q}+e^{\beta\kappa Q})$	[100]	$\Lambda^4 e^{-\lambda Q}(1+A\sin\nu Q)$	[139]
$\Lambda^4[(Q-B)^{\alpha}+A]e^{-\lambda Q}$	[118]	$\Lambda^4[1+\cos(Q/f)]$	[74]
$\Lambda^4\left(\frac{1}{Q^{\alpha}}+\frac{1}{Q^{\beta}}\right)$	[80]	$\Lambda^4(e^{1/Q}-1)$	[79]

Table 5.1: Quintessence potentials that have been used in the litterature.

on w_Q^0 would be to constrain directly the quintessence potential. However this could result in a difficult challenge, for instance in Table 5.1 we show a list of proposed tracker quintessence potentials. Therefore, because there are no fundamental physical principles that can specify the nature of the dark energy, we are left with a potentially infinite set of families of theoretical models to compare with the data. As a consequence of this it is to be hoped that a more general way of constraining the dark energy can be developed. A simple method to take into account a large number of dark energy models is to consider a constant effective equation of state defined by Eq. (4.3). Using the energy conservation equation, the redshift evolution of the dark energy density is given by

$$\rho_{de}(z)=\rho_{de}^0(1+z)^{3(1+w_{eff})}. \tag{5.1}$$

The effective equation of state appears through the Hubble equation in the coordinate distance defined by:

$$r(z)=\frac{1}{H_0}\int_0^z\frac{dz'}{\sqrt{\Omega_m(1+z')^3+\Omega_r(1+z')^4+\Omega_{de}(1+z')^{3(1+w_{eff})}}}. \tag{5.2}$$

Hence the value of w_{eff} can be constrained by measurements of the luminosity distance and the angular diameter distance, that in a flat space-time read as $d_L(z)=(1+z)r(z)$ and $d_A(z)=r(z)/(1+z)$ respectively. There is a general consensus that an accurate determination of d_L from high redshift Sn Ia measurements with the proposed SNAP satellite [140] can determine w_{eff} to better than 5 per cent [141]. In such a case if w_{eff} is much larger than -1 it will be possible to rule out the ΛCDM model. However if $w_{eff}\approx -1$ the results of the data analysis have to be carefully considered. In fact it has

been shown by Maor *et al.* [142] that assuming a constant w_{eff} introduces a bias that leads to misleading conclusions about the properties of the dark energy. In order to make this point clear, let us consider a sample of mock data generated from a dark energy model with an equation of state of the form

$$w_Q(z) = w_0 + w_1 z, \tag{5.3}$$

with $w_0 < -1/3$ and $w_1 > 0$. The constraints on a constant equation of state w_{eff} obtained from the statistical analysis of such a sample, will push the bounds towards values of $w_{eff} < w_0$. This effect has been noticed also in other works, see for instance [145, 146] and can be explained as follows. For a model with w_Q given by Eq. (5.3) the energy density evolves as:

$$\rho_{de}(z) = \rho^0_{de}(1+z)^{3(w_0-w_1+1)} exp\left[\frac{3w_1 z}{1+z}\right]. \tag{5.4}$$

As we may note, comparing Eq. (5.1) with Eq. (5.4), if $w_0 < 0$ and $w_1 > 0$, fitting the data with a constant equation of state roughly requires $w_{eff} \approx w_0 - w_1 < w_0$. In other words the fitting procedure will pick out values of w_0 that are more negative than the fiducial one. Hence a time varying dark energy component can be confused with a cosmological constant, while allowing w_{eff} to vary in a range of values more negative than -1, will shift the best fit models towards $w_{eff} < -1$. Therefore it is very possible that the claims for the existence of *phantom* matter (with $w_Q < -1$) [143, 144] are just a consequence of assuming a constant equation of state in the data analysis.

5.2 Cosmological distance fitting functions

Several methods to constrain the time dependence of the dark energy equation of state have been discussed in the literature [115, 145–153]. Since the dark energy became dominant only recently, it is reasonable to concentrate on local redshift measurements, such as the Sn Ia. The coordinate distance and the Hubble parameter are uniquely related by $H(z) = (dr/dz)^{-1}$. Thus we can estimate $r(z)$ from cosmological distance indicators and unambiguously calculate $H(z)$ and dH/dz. This allows us to reconstruct $w(z)$ provided the value of Ω_m is given. In fact the Hubble equations in the presence of matter and a scalar field are:

$$H^2 = \frac{8\pi G}{3}\left[\rho_m + \frac{1}{2}\dot{Q}^2 + V(Q)\right] \tag{5.5}$$

and

$$\dot{H} = -4\pi G(\rho_m + \dot{Q}^2), \tag{5.6}$$

where the dot is the derivative with respect to the time. These equations can be rewritten in the form:

$$\frac{8\pi G}{3H_0^2}V(x) = \frac{H^2}{H_0^2} - \frac{x}{6H_0^2}\left(\frac{dH}{dx}\right)^2 - \frac{1}{2}\Omega_m x^3, \tag{5.7}$$

$$\frac{8\pi G}{3H_0^2}\left(\frac{dQ}{dx}\right)^2 = \frac{2}{3H_0^2 x} - \frac{\Omega_m x}{H^2}, \tag{5.8}$$

where $x = 1 + z$. Using the definition of the scalar field equation of state we find:

$$w(z) = \frac{\frac{2x}{3}\frac{dlnH}{dx} - 1}{1 - \frac{H^2}{H_0^2}\Omega_m x^3}. \tag{5.9}$$

The idea is then to introduce a fitting function for the coordinate distance, so that once its parameters have been determined from the data analysis, its first and second derivatives with respect to the redshift can be analytically calculated. The authors of [115] suggest

$$r^{fit}(z) = \frac{2}{H_0}\left[\frac{x - \alpha\sqrt{x} - 1 + \alpha}{\beta x + \gamma\sqrt{x} + 2 - \alpha - \beta - \gamma}\right], \tag{5.10}$$

where α, β and γ are fitting parameters, while Huterer & Turner [147] consider both a polynomial fitting function

$$r^{fit}(z) = \sum_i c_i z^i \tag{5.11}$$

and a Pade' approximate

$$r^{fit}(z) = \frac{z(1 + az)}{1 + bz + cz^2}. \tag{5.12}$$

It has been pointed out in [146] that such a general method fails to accurately reproduce the correct behaviour of given scalar field models, even assuming strong priors on the value of Ω_m. The difficulty arises because the formula Eq. (5.9) depends on the derivatives of $r(z)$. Therefore even though $r^{fit}(z)$ can mimic the $r(z)$ of a specific model, this may be not true for its derivatives.

5.3 *Statefinder* method

A different approach has been developed by Sahni *et al.* [154,155]. They suggest a method to distinguish amongst different dark energy scenarios by measuring geometrical parameters that are constructed in such a way they are more sensitive to the expansion rate of the Universe. Such parameters, called *Statefinder* pair, are defined by:

$$r = \frac{\dddot{a}}{aH^3}, s = \frac{r-1}{3(q-1/2)}. \tag{5.13}$$

For a flat Universe the relation to the dark energy equation of state w and its time derivative $\dot{w}$ is:

$$r = 1 + \frac{9}{2}\Omega_{de} w(1+w) - \frac{3}{2}\Omega_{de}\frac{\dot{w}}{H}, \tag{5.14}$$

$$s = 1 + w - \frac{1}{3}\frac{\dot{w}}{wH}, \tag{5.15}$$

where H is the Hubble parameter. In general the value of such parameters evolves with the time, but for the cosmological constant ($w = -1$) we have $(r, s) = (1, 0)$ at all the times. Moreover, since (r, s) are geometrical quantities, they can naturally take into account braneworld models in which the accelerated expansion is caused by five dimensional gravity effects and which lead to modifications of the Hubble equations. The Statefinder pair can be estimated using the following ansatz for the Hubble parameter,

$$H(x) = H_0 \left[\Omega_m x^3 + A_1 + A_2 x + A_3 x^2\right]^{\frac{1}{2}}, \tag{5.16}$$

where $x = 1 + z$, and $A_1 + A_2 + A_3 = 1 - \Omega_m$. In such a case (r, s) are of the form:

$$r = 1 - \frac{A_1 + \Omega_m x^3}{\Omega_m x^3 + A_1 + A_2 x + A_3 x^2}, \tag{5.17}$$

$$s = \frac{2(A_2 x + A_3 x^2)}{3(3A_1 + 2A_2 x + A_3 x^2)}. \tag{5.18}$$

The value of the fitting parameters A_i can be inferred from a likelihood analysis of cosmological distance measurements, such as the Sn Ia. From Eq. (5.17) it appears obvious that an accurate estimation of r needs a precise knowledge of the amount of non-relativistic matter. In [155] it has been shown that imposing a Gaussian prior probability distribution on Ω_m with variance $\sigma_{\Omega_m} = 0.05$, the high redshift Sn Ia measurements provided by the proposed SNAP satellite will accurately determine the Statefinder pair offering the chance to distinguish between different dark energy models. Therefore the Statefinder method

seems to be highly sensitive to the nature of dark energy and avoids the main difficulties of the reconstructing procedure. In fact it only needs to constrain fitting parameters that appear in the Hubble equation and does not constrain directly the equation of state that affects the expansion rate apart from through a time integrated effect. A potential limitation of such an approach is that the determined values of (r, s) do not give us any information about the physical properties of the dark energy, unless their values are *a priori* known for specific classes of models.

5.4 Low redshift parameterization

In the absence of theoretically motivated dark energy models we can consider a low redshift expansion for $w_Q(z)$ and the parameters of such an expansion can be interpreted as fundamental dark energy parameters. Therefore the constraints on a parameterization of the equation of state would provide a model independent determination of the dark energy properties. Such a parameterization should satisfy the following requirements:

- it should depend on a minimal number of parameters θ_i that specify the physical properties of the dark energy;
- the functional form of the parameterization has to be such that for a given set $(\tilde{\theta}_i)$ the behavior of the equation of state $w_Q(z, \tilde{\theta})$ reproduces the $w(z)$ predicted by proposed quintessence models and can account also for more general cases.

In [146, 148] it was suggested the use of a logarithmic expansion,

$$w_Q^p(z) = w_0 - \alpha \log(1 + z), \tag{5.19}$$

while the authors of [145, 151, 153] used a polynomial fitting function,

$$w_Q^p = \sum_i c_i z^i. \tag{5.20}$$

The general drawback of using a redshift expansion formula for the dark energy equation of state is that the number of fitting parameters is now larger than assuming a simple time constant behaviours and consequently the degeneracy in the dark energy parameter space is enlarged. In fact the coordinate distance is related by a multi-integral expression to the equation of state and therefore widely different $w(z, \theta_i)$ can have the same multi-integral value. There is a general consensus that assuming strong priors on the value of

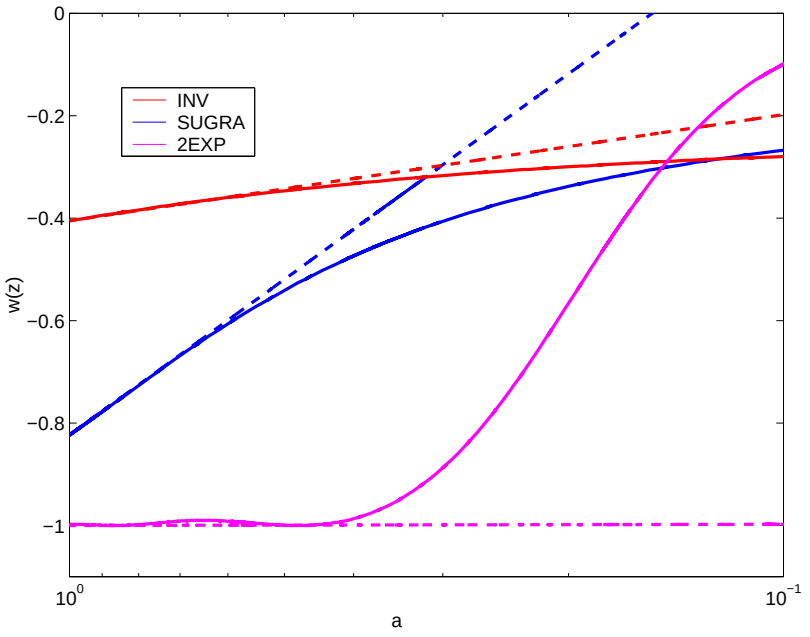

Figure 5.1: Low redshift approximation to the quitenssence equation of state for different types of potentials: Inverse Power Law (red), Inverse Power Law times Exponential (blue) and Two Exponential (magenta). The solid line corresponds to the exact numerical solution of the Klein-Gordon equation, while the dash line is the approximated behaviour provided by Eq.(5.19).

Ω_m it will be possible to tightly constrain $w_0 = \theta_1$, but it will be more difficult to put tight bounds on the other parameters. The solution would be to combine different data sets that can break the degeneracy in the parameter space. The expansions specified by Eq. (5.19) and Eq. (5.20) both have limited applicability. For instance Eq. (5.19) can take into account only for quintessence models with slowly varying behaviours and breaks down at large redshifts, as we can see in figure 5.1. On the other hand the polynomial expansion Eq. (5.20) introduces a number of unphysical parameters whose values are not directly related to the properties of a dark energy fluid. The consequence is that, unless we pay the cost of considering very unphysical values, their application is limited to low redshift measurements and cannot be extended to the analysis of high redshift data sets such as the CMB data. An interesting alternative to the fitting expansion approach, has recently been proposed in [156]. The authors of this study developed a method to reconstruct the time behavior of the equation of state from cosmological distance measurements without assuming the form of its parameterization. In spite of the efficiency of such an approach,

it does not take into account the effects of the possible clustering properties of dark energy which become manifest at higher redshifts. Hence its application has to be limited to the effects dark energy can produce on the expansion rate of the universe at low redshifts. On the other hand, it has been argued that dark energy does not leave a detectable imprint at higher redshifts, since it has only recently become the dominant component of the universe. Such a statement, however, is model dependent, on the face of it there is no reason why the dark energy should be negligible deep in the matter dominated era. For instance CMB observations constrain the dark energy density at decoupling to be less then 10 per cent of the critical one [104]. Such a non negligible contribution can be realized in a large class of models and therefore cannot be *a priori* excluded. Consequently it is of crucial importance to find an appropriate parameterization for the dark energy equation of state that allows us to take into account the full impact dark energy has on different types of cosmological observations.

5.5 An exact parameterization for the dark energy equation of state

Our goal is to determine an appropriate analytical form of the equation of state $w_Q^p(a)$ valid at all redshifts in terms of physical quantities, so that it can describe a general fluid and take into account most of the proposed dark energy models. In Chapter 2 we have seen that the specific evolution of $w_Q(a)$, depends on the shape of the potential, however there are some common features in its behaviour that can be described in a model independent manner and which allow us to introduce some physical parameters. As we have seen in Chapter 2 a large number of quintessence models are characterized by the existence of the 'tracker regime'. It consists of a period during which the scalar field, while it is approaching a late time attractor, evolves with an almost constant equation of state whose value can track that of the background component. Here we consider a broad class of tracking potentials. These include models for which $w_Q(a)$ evolves smoothly, as with the inverse power law [73], $V(Q) \sim 1/Q^\alpha$ (INV) and the supergravity inspired potential [96], $V(Q) \sim 1/Q^\alpha e^{Q^2/2}$ (SUGRA). Late time rapidly varying equation of states arise in potentials with two exponential functions [100], $V \sim e^{-\alpha Q} + e^{\beta Q}$ (2EXP), in the so called 'Albrecht & Skordis' model [118] (AS) and in the model proposed by Copeland et al. [101] (CNR). To show this in more detail, in figure 5.2 we plot the equation of state

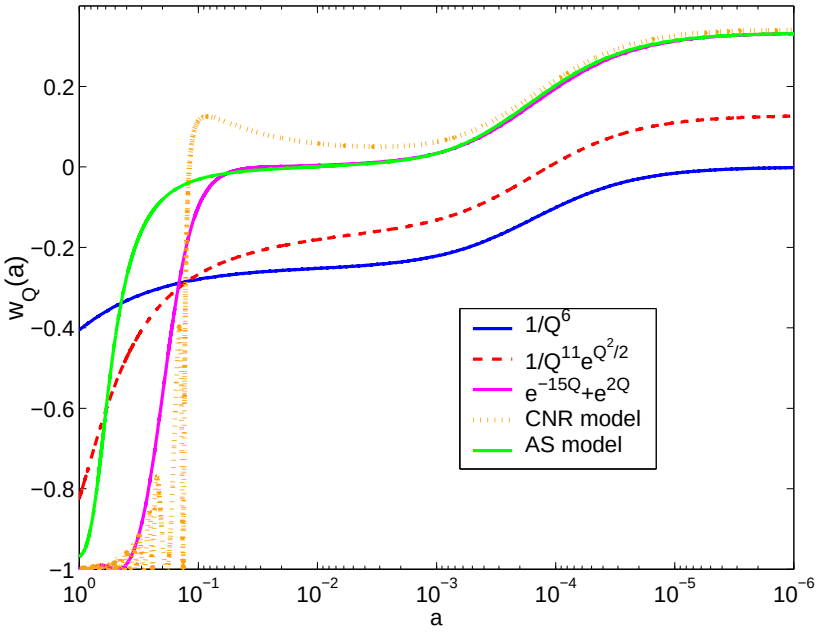

Figure 5.2: Evolution of w_Q against the scale factor for an Inverse Power Law model (solid blue line), SUGRA model ([96]) (dash red line), two exponential potential model ([100]) (solid magenta line), AS model ([118]) (solid green line) and CNR model ([101]) (dot orange line).

obtained by solving numerically for each of these potentials the scalar field equation of motion defined by Eq. (2.8) and Eq. (2.9).

There are some generic features that appear to be present, and which we can make use of in our attempts to parameterize w_Q. For a large range of initial conditions of the quintessence field, the tracking phase starts before matter-radiation equality. In such a scenario $w_Q(a)$ has three distinct phases, separated by two 'phase transitions'. Deep into both the radiation and matter dominated eras the equation of state, $w_Q(a)$, takes on the values w_Q^r and w_Q^m respectively, values that are related to the equation of state of the background component w_B through:

$$w_Q \approx \frac{w_B - 2(\Gamma - 1)}{2\Gamma - 1}, \tag{5.21}$$

where $\Gamma = V''V/(V')^2$ and $V' \equiv dV/dQ$ etc. For the case of an exponential potential, $\Gamma = 1$, with $w_Q = w_B$, but in general $w_Q \neq w_B$. Therefore if we do not specify the quintessence potential the values of w_Q^r and w_Q^m should be considered as free parameters. The two transition phases can each be described by two parameters; the value of the scale factor $a_c^{r,m}$ when the equation of state w_Q begins to change and the width $\Delta_{r,m}$ of the

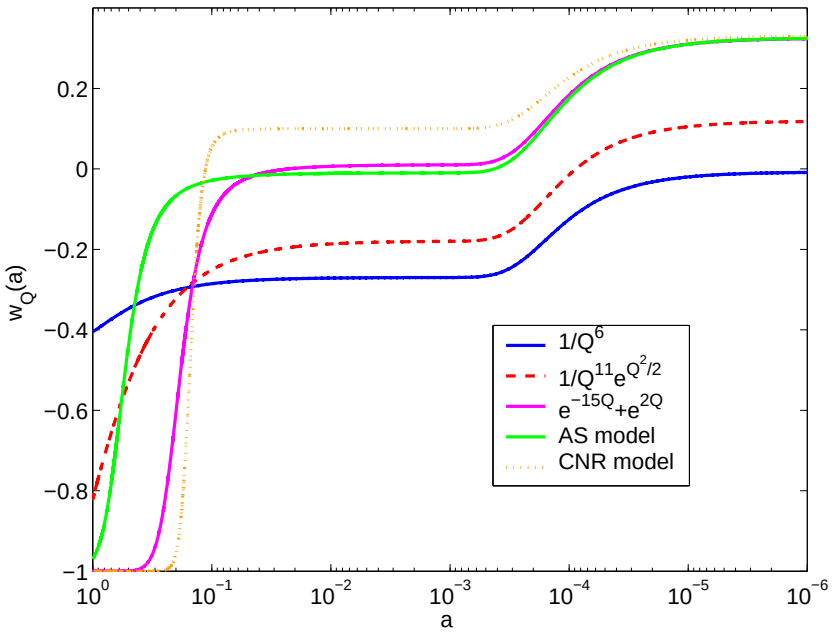

Figure 5.3: Plot of $w_Q^p(a)$ (Eq. 5.22) best fit for different potentials.

transition. Since Γ is constant or slowly varying during the tracker regime, the transition from w_Q^r to w_Q^m is always smooth and is similar for all the models (see figure 5.2). To be more precise, we have found that $a_c^r \sim 10^{-5}$ and $\Delta_r \sim 10^{-4}$ during this transition, the former number expected from the time of matter-radiation equality and the latter from the transition period from radiation to matter domination. However, when considering the transition in w_Q from w_Q^m to the present day value w_Q^0, we see from figure 5.2 that this can be slow ($0 < a_c^m/\Delta_m < 1$) or rapid ($a_c^m/\Delta_m > 1$) according to the slope of the quintessence potential. For instance in models with a steep slope followed by a flat region or by a minimum, as in the case of the two exponentials, the AS potential or the CNR model, the scalar field evolves towards a solution that approaches the late time attractor, finally deviating from the tracking regime with the parameter Γ rapidly varying. In contrast the inverse power law potential always has a slower transition since Γ is constant for all times. Given these general features we conclude that the behavior of $w_Q(a)$ can be explained in terms of functions, $w_Q^p(a)$, involving the following parameters: w_Q^0, w_Q^m, w_Q^r, a_c^m and Δ_m. The authors of [135] have recently used an expansion in terms of a Fermi-Dirac function in order to constrain a class of dark energy models with rapid late time transitions.

In what follows we find that a generalisation of this involving a linear combination of such functions allows for a wider range of models to be investigated. To be more precise,

	w_Q^0	w_Q^m	w_Q^r	a_c^m	Δ_m
INV	-0.40	-0.27	-0.02	0.18	0.5
SUGRA	-0.82	-0.18	0.10	0.1	0.7
2EXP	-1	0.01	0.31	0.19	0.043
AS	-0.96	-0.01	0.31	0.53	0.13
CNR	-1.0	0.1	0.32	0.15	0.016

Table 5.2: Best fit values of the parameters of the expansion (5.22).

we propose the following formula for $w_Q^p(a)$:

$$w_Q^p(a) = F_1 f_r(a) + F_2 f_m(a) + F_3, \tag{5.22}$$

with

$$f_{r,m}(a) = \frac{1}{1 + e^{-\frac{a - a_c^{r,m}}{\Delta_{r,m}}}}. \tag{5.23}$$

The coefficients F_1, F_2 and F_3 are determined by demanding that $w_Q^p(a)$ takes on the respective values w_Q^r, w_Q^m, w_Q^0 during radiation (a_r) and matter (a_m) domination as well as today (a_0). Solving the algebraic equations that follow we have:

$$F_1 = \frac{\left(w_Q^m - w_Q^r\right)\left(f_m(a_0) - f_m(a_r)\right) - \left(w_Q^0 - w_Q^r\right)\left(f_m(a_m) - f_m(a_r)\right)}{\left(f_r(a_m) - f_r(a_r)\right)\left(f_m(a_0) - f_m(a_r)\right) - \left(f_r(a_0) - f_r(a_r)\right)\left(f_m(a_m) - f_m(a_r)\right)}, \tag{5.24}$$

$$F_2 = \frac{w_Q^0 - w_Q^r}{f_m(a_0) - f_m(a_r)} - F_1 \frac{f_r(a_0) - f_r(a_r)}{f_m(a_0) - f_m(a_r)}, \tag{5.25}$$

$$F_3 = w_Q^r - F_1 f_r(a_r) - F_2 f_m(a_r), \tag{5.26}$$

where $a_0 = 1$, and the value of and a_r and a_m can be arbitrarily chosen in the radiation and matter era because of the almost constant nature of w_Q during those eras. For example in our simulations we assumed $a_r = 10^{-5}$ and $a_m = 10^{-3}$. In table 5.2 we present the best fit parameters obtained by minimizing a chi-square for the models we have considered and in figure 5.3 we plot the associated fitting functions $w_Q^p(a)$. It is encouraging to see how accurately the Fermi-Dirac functions mimic the exact time behavior of $w_Q(a)$ for the majority of the potentials.

In figure 5.4 we plot the absolute value of the difference $\Delta w(a)$ between $w_Q(a)$ and $w_Q^p(a)$. The discrepancy is less then 1% for redshifts $z < 10$ where the energy density of the dark energy can produce observable effects in these class of models and it remains below 9%

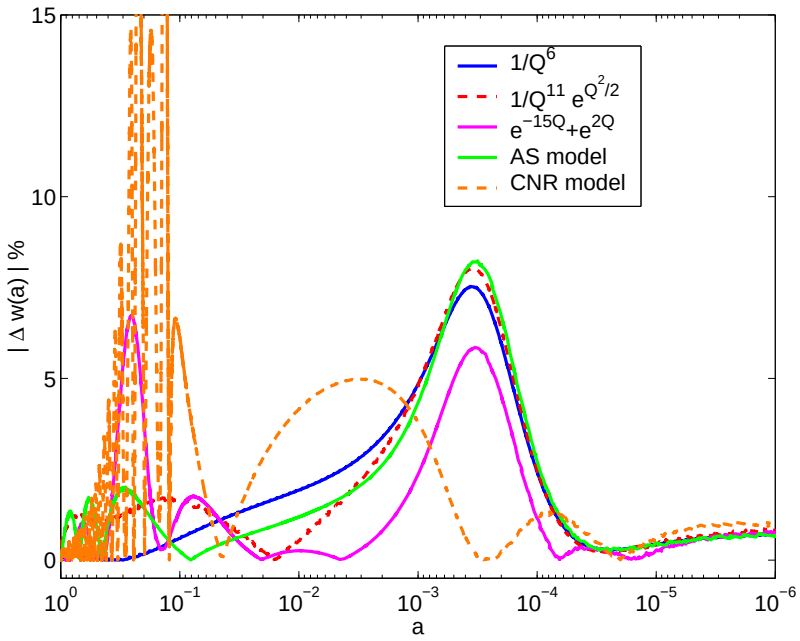

Figure 5.4: Absolute value of the difference between $w_Q(a)$ and $w_Q^p(a)$ for the models of figure 5.2.

between decoupling and matter-radiation equality. Only the CNR case is not accurately described by $w_Q^p(a)$ due to the high frequency oscillations of the scalar field which occur at low redshift as it fluctuates around the minimum of its potential. In fact these oscillations are not detectable, rather it is the time-average of $w_Q(a)$ which is seen in the cosmological observables, and can be described by the corresponding $w_Q^p(a)$. There are a number of impressive features that can be associated with the use of $w_Q^p(a)$ in Eq. (5.22). For instance it can mimic the behavior of more general models. As an example of this in figure 5.5 we plot $w_Q^p(a)$ that approximately corresponds to three cases: a K-essence model [157] (blue solid line); a rapid late time transition [158] (red dash-dot line) and finally one with an equation of state $w_Q^0 < -1$ (green dash line). The observational constraints on w_Q^0, w_Q^m, w_Q^r, a_c^m and Δ_m lead to constraints on a large number of dark energy models, but at the same time it provides us with model independent information on the evolution of the dark energy. It could be argued that the five dimensional parameter space we have introduced is too large to be reliably constrained. Fortunately this can be further reduced without losing any of the essential details arising out of tracker solutions in these Quintessence models. In fact nucleosynthesis places tight constraints on the allowed energy density of any dark energy component, generally forcing them to be negligible in the radiation

era [103, 159]. The real impact of dark energy occurs after matter-radiation equality, so we can set $w_Q^r = w_Q^m$. Consequently we end up with four parameters: w_Q^0, w_Q^m, a_c^m and Δ_m. Although they increase the already large parameter space of cosmology, they are necessary if we are to answer fundamental questions about the nature of the dark energy. The parameters make sense, if $w_Q(a)$ evolves in time, we need to know when it changed (a_c^m), how rapidly (Δ_m) and what its value was when it changed (w_Q^m). Neglecting the effects during the radiation dominated era it proves useful to provide a shorter version of Eq. (5.22), in fact since we can neglect the transition from radiation to matter dominated eras, then the linear combination Eq. (5.22) can be rewritten as [1]:

$$w_Q^p(a) = w_Q^0 + (w_Q^m - w_Q^0) \times \frac{1 + e^{\frac{a_c^m}{\Delta_m}}}{1 + e^{-\frac{a - a_c^m}{\Delta_m}}} \times \frac{1 - e^{-\frac{a-1}{\Delta_m}}}{1 - e^{\frac{1}{\Delta_m}}}. \tag{5.27}$$

As we can see in figure 5.6, the relative difference between the exact solution $w_Q(a)$ of the Klein-Gordon equation and Eq. (5.27) is smaller than 5% for redshifts $z < 1000$, therefore it provides a very good approximation for the evolution of the quintessence equation of state. Both Eq. (5.22) and Eq. (5.27) are very useful in that they allow us to take into account the clustering properties of dark energy (see for instance [160]) and to combine low redshift measurements with large scale structure and CMB data.

[1] We thank Eric Linder for pointing this out to us.

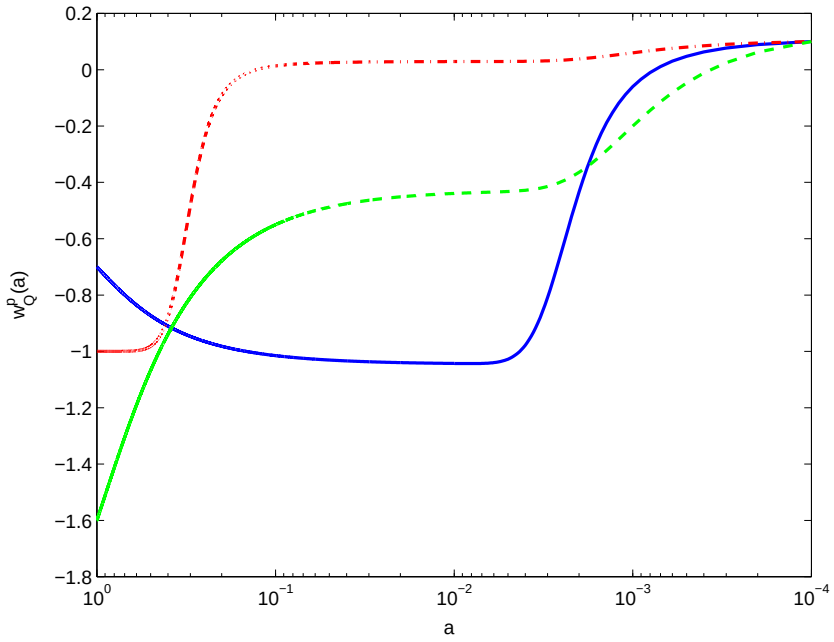

Figure 5.5: Time evolution of $w_Q^p(a)$ as in the case of K-essence (blue solid line), late time transition (red dash-dot line) end with $w_Q^o < -1$ (green dash line).

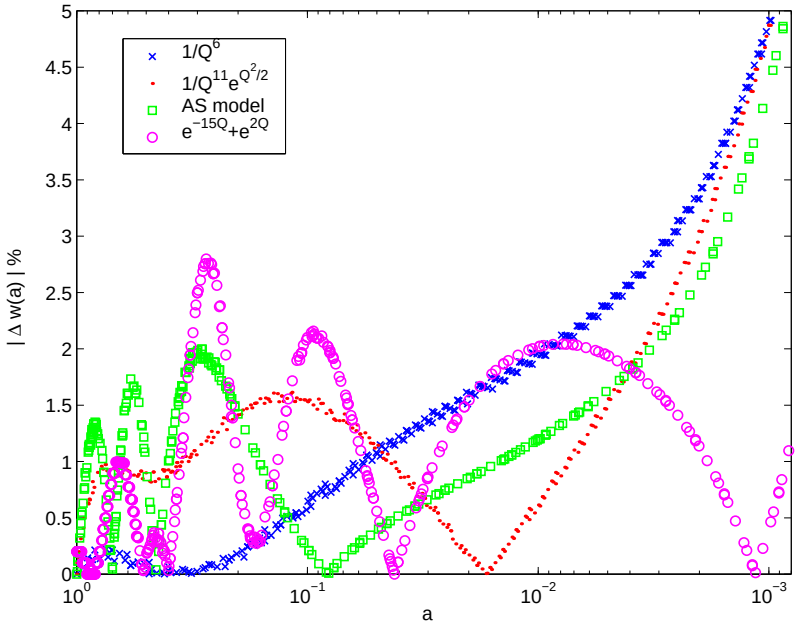

Figure 5.6: Absolute value of the difference between $w_Q(a)$ and the low redshift formula Eq. (5.27) for the models of figure 5.2.

Chapter 6

Dark energy effects in the Cosmic Microwave Background Radiation

The physics of the Cosmic Microwave Background radiation has been deeply studied during the past 30 years. The theoretical developments in understanding the different processes responsible for the temperature anisotropies have given to us the possibility to accurately predict the spectrum of the CMB fluctuations for a given cosmological model. The existence of these cosmological temperature fluctuations was initially confirmed by the COBE satellite [163], but it is only with the recent generation of balloon and ground experiments, such as Boomerang [19], Maxima [23] and DASI [24], that the observations reached the level of accuracy necessary for testing different cosmological scenarios. As we have reviewed in Chapter 1, these measurements have detected the multiple peak structure of the CMB power spectrum, providing an accurate determination of the cosmological parameters. The improvements in the CMB experiments are mainly due to the high performance of the new high frequency microwave detectors. The recent WMAP satellite, using this technology has started a new generation of satellite experiments that will measure the temperature and polarization anisotropies close to the theoretical 'cosmic variance' limit. It is therefore of crucial importance to study the imprint dark energy leaves in the anisotropy power spectrum. In this Chapter we start reviewing the main concepts of the CMB physics. Using a model independent approach we study the impact of different dark energy models in the CMB spectrum. In particular we find that features of the dark energy equation of state can leave a characteristic imprint in the Integrated Sachs-Wolfe effect [161, 162].

We will identify the dark energy models that are distinguishable from the cosmological constant. In conclusion we will show the limits on a class of dark energy models that can be obtained by cosmic variance limited experiments.

6.1 A beginner's guide to CMB physics

The starting point of the CMB anisotropy calculation is the kinetic theory of photons in a perturbed space-time. Here we shall briefly review the main concept of the subject and for more authoritative reviews we refer to [121, 126, 164].

6.1.1 Basic equations

Let us consider a flat pertubed background. In the Newtonian gauge the metric element is

$$ds^2 = a^2(\eta)[-(1+2\Psi)d\eta^2 + (1-2\Phi)dx^i dx_i], \tag{6.1}$$

where Ψ and Φ are the metric perturbations and η is the conformal time. The properties of a gas of photons propagating in this space-time are described by the distribution function $f(x^i, P_i)$ that depends on the three spatial coordinates x^i and the three conjugate momenta P_i. In the Newtonian gauge the relation between P_i and the proper momentum p_i measured by an observer at a fixed spatial coordinate is given by $P_i = a(1-\Phi)p_i$. In order to eliminate the metric perturbations from the definition of the momenta it is convenient to replace P_i with $q_i = ap_i$, where $q_i = q\gamma_i$, q and γ_i being the module and the cosine directions respectively. In the early Universe the photons propagate in a hot ionized medium and interact through the Compton scattering with free electrons and ions. As a consequence of this the distribution function is conserved along the perturbed geodesic apart for a collisional term. The evolution of the distribution function is described by the Boltzmann equation:

$$\frac{df}{d\eta} \equiv \frac{\partial f}{\partial \eta} + \frac{\partial f}{\partial x^i}\frac{dx^i}{d\eta} + \frac{\partial f}{\partial q}\frac{dq}{d\eta} + \frac{\partial f}{\partial \gamma^i}\frac{d\gamma^i}{d\eta} = C[f], \tag{6.2}$$

where $C[f]$ accounts for the Compton scattering and the geodesic equation

$$\frac{1}{q}\frac{dq}{d\eta} = \dot{\Phi} - \gamma_i \frac{\partial \Psi}{\partial x_i}. \tag{6.3}$$

In addition the linearized Einstein equations determine the equations for the metric perturbations Φ and Ψ in term of the perturbations in the multiple fluids system. At the

zeroth order we can consider the Universe as being unperturbed, in such a case f is independent of x^i and γ_i and if the collision between photons and charged particles conserve energy, then $q = ap$ is time independent and consequently f is as well. This is a good approximation, since the free electrons are non-relativistic and the Compton scattering is primarily Thomson scattering in which momentum and not energy is transferred. The equilibrium distribution function f is

$$f_{eq} = \frac{2}{\exp\left(\frac{q}{T_0}\right) - 1}, \tag{6.4}$$

where the factor 2 accounts for the number of polarization states of the photon and T_0 is the temperature of the radiation today. The effects of the perturbed background can be described by expanding the distribution function f about the equilibrium state,

$$f = f_0(q) + f_1(\eta, x^i, \gamma_i, q), \tag{6.5}$$

where $f_0(q)$ is given by Eq. (6.4) and f_1 is the perturbed part of the distribution function. Substituting Eq. (6.5) into Eq. (6.2) and taking only the first order terms we obtain:

$$\frac{\partial f_1}{\partial \eta} + \gamma^i \frac{\partial f_1}{\partial x^i} + q\frac{df_0}{dq}\left(\dot{\Phi} - \gamma^i \frac{\partial \Psi}{\partial x^i}\right) = C[f]. \tag{6.6}$$

For practical purposes it is convenient to write the perturbed part of the distribution function in term of the brightness function $\Theta(\eta, x^i, \gamma_i)$, that is the fractional perturbation in the effective temperature of the photons, $T = T_0(1+\Theta)$. Expanding f around $T_0(1+\Theta)$ we have:

$$\begin{aligned} f &= \frac{2}{\exp\left[\frac{q}{T_0(1+\Theta)}\right] - 1} \\ &\approx \frac{2}{\exp\left(\frac{q}{T_0}\right) - 1} - 2\frac{q}{\left[\exp\left(\frac{q}{T_0}\right) - 1\right]^2}\frac{\exp\left(\frac{q}{T_0}\right)}{T_0}\Theta \\ &= f_0 - q\frac{df_0}{dq}\Theta. \end{aligned} \tag{6.7}$$

Comparing Eq. (6.5) with Eq. (6.7) we obtain

$$f_1 = -q df_0/dq\Theta. \tag{6.8}$$

Substituting Eq. (6.8) into Eq. (6.6) and taking the Fourier transform the Boltzmann equation becomes [18]:

$$\dot{\Theta} + ik\mu(\Theta + \Psi) = -\dot{\Phi} + S_C, \tag{6.9}$$

where $\mu = \frac{\gamma^i k_i}{k}$ and

$$S_C = \dot{\tau}\left(\Theta_0 - \Theta + \gamma_i V_b^i + \frac{1}{16}\gamma_i\gamma_j\Pi_r^{ij}\right), \tag{6.10}$$

where $\dot{\tau} = x_e n_e \sigma_T a$ is the differential optical depth, with x_e the ionization fraction, n_e the electron number density and σ_T the Thomson cross section; Θ_0 is the isotropic component of Θ, V_b^i is the baryon velocity and Π_r^{ij} is the anisotropic stress perturbation for the photons. Hence the collisional term couples the evolution of the photon perturbation to that of the baryons. The equations for the baryon perturbations are obtained by linearizing the conservation equation of the stress energy tensor:

$$\dot{\delta}_b = -k(V_b - V_r) - 3\dot{\Phi}, \tag{6.11}$$

$$\dot{V}_b = -\frac{\dot{a}}{a}V_b + k\Psi + \dot{\tau}(V_r - V_b)/R, \tag{6.12}$$

where V_r is the velocity perturbation of the photons. It is useful to expand the brightness function in a Legendre series:

$$\Theta = \sum_{l=0}^{\infty}(-i)^l(2l+1)\Theta_l P_l(\mu). \tag{6.13}$$

Using the definition of the photon stress energy tensor in term of the distribution function f, it can be shown that $\Theta_0 = \delta_r/4$ and $\Theta_1 = V_r$. Substituting Eq. (6.13) in Eq. (6.9) and using the explicit form of the Compton scattering term Eq. (6.10) we obtain the hierarchy equations [165, 166]:

$$\dot{\Theta}_0 = -\frac{k}{3}\Theta_1 - \dot{\Phi}, \tag{6.14}$$

$$\dot{\Theta}_1 = k\left[\Theta_0 + \Psi - \frac{2}{5}\Theta_2\right] - \dot{\tau}(\Theta_1 - V_b), \tag{6.15}$$

$$\dot{\Theta}_2 = k\left[\frac{2}{3}\Theta_1 - \frac{3}{7}\Theta_3\right] - \frac{9}{10}\dot{\tau}\Theta_2, \tag{6.16}$$

$$\dot{\Theta}_l = k\left[\frac{l}{2l-1}\Theta_{l-1} - \frac{l+1}{2l+3}\Theta_{l+1}\right] - \dot{\tau}\Theta_l \ (l > 2). \tag{6.17}$$

The anisotropy power spectrum is defined as:

$$\frac{2l+1}{4\pi}C_l = \frac{1}{2\pi^2}\int d\eta \frac{dk}{k}\frac{k^3|\Theta_l(k,\eta)|^2}{2l+1}. \tag{6.18}$$

From Eq. (6.9) we note there are two sources of anisotropy formation, the Compton scattering that couples the photons to the baryons and the gravitational effect produced by the presence of density fluctuations in all the matter components.

6.1.2 CMB anisotropies

Acoustic Oscillations

Before recombination the differential optical depth $\dot{\tau}$ is very large and the scattering between photons and baryons is extremely rapid and efficient. In this regime, called the *tight coupling* limit ($\dot{\tau}/k >> 1$), the photons and the baryons behave as a single fluid. Because of this the baryons and photons velocity are the same at the zeroth order, $V_b \approx V_r = \Theta_1$. In such a case Eq. (6.12) becomes:

$$\dot{\Theta}_1 = -\frac{\dot{R}}{R}\Theta_1 + k\Psi + \frac{\dot{\tau}}{R}(\Theta_1 - V_b), \tag{6.19}$$

where $R = 3\rho_b/4\rho_r$ is the baryon to photon ratio. Inverting this equation in terms of $\dot{\tau}(\Theta_1 - V_b)$ and substituting in Eq. (6.15) we obtain the iterative first order solution,

$$\dot{\Theta}_0 = -\frac{k}{3}\Theta_1 - \dot{\Phi}, \tag{6.20}$$

$$\dot{\Theta}_1 = -\frac{\dot{R}}{1+R}\Theta_1 + \frac{k\Theta_0}{1+R} + k\Psi. \tag{6.21}$$

These equations can be combined into a single second order equation [167],

$$\ddot{\Theta}_0 + \frac{\dot{a}}{a}\frac{R}{1+R}\dot{\Theta}_0 + k^2 c_s^2 \Theta_0 = F(\eta), \tag{6.22}$$

where $c_s^2 = \frac{1}{3}(1+R)^{-1}$. The source function $F(\eta)$ arises from the gravitational potentials and is given by

$$F(\eta) = -\ddot{\Phi} - \frac{\dot{a}}{a}\frac{\dot{R}}{1+R}\dot{\Phi} - \frac{k^2}{3}\Psi. \tag{6.23}$$

From Eq. (6.22) we can distinguish three different contributions to the evolution of the isotropic part of the brightness function during the tight coupling regime:

- the radiation pressure given by the term $k^2 c_s^2 \Theta_0$ which dominates on subhorizon scales and supports oscillations of the photon-baryon plasma;
- the gravitational infall of the photon-baryon fluctuations in the potential well, $k^2\Psi$;
- the $\ddot{\Phi}$ term that sources the oscillations at scales that enter in the horizon between the epochs of matter-radiation equality and decoupling. The $\dot{\Phi}$ term contribute as a friction term.

Neglecting time variations in the gravitational potentials, Eq. (6.22) describes a forced harmonic oscillator equation. On subhorizon scales the photon pressure balances the

gravitational collapse of the perturbations and causes the propagation of pressure waves in the photon-baryon plasma. The characteristic scale upon which these waves can propagate is fixed by the size of the sound horizon $r_s = \int c_s(\eta) d\eta$. When the photons last scatter, the imprint of these compression and rarefaction regions will appear as a series of peaks in the anisotropy power spectrum on the angular scales smaller than the angle subtended by the sound horizon at the decoupling. The odd and the even peaks correspond to photons coming from regions that are respectively in compression and expansion phases at last scattering. However the compression and rarefaction phases are not completely equivalent. In fact the baryons increase the effective mass of the barotropic fluid and consequently the gravitational infall generated by the density fluctuations leads to a deeper trough during the compression phase (*baryon drag*). The compression is enhanced over rarefaction resulting in a larger amplitude of the odd peaks relative to the even ones. Therefore the relative heights of the acoustic peaks is extremely sensitive to the baryon density $\Omega_b h^2$. An additional source of anisotropies is due to the motion of the fluid at the last scattering surface due to the Doppler shift of the CMB photons. However due to the large value of R this effect is subdominant.

Sachs-Wolfe effect

In the large wavelength limit ($k\eta << 1$) the Boltzmann equation Eq. (6.14) reduces to the form $\dot{\Theta}_0 = -\dot{\Phi} \approx \dot{\Psi}$ ($\Phi = -\Psi$). The solution of this equation depends on the initial condition of the solution of the linear density perturbation equations. In fact $\Theta_0 = \delta_r$ and for adiabatic initial conditions $\delta_r(0) = -\frac{1}{2}\Psi(0)$, reflecting the fact that the photons are overdensities inside the potential well. However due to the decay of the gravitational potential after matter-radiation equality the photon temperature at decoupling becomes $\Theta_0(\eta_*) = -\frac{2}{3}\Psi(\eta_*)$, where η_* is the conformal time at decouplings. When the photons last scatter they climb out of the potential well Ψ so that the effective superhorizon perturbations in the photon temperature is:

$$[\Theta_0 + \Psi](\eta_*) = \frac{1}{3}\Psi(\eta_*). \tag{6.24}$$

This is the so called Sachs-Wolfe effect [168]. It is the dominant source of anisotropies on large angular scales and is responsible for the plateau at the low multipoles in the CMB power spectrum. Since these scales are superhorizon at the time of decoupling the amplitude of this Sachs-Wolfe depends on the primordial spectrum of the density

fluctuations.

The Integrated Sachs-Wolfe effect

The time evolution of the gravitational potentials is a source of primary anisotropies, in fact as the photons free stream after decoupling the solution to the Boltzmann equation is given by [169]:

$$\frac{\Theta_l(\eta)}{2l+1} = [\Theta_0 + \Psi](\eta_*) j_l(k(\eta - \eta_*)) + \int_{\eta_*}^{\eta} (\dot{\Psi} - \dot{\Phi}) j_l(k(\eta - \eta')) d\eta', \tag{6.25}$$

where $j_l(k\eta)$ are the Bessel functions. The first term represents the contribution of the Sachs-Wolfe effect, while the second term is the Integrated Sachs-Wolfe effect (ISW) [170]. We can distinguish two contributions to the ISW: an early and a late ISW. The former is due to the decays of the gravitational potentials after horizon crossing at the end of the radiation dominated era. The latter occurs in dark energy dominated cosmologies, as the Universe starts accelerating the rapid expansion causes the decay of the density fluctuations that drive the decay of the gravitational potentials. The combined effect of the SW and the two components of the ISW can be studied by analysing the the anisotropy power spectrum per logarithmic k and l interval defined by

$$C_l(k) = \frac{1}{l(l+1)} \int_{\eta*}^{\eta} |\Theta(k, \eta')|^2 d\eta'. \tag{6.26}$$

In figure 6.1 we show the density plots of Eq. (6.26) integrated up to $z = 5$ (*left panel*) and to $z = 0$ (*right panel*) for a ΛCDM with $\Omega_\Lambda = 0.7$. The brighter regions correspond to values of the wavenumbers and multipoles where there is more power. Since for the model we have considered the acceleration starts at redshift $z = 0.7$, the contribution of the late ISW can be emphasized by comparing the distribution of power in the left panel with that in the right panel. As we expect, we note that due to the projection onto the last scattering surface the wavenumbers k and the multipoles l are strongly correlated. As a consequence of this the power at redshift $z = 5$ is shifted toward lower multipoles than at $z = 0$. This is simply because the last scattering surface is closer to the observer at redshift $z = 5$ and different scales are projected on larger angles. The filamentary and periodic structure of the density plots are due to the Bessel functions. We therefore expect a different structure in the case of an open or closed space-time. Note that the power is distributed along an upper and a lower ridge respectively. The latter is the contribution of the Sachs-Wolfe effect caused by modes that are superhorizon at decoupling ($k \sim 10^{-3}$)

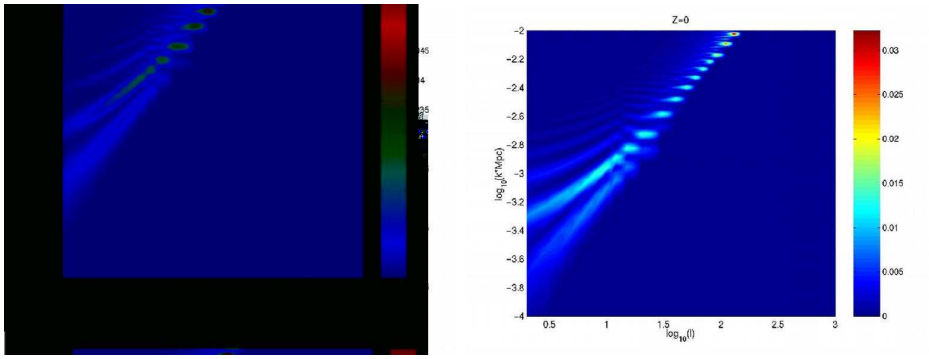

Figure 6.1: Density plots of $C_l(k)$ in the $k-l$ plane for a ΛCDM model. The modes in the left panel are integrated up to redshift $z = 5$ and those in the right panel are integrated up to $z = 0$.

while the upper ridge is produced by the early ISW. Since this latter effect arises closer to the present time, the corresponding anisotropies are projected on angular scales larger than the SW effect itself. The bright spot at the top of the panels correspond to the rise of the first Doppler peak, the other peaks do not appear in these plots since we limited our analysis to scales larger than the horizon at decoupling ($k < 10^{-3}$). As we can see in the right panel, integrating the modes over the period of time when the Universe started to accelerate boosts the power at lower multipoles. In fact the signature of the late ISW can be noticed from the fact that the upper ridge becomes brighter than that in the right panel. Note that the two plots have slightly different brightness scales, this is because the late ISW overlaps with the SW leading to a different distribution of the power on the large angular scales.

Damping mechanisms

The overall amplitude of the CMB power spectrum is suppressed by the effects of diffusive mechanisms. The most important of these effects is due to the diffusion of the photons on scales smaller than their mean free path λ_C. In fact due to the Compton scattering the photons randomly walk through the baryons with a mean free path $\lambda_C \approx \dot{\tau}^{-1}$. After N collisions the diffusive length is $\lambda_D \sim \sqrt{N}\lambda_C$. Consequently on scales $\lambda < \lambda_D$ the diffusion exponentially suppresses the amplitude of anisotropies. The baryons suffer a similar effect, in fact from Eq. (6.12) we can see that on scales $k << \dot{\tau}/R$ the Compton scattering can drag the baryons in and out of the potential wells leading to a destruction of the baryonic oscillations (*Silk damping* [171]). Another damping effect arises from the

fact that he last scattering process is not instantaneous. The photons we observe today in a given direction of the sky may have decoupled from different points along the line of sight. Therefore fluctuations on scales smaller then the thickness of the last scattering surface have destructively interfered causing a 'washing out' of the anisotropies on very small angular scales. The reionization history of the Universe also contributes to the overall damping of the temperature anisotropy power spectrum. In fact when the first stars form they reionize the intergalactic medium, therefore a fraction of the CMB photons are scattered on scales smaller then size of the horizon at the epoch of reionization. This lead to a suppression of the power at large multipoles. In light of the recent WMAP measurements of the temperature-polarization cross power spectrum, it is worth mentioning that the reionization sources the polarization of the anisotropies. Consequently a late reionization, $z_{ion} < 100$, will produce significant power at low multipoles in the temperature-polarization spectrum.

6.2 Dark energy and the Integrated Sachs-Wolfe effect

We have previously discussed the importance of distinguishing between different dark energy models from the "concordance" ΛCDM model. The ISW is particularly sensitive to the late time evolution of the Universe. In fact during the matter dominated era the gravitational potential Φ associated with the density perturbations is constant and there is no ISW effect. However, we have seen that in ΛCDM models Φ starts decaying at redshifts when Λ starts to dominate, producing large angular scale anisotropies [172]. In dark energy scenarios the cosmic acceleration is not the only contribution to the decay of Φ: on large scales the clustering properties alter the growth rate of matter perturbations [76, 173]. It is the signal of this clustering [174] that we are hunting in as model-independent a way as possible. We assume a flat spatial geometry and fix the value of the Hubble constant $H_o = 70$ Kms$^{-1}Mpc^{-1}$, and the amount of matter (CDM) $\Omega_m = 0.3$. We can usefully distinguish two classes of models,

- those with a slowly varying equation of state for which $0 < a_c^m/\Delta < 1$, as in the case of the inverse power law potential [79];
- a rapidly varying $w(z)$, such as the 'Albrecht-Skordis' model [118] and the two exponential potential [100], with $a_c^m/\Delta > 1$. This class also includes many interesting rad-

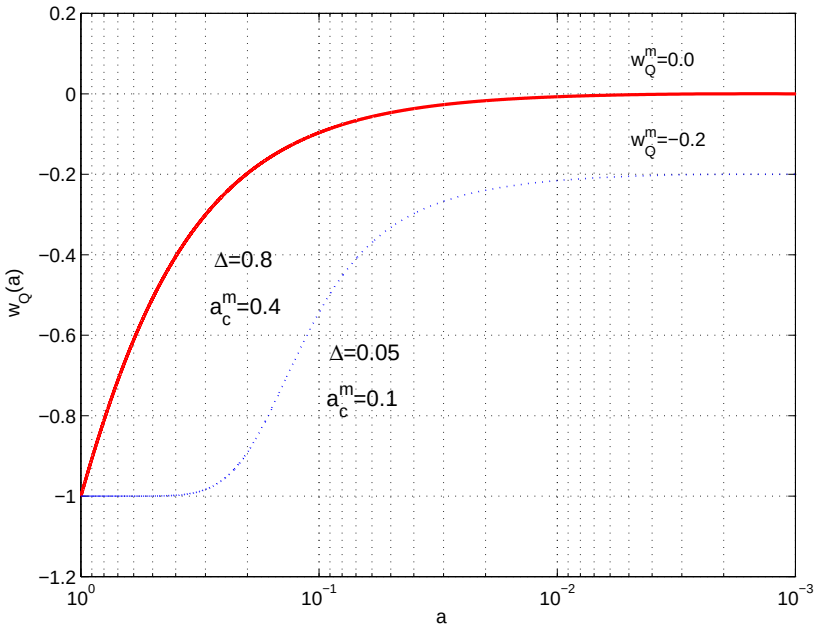

Figure 6.2: Time evolution of the equation of state for two classes of models, with slow (red solid line) and rapid transition (blue dotted line). The dark energy parameters specify the features of $w_Q(a)$

.

ical models such as vacuum metamorphosis [175], late-time phase transitions [176], and backreaction-induced acceleration [177].

We show these two classes in figure 6.2. The red solid line corresponds to dark energy that tracks the dust during the matter era ($w_Q^m = 0.0$) and evolves slowly toward $w_Q^o = -1$, and the blue dotted line corresponds to a model with a rapid transition in its equation of state at $a_c^m = 0.1$ ($z = 9$). Given current data it is worth studying the case with $w_Q^o = -1$, (since it is also the most difficult to distinguish from ΛCDM) whilst allowing the other parameters w_Q^m and a_c^m, to vary. We have modified the CMBFAST code [178] in order to include the effects of a dark energy fluid and its perturbations by specifying the time evolution of the equation of state. Figure 6.3 shows the anisotropy power spectrum, C_l^{ISW}, produced through the integrated Sachs-Wolfe effect by a rapidly evolving (*top panels*) and a slowly evolving (*bottom panels*) equation of state; the red (solid) line corresponds to the ΛCDM model. As we can see in the top left panel (figure 6.3a), varying a_c^m can produce a strong ISW. The effect is larger if the transition in the equation of state occurs at redshifts $z < 3$. On the other hand the C_l^{ISW} is the same as in the cosmological constant regime if $a_c^m < 0.2$

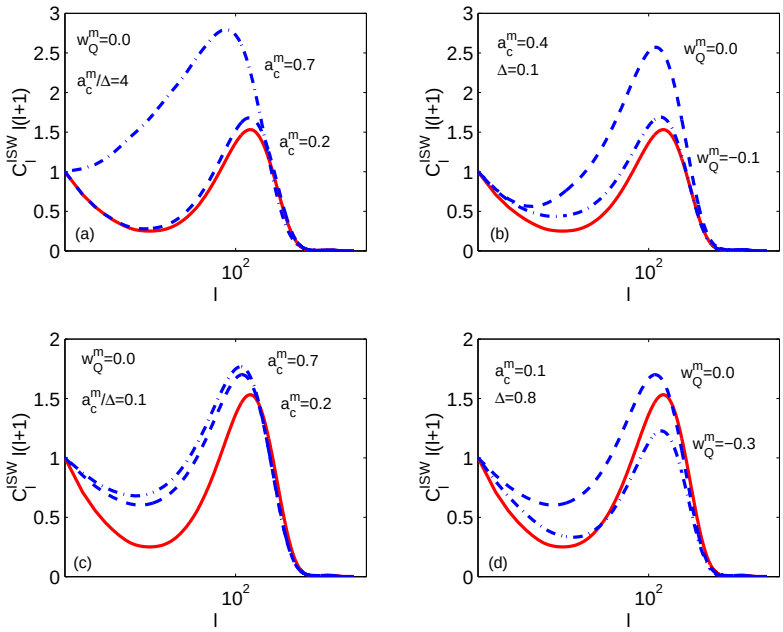

Figure 6.3: Power spectrum of the ISW for rapidly varying models (top panels) and slowly varying ones (bottom panels). The solid red line is the ISW effects produced in the cosmological constant case. Detailed explanation in the text.

($z > 4$). In the top right panel (figure 6.3b) we plot the ISW for two different values of w_Q^m, corresponding to $w_Q^m = 0.0$ (dashed line) and $w_Q^m = -0.1$ (dot-dash line). We note that the signal is larger if the quintessence field is perfectly tracking the background component. But as w_Q^m diverges from the dust value the ISW effect approaches that of ΛCDM. This means that even for rapidly varying $w(z)$ (small Δ), the ISW is distinguishable from that in the ΛCDM scenario only if $w(z)$ during matter domination closely mimics the dust value and the transition occurs at low redshifts, $z < 3$. We can see that the amplitude of the integrated Sachs-Wolfe effect is smaller in slowly varying models (*bottom panels*). As we expect the C_l^{ISW} is independent of a_c^m (figure 6.3c), since for these models a different value in the transition redshift does not produce a large effect on the evolution of the dark energy density. In figure 6.3d, the ISW power spectrum is large for $w_Q^m = 0.0$ (dash line) and becomes smaller than the cosmological constant on horizons scales as w_Q^m has negative values (dot-dashed line), and increases toward Λ for w_Q^m approaching -1. This class of models is then more difficult to distinguish from the ΛCDM if the equation of state today is close to $w_\Lambda = -1$. This can be qualitatively explained noting that perfect tracking between dark energy and CDM causes a delay in the time when the gravitational

potential starts to decay, compared to the case of ΛCDM. This effect is stronger for models with a rapidly varying equation of state since the rapid change in w_Q produces a stronger variation in the gravitational potential.

6.3 Differentiating dark energy models with CMB measurements

The information in the CMB power spectrum can be encoded in the position of the first three Doppler peaks, l_1, l_2 and l_3 and in three parameters, H_1, H_2 and H_3 that account for the amplitude [179]. These are the height of the first peak relative to the power at $l = 10$,

$$H_1 \equiv \frac{l_1(l_1+1)C_{l_1}}{l_{10}(l_{10}+1)C_{l_{10}}}, \tag{6.27}$$

the height of the second peak relative to the first,

$$H_2 \equiv \frac{l_2(l_2+1)C_{l_2}}{l_1(l_1+1)C_{l_1}}, \tag{6.28}$$

and the height of the third peak relative to the first,

$$H_3 \equiv \frac{l_3(l_3+1)C_{l_3}}{l_1(l_1+1)C_{l_1}}. \tag{6.29}$$

In principle the position of the second and third peaks is not necessary to characterize the CMB power spectrum, since their value is set by the position of the first peak through the harmonic relation Eq. (4.6). However, as we have previously discussed in Chapter 4 this relation is affected by pre-recombination effects and therefore the value of l_2 and l_3 carry information about a combination of the cosmological parameters. Since H_1, H_2 and H_3 quantify the amplitude of the power spectrum on different multipoles we expect they are sensitive in different ways to the cosmological parameters. For instance since H_1 depends on the ratio between C_{l_1} and $C_{l_{10}}$ it mainly depends on the scalar spectral index n, the physical baryon density $\Omega_b h^2$ due to the baryon drag that changes C_{l_1}, Ω_Λ through the ISW and the reionization since increasing τ will lower the first peak. On the other hand H_2 is sensitive only to $\Omega_b h^2$ and n. Since the baryons affect in the same way the height of the third and first peak, H_3 depends only on the matter density Ω_m and n. This implies that if the amplitude of the first three peaks is accurately determined the degeneracy between $\Omega_b h^2$ and n can be broken and their value can be measured with high precision. We use H_1, H_2 and H_3 to determine the overall effect of the dark energy in the CMB spectrum.

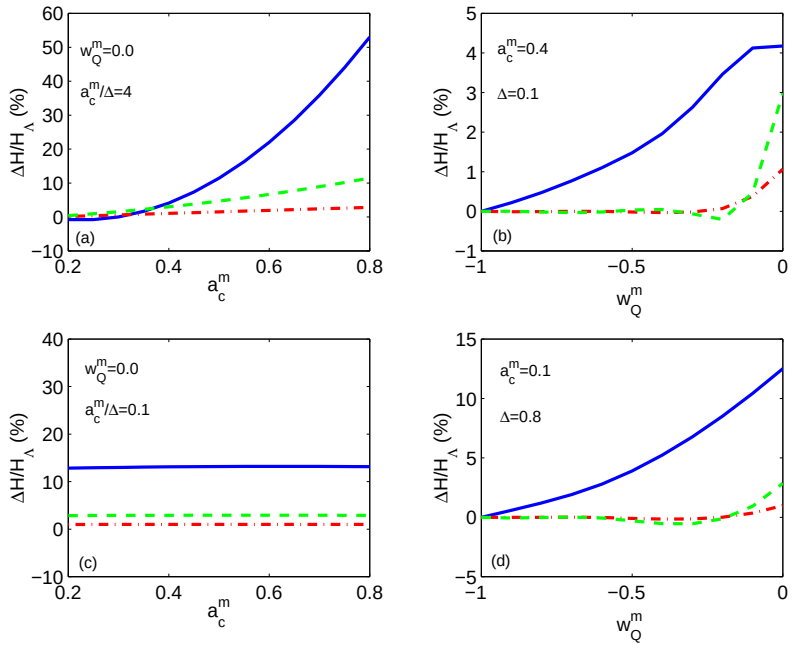

Figure 6.4: Relative difference of H_1 (blue solid line), H_2 (green dash line) and H_3 (red dash-dot line) to the ΛCDM model, for rapidly varying models (*top panels*), and with slow transition (*bottom panels*). For these models the present value of the equation of state is $w_Q^o = -1$.

In particular we expect H_1 to be extremely sensitive to a quintessential effect through the ISW, while H_2 and H_3 are weak indicators of such a signal. We have computed the CMB spectra for the class of models with $w_Q^o = -1$ described in the previous section and we have inferred the values of H_i and compared them with those of the ΛCDM model for the same values of the cosmological parameters. In figure 6.4 we plot the absolute value of the relative difference of H_1, H_2 and H_3 to the ΛCDM model. The rapidly varying models are shown in the top panels. We can see the strong ISW effects produced by changing a_c^m are now evident in the large discrepancy between H_1 and H_1^Λ (blue line) (figure 6.4a): it can be larger then 20 per cent for $a_c^m > 0.6$. The effect on H_2 and H_3 is smaller. However varying w_Q^m (figure 6.4b) produces a discrepancy of only order 4 per cent on H_1, while H_2 and H_3 remain the same as in ΛCDM. For a slowly varying equation of state, H_1, H_2 and H_3 are independent of a_c^m (figure 6.4c). The dark energy imprint is only on H_1 for which the discrepancy to the Λ case is about 10 per cent. This discrepancy decreases when changing the value of the quintessence equation of state during matter from $w_Q^m = 0.0$ to $w_Q^m = -1$ (figure 6.4d). Values of the equation of state today $w_Q^o > -1$ imply a stronger ISW effect.

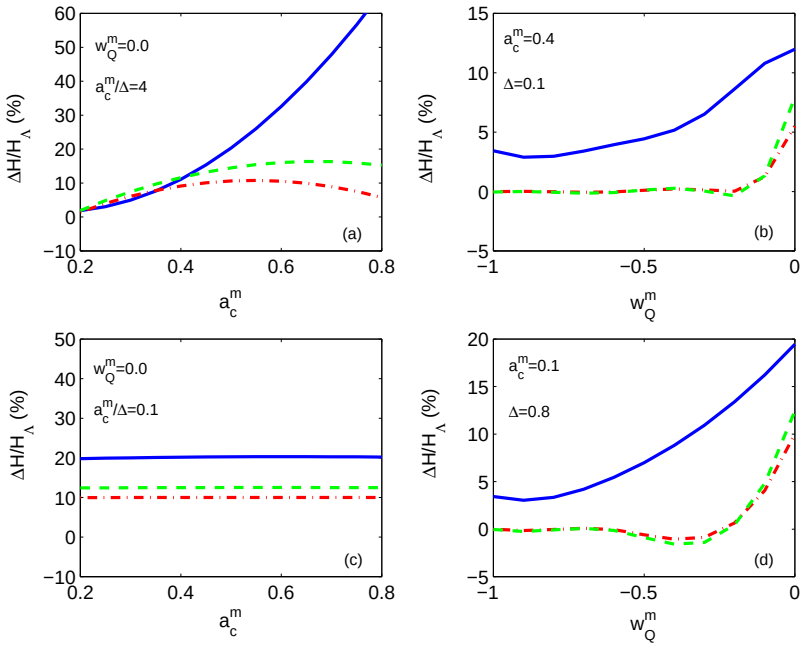

Figure 6.5: As in figure 6.4 for $w_Q^o = -0.88$.

Consequently the curves of fig.3 are shifted upwards. For instance in figure 6.5 we plot the class of models previously analysed, with $w_Q^o = -0.88$. We note the same behavior as we vary the dark energy parameters, but the discrepancy with the ΛCDM model is now larger. In figure 6.5d it is worth noticing the case $w_Q^m = -1$, that corresponds to a model very similar to a 'k-essence' model [157]. We can see that the relative difference with the ΛCDM case is of the order of a few percent, in agreement with [180] for the same value of $w_Q^o = -0.88$. At this point we ask the key question whether such differences are observable. We have shown that H_1 is a good estimator of the ISW effect, and that it is a tracer of the dark energy imprint on the CMB. However its estimation from the data will be affected by cosmic variance at $l = 10$. Hence with even perfect measurements of the first acoustic peak the uncertainty on H_1 will be dominated by the 30 per cent uncertainty due to cosmic variance. With the plots of figures 6.4-6.5 in mind, this means that if the present value of the equation of state is close to -1, slowly varying dark energy models are hardly distinguishable from ΛCDM, while rapidly varying ones can produce a detectable signature only if the transition in the equation occurred at $a_c^m > 0.7$, but in any case it will be difficult to constrain w_Q^m. Moreover it should be taken into account that H_1 is degenerate with other cosmological parameters, such as the scalar spectral index n, the optical depth τ and the scalar to tensor ratio r. Hence only an accurate determination

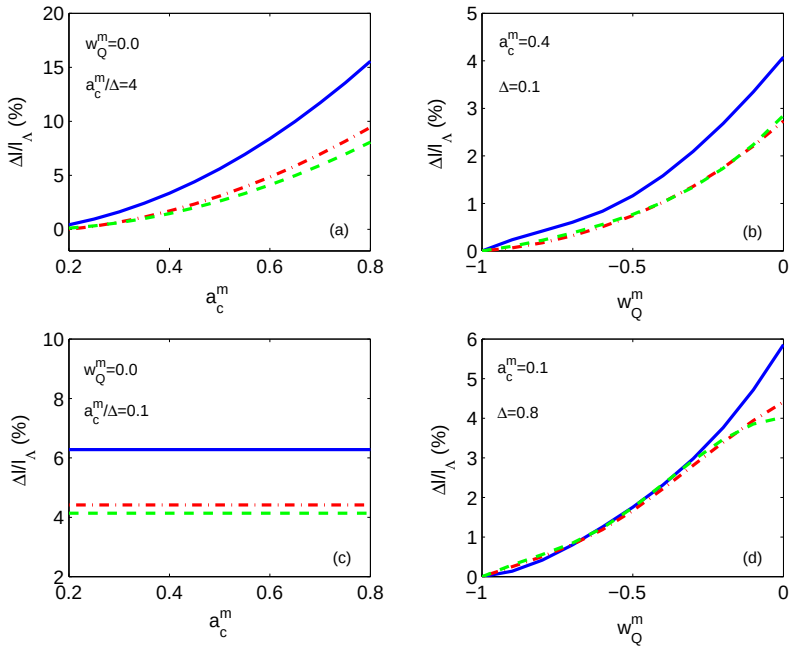

Figure 6.6: Relative difference of l_1 (blue solid line), l_2 (green dashed line) and l_3 (red dot-dashed line) to the ΛCDM model, for rapidly varying models (*top panels*), and with slow transition (*bottom panels*). For these models the present value of the equation of state is $w_Q^o = -1$.

of the angular diameter distance, inferred from the location of the acoustic peaks, would allow detection of such deviations from the cosmological constant model. The shift of the multipole positions (ℓ_i) of the acoustic peaks caused by the evolution of the dark energy in the class of models analysed in figure 6.3 can be seen in figure 6.6, where we plot the relative difference of l_1, l_2 and l_3 to the Λ case. We note that due to the additional shift induced on the first acoustic peak by the ISW effect the difference with the ΛCDM model for the first peak is generally larger than for the second and third peaks. As with the comparison of the amplitude of the CMB spectrum, the largest effect is produced by models with a rapid transition occurring at small redshifts. However the degeneracy of the angular diameter distance, in particular with the value of Hubble constant and the amount of dark energy density, will limit our ability to put tight constraints on the dark energy parameters. There are alternative ways in which these problems can be alleviated, for instance cross-correlating the ISW effect with the large scale structure of the local universe [181–183]. An efficient approach would be to combine different observations in order to break the degeneracies with the cosmological parameters [184, 185].

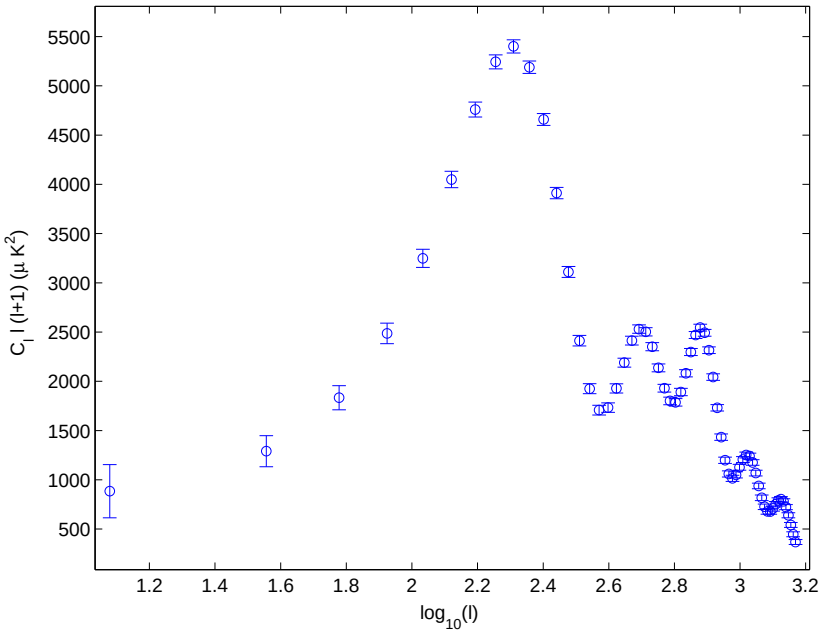

Figure 6.7: CMB power spectrum for a fiducial dark energy models, the errorbars are the cosmic variance errors.

6.4 Testing dark energy with ideal CMB experiments

The new generation of CMB satellite experiments is going to provide an estimation of the anisotropy power spectrum close to the ideal case, where the only source of indetermination is due to the cosmic variance. It is therefore interesting to test the sensitivity of such CMB measurements to the dark energy effects. As we have described in the previous section, the class of models most difficult to distinguish from the ΛCDM case corresponds to a dark energy fluid with a slowly varying equation of state characterized by $w_Q^0 = -1$. This can be considered as the most pessimistic situation since it can prevent us from understanding the nature of the dark energy. We have studied the information on this class of models that can be inferred from cosmic variance limited measurements [162] and generated a sample of ideal CMB power spectrum data assuming a fiducial model specified by the following values of the cosmological parameters: $\Omega_Q = 0.68$, $H_o = 70$ Km s^{-1} Mpc^{-1}, $w_Q^o = -1$, $w_Q^m = -0.4$, $a_c^m = 0.2$, $\Delta = 0.3$. Assuming a flat geometry, no tensor contribution, the scalar spectral index $n = 1$ and the baryon density $\Omega_b h^2 = 0.021$, we have binned the input power spectrum in 62 data points plotted in figure 6.7. A library of CMB spectra has then been generated using a modified version of CMBFAST [178] assuming the following uniform priors: $\Omega_Q \in (0.5, 0.8)$, $H_0 \in (0.5, 0.8)$, $w_Q^0 \in (-0.1, -0.4)$, $w_Q^m \in (-1.0, 0.0)$ and

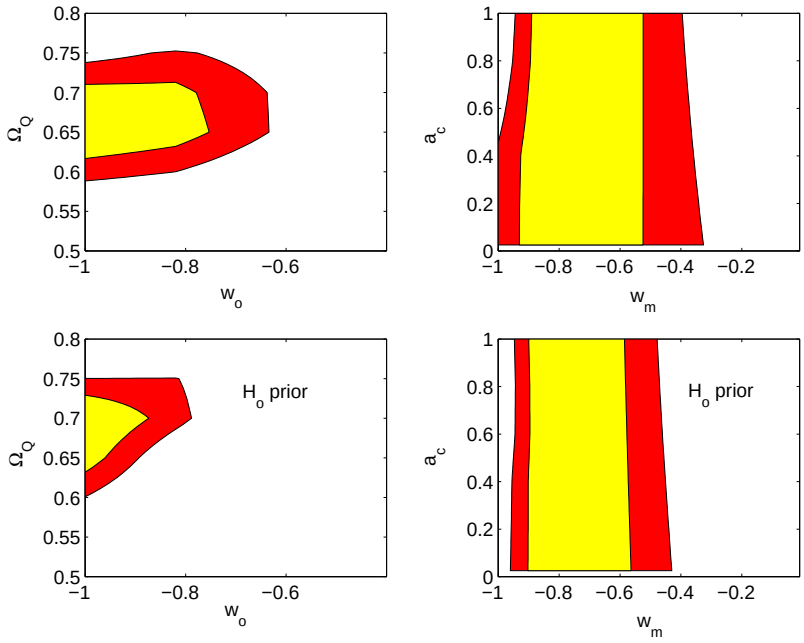

Figure 6.8: Simulated 2-D likelihood contour plots for an ideal experiment, with no priors (*top panels*) and H_o prior (*bottom panels*). The yellow and red contours correspond to 1 and 2σ respectively.

$a_c^m \in (0.01, 1.0)$. As extra priors we have assumed $\Delta = 0.5$ (slowly varying equation of state) and the remaining parameters have been set as follows: $n = 1$, $\Omega_b = 0.05$ and $\tau = 0$. Since we are not considering the effect of systematics, but only cosmic variance errors we evaluate a simple likelihood defined as

$$L(\alpha_j) = \mathscr{N} \exp\left[-\sum_i \frac{C_l^t(l_i;\alpha_j) - C_l^d(l_i)}{\sigma_i^2}\right], \tag{6.30}$$

where α_j are the likelihood parameters, $\mathscr{N}$ is a normalization constant and σ_i is the cosmic variance at $l = l_i$. The superscripts t and d refer to the theoretical quantity and to the real data respectively. The results are shown in figure 6.8, where we plot the two dimensional likelihood contours in the $w_Q^0 - \Omega_Q$ (left panels) and $w_Q^m - a_c^m$ (right panels) planes respectively. We find $\Omega_Q = 0.68 \pm^{0.05}_{0.08}$, $w_Q^0 \leq -0.78$, whereas assuming a prior on H_0 improves the constraints on w_Q^0 to $w_Q^0 \leq -0.85$ at 1σ. The likelihood plot in the $w_Q^m - a_c^m$ plane shows that a_c^m is undetermined. This result is expected since for this class of models the value of a_c^m does not affect the evolution of the dark energy. On the contrary we find $w_Q^m = -0.79 \pm^{0.2}_{0.1}$, but the Λ case cannot be excluded at 2σ. The constraint does not improve assuming the H_o prior. This is because w_Q^o and w_Q^m are degenerate, hence marginalizing the likelihood over w_Q^o shifts the best fit value of w_Q^m towards more negative

values. However it is remarkable that there is still some sensitivity to the value of w_Q^m, such that the best fit is not for $w_Q^m = -1$. Therefore we can conclude that if $w_Q^0 \approx -1$, a large class of models will not be distinguished from a ΛCDM scenario even with ideal CMB measurements. It is possible that by combining different cosmological data, as Sn Ia, large scale structure and quasar clustering the degeneracy between w_Q^m and w_Q^0 can be broken and more information on this class of dark energy models can be inferred [185].

Chapter 7

Alternative cosmological test with higher order statistics

In the recent past the number of papers devoted to the analysis of high order statistics of the CMB anisotropy has dramatically increased. In fact the simplest inflationary models predict to first order a Gaussian distribution of temperature fluctuations, and deviations from gaussianity could be the signature of other phenomena occurring in the anisotropy formation process. On top of that different mechanisms can also be a source of non-Gaussian signals at different angular scales. This is the case of non-linear effects during the inflationary epoch or the presence of topological defects. The present CMB data strongly constrains the level of non-gaussianity on the scales so far probed by the experiments. In this Chapter we will briefly review the higher order statistics of the CMB anisotropies. We will focus on the use of the angular bispectrum as an estimator of non-gaussianity, and introduce a formalism that allows us to analytically calculate the spectrum and bispectrum in the case of a random distribution of localized anisotropies in the CMB sky. We will argue that applying this analytical approach to the analysis of localized anisotropies such as the Sunyaev-Zeldovich effect or radio point sources, it is possible to constrain the clustering properties of these objects and determine the cosmological parameters.

7.1 Higher order statistics

Let us expand the temperature fluctuation field in the direction $\hat{\gamma}$ of the sky into spherical harmonics:

$$\frac{\Delta T(\hat{\gamma})}{T} = \sum_{l,m} a_{lm} Y_l^m(\hat{\gamma}), \tag{7.1}$$

the a_{lm} are the multipole coefficients that contain all the statistical information of the anisotropy field. For $m \neq 0$ these are complex numbers satisfying the condition $a_{l-m} = (-1^m)a_{lm}^*$. The statistics of the CMB anisotropies depends on the physical process responsible for the generation of the initial density perturbations. Simple inflationary models predicts a Gaussian spectrum of fluctuations [186, 187], consequently we expect the anisotropy field to be Gaussian. In such a case the a_{lm} are random Gaussian variables with Gaussian distributed amplitudes and with uniformly distributed phases. As consequence of this the statistical distribution of the CMB anisotropies is entirely specified by its second order moment (*i.e.* the power spectrum),

$$C_l = \sum_{m=-l}^{l} |a_{lm}|^2. \tag{7.2}$$

In this Gaussian case the higher odd moments of the distribution vanish, while the even moments can be expressed in term of the variance C_l. Therefore any deviation from gaussianity will inevitably produce non vanishing high order statistics. Since there is a potentially infinite number of higher moments, the non-Gaussian hypothesis cannot be disproved. Several methods have been proposed in the literature to measure statistical estimators of the skewness (third moment) and (kurtosis) from the analysis of CMB maps (for a list of these methods we refer to [188]). A simple method is to measure the correlation between the temperature fluctuations in different directions of the sky. In this case the higher order moments are estimated by the angular correlation functions. For instance the $m - point$ angular correlation function is defined as:

$$C_m(\hat{\gamma}_1, \hat{\gamma}_2, ..., \hat{\gamma}_m) \equiv \left\langle \frac{\Delta T}{T}(\hat{\gamma}_1) \frac{\Delta T}{T}(\hat{\gamma}_2) ... \frac{\Delta T}{T}(\hat{\gamma}_m) \right\rangle, \tag{7.3}$$

where $\hat{\gamma}_1, .., \hat{\gamma}_m$ are unitary vectors pointing at $1, .., m$ directions of the sky and the average $\langle .. \rangle$ is taken over the whole sky. In particular an estimate of the skewness is provided by the collapsed three-point correlation functions $C_3(\alpha)$, that is a specific configuration of

the three-point correlation function between two points of the sky separated by an angle α and defined as:

$$C_3(\alpha) \equiv \left\langle \frac{\Delta T}{T}(\hat{\gamma}_1)\frac{\Delta T}{T}(\hat{\gamma}_1)\frac{\Delta T}{T}(\hat{\gamma}_2)\right\rangle, \tag{7.4}$$

where $\cos(\alpha) = \hat{\gamma}_1 \cdot \hat{\gamma}_2$. In terms of the multipoles it reads as:

$$C_3(\alpha) = \sum_{l_1,l_2,l_3}\sum_{m_1,m_2,m_3} P_{l_1}(cos\alpha)a_{l_1m_1}a_{l_2m_2}a_{l_3m_3}\mathscr{W}_{l_1}\mathscr{W}_{l_2}\mathscr{W}_{l_3}\mathscr{H}^{m_1m_2m_3}_{l_1l_2l_3}, \tag{7.5}$$

where $P_{l_1}(\cos\alpha)$ is the Legendre polynomial of degree l_1, $\mathscr{W}_l$ is the experimental window function in the multipole space and

$$\bar{\mathscr{H}}^{m_1m_2m_3}_{\ell_1\ell_2\ell_3} = \sqrt{\frac{(2\ell_1+1)(2\ell_2+1)(2\ell_3+1)}{4\pi}}\begin{pmatrix}\ell_1 & \ell_2 & \ell_3\\ 0 & 0 & 0\end{pmatrix}\begin{pmatrix}\ell_1 & \ell_2 & \ell_3\\ m_1 & m_2 & m_3\end{pmatrix}. \tag{7.6}$$

are a combination of the Wigner-3J symbols. The $C_3(\alpha)$ measured from the COBE-DMR sky maps has been found to be consistent with the Gaussian hypothesis within the cosmic variance errors [188]. These results strongly limit the allowed amount of non-gaussianity in the CMB anisotropies at large angular scales, in particular they constrain the parameter space of a class of non-Gaussian models [189–192]. Similarly the collapsed three-point correlation function inferred from the WMAP data is also consistent with Gaussian expectations [193]. Any non-gaussian analysis can be carried out in the multipole space as well, in this case the equivalent of the three-point correlation function is the angular bispectrum defined by:

$$B_{l_1l_2l_3} = \sum_{m_1,m_2,m_3}\begin{pmatrix}\ell_1 & \ell_2 & \ell_3\\ m_1 & m_2 & m_3\end{pmatrix}a^{m_1}_{l_1}a^{m_2}_{l_2}a^{m_3}_{l_3}. \tag{7.7}$$

This estimator is rotationally invariant [194, 195] and satisfies geometrical conditions such that the only non vanishing $B_{l_1l_2l_3}$ are those with $|l_i - l_j| \leq l_k \leq l_i + l_j$ $(i \neq j \neq k)$ for all permutations of indices and $l_1 + l_2 + l_3 = even$. A normalized version of the angular bispectrum has been applied to the analysis of COBE-DMR maps for the configuration $l_1 = l_2 = l_3$ [196–199]. More recently the bispectrum has been estimated from the WMAP map and has been found to be consistent with the Gaussian hypothesis [200].

7.2 Frequentist approach and estimation of higher moments

The frequentist approach is the usual procedure adopted to test gaussianity. This implies the measured value of a higher order statistical estimator is compared against the probability distribution function obtained from random Gaussian simulations of the data

sample. If there is a low probability that the measured value is consistent with the Gaussian simulation, then the Gaussian hypothesis is ruled out. For instance this approach allowed the authors of [196] to rule out the gaussianity of the anisotropies at multipole $l = 16$ in the COBE-DMR data. However it is worth mentioning that so far only the diagonal component of the bispectrum has been measured and in order to be statistically significant the data analysis should be extended to the estimation of the non-diagonal term of the bispectrum. If this is not a problem at low multipoles it could be a computationaly challenge at higher orders. On the other hand it has been pointed out in a number of papers [199, 201] that within the frequentist approach some non-Gaussian theories will be indistinguishable from the Gaussian one. We will try to make this point more clear with a specific example and we refer to the fundamental statistics textbook [202] for a more detailed derivation of the formula used in what follows.

Let us consider a sample of data $\{x_i\}$ $(i = 1, .., N)$ generated from a random Gaussian process $f(x)$ such that each x_i is an independent Gaussian random variable with zero mean $\mu_1 = 0$ and the second order moment $\mu_2 = \sigma^/2$,

$$f(x) = \frac{1}{\sqrt{2\pi}\sigma} e^{-\frac{x^2}{2\sigma^2}}. \tag{7.8}$$

In order to avoid confusion we will use Greek letters for the moments of the generating function $f(x)$, μ_r its r-th moment and Roman letters for the moments obtained from the statistics of the data sample. In particular the r-th moment m_r is given by:

$$m_r = \frac{1}{N} \sum_{i=1}^{n} (x_i - \langle x \rangle)^r, \tag{7.9}$$

where $\langle x \rangle = m_1$ is the mean value of the sample. Making K realizations of this data sample, $\{x_i\}_j$ $(j = 1, .., K)$, we can infer the distribution function $P_{gauss}(m_r)$ of the $r-th$ moment statistic m_r, which is the frequency (number of times to the total number of realizations) of a certain value m_r appearing in the sample x_{ij}. The expectation value of this distribution $E(m_r)$ (the mean value of m_r estimated from the K realizations) will be indicative of the r-th moment μ_r of the generating Gaussian distribution function. The expectation value $E(m_r)$ and the variance $var(m_r)$ can be related to the moments μ_r of the generating function through approximate relations valid up to $(K \cdot N)^{-1/2}$ [202]. It can be shown that:

$$E(m_r) = \mu_r. \tag{7.10}$$

$$var(m_r) = \frac{1}{N \cdot K} (\mu_{2r} - \mu_r^2 + r^2 \mu_2 \mu_{r-1}^2 - 2r\mu_{r-1}\mu_{r+1}). \tag{7.11}$$

For practical purposes we prefer to work in terms of cumulants k_r, that are an equivalent set of numbers characterizing the generating function $f(x)$. The cumulants k_r and the moments μ_r are related through Eq. (3.33) in [202]. Let us consider the third order moment-statistic m_3, from Eq. (7.10) and Eq. (7.11) and using the relation between moments and cumulants we have:

$$E(m_3) = k_3, \tag{7.12}$$

$$var(m_3) = \frac{1}{N \cdot K}(k_6 + 9k_2k_4 + 6k_2^3 + 9k_3^2). \tag{7.13}$$

For the Gaussian generating function we have considered $k_2 = \mu_2 = \sigma^2/2$, $k_3 = 0$, $k_4 = 0$ and $k_6 = 45\sigma^6$, consequently we obtain:

$$E(m_3) = 0, \tag{7.14}$$

$$var(m_3) = \frac{183}{4N \cdot K}\sigma^6. \tag{7.15}$$

On the other hand let us consider a sample of data generated from a non-Gaussian random process. A general non-Gaussian random generating function can be constructed by using an Edgeworth expansion around the Gaussian distribution defined by

$$g(x) = f(x)(1 + \frac{1}{6}k_3H_3(x) + \frac{1}{24}k_4H_4(x) + ...), \tag{7.16}$$

where $f(x)$ is given by Eq. (7.8), the H_i are the Hermite polynomials and the cumulants k_r are free parameters. It can be shown that Eq. (7.16) gives a good approximation to any distribution function provided all moments are defined and the higher order terms do not dominate over the Gaussian one. We can limit the non-gaussianity to first order by imposing only the presence of a non vanishing skewness k_3 and kurtosis k_4. In this case Eq. (7.10) and Eq. (7.11) becomes:

$$E(m_3) = k_3, \tag{7.17}$$

$$var(m_3) = \frac{1}{N \cdot K}(\frac{9}{2}k_4\sigma^2 + \frac{3}{4}\sigma^6 + 9k_3^2). \tag{7.18}$$

Note from Eq. (7.18) the kurtosis and the skewness can sum up in such a way that they cancel each other. In such a case the frequency distributions of the third order moment-statistic m_3 inferred from the K realizations of the Gaussian and non-Gaussian process, $P_{gauss}(m_3)$ and $P_{n-gauss}(m_3)$ respectively, will have the same variance. This makes difficult to establish whether the population of the data had been generated from a

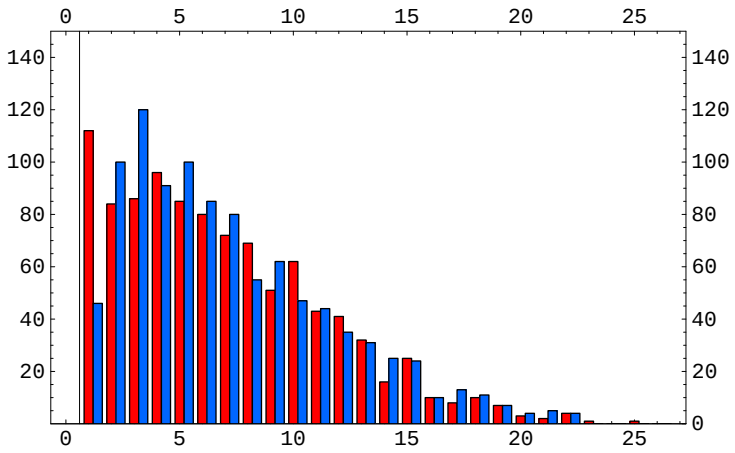

Figure 7.1: Probability distribution functions of the third order moment m_3 estimated from Monte-Carlo simulation of randomly generated data for a Gaussian (red bars) and a non-Gaussian process (blue bars).

Gaussian or a non-Gaussian process by estimating m_3. This analysis is confirmed by the numerical simulations in which we simulated two populations of data from two different random processes. The Gaussian sample has been generated assuming the generating function Eq. (7.8) with $k_1 = 0$, $k_2 = 1$, while the non-Gaussian population has been obtained assuming Eq. (7.16) with $k_1 = 0$, $k_2 = 1$, $k_3 = 3$ and $k_4 = -153/18$. From these two populations we inferred the distribution functions of the third moment-statistic m_3. The results are shown in figure 7.1, where we plot $P_{gauss}(m_3)$ (*red bars*) and $P_{n-gauss}(m_3)$ (*blue bars*). Note that $P_{n-gauss}(m_3)$ is peaked at $m_3 \neq 0$, while $P_{gauss}(m_3)$ has a maximum at $m_3 = 0$. Even so the variances of the two distributions are the same. This naive argument shows that for some non-Gaussian models little information can be obtained using a frequentist approach when analysing the third order statistics unless higher order moments of the CMB anisotropies fields are measured as well. Such simulations are necessary to take into account the systematic experimental sources of non-gaussianity. However they make these tests computationally expensive. Therefore it is important to have a theoretical prediction of the amplitude of non-Gaussianity at least for known non-Gaussian anisotropies such as the secondary ones.

7.3 Modelling localized non-Gaussian anisotropies

Localized patterns of anisotropies produce a non-Gaussian signature in the CMB statistics. This is the case of secondary sources of anisotropies such as radio point sources or the Sunyaev-Zeldovich (SZ) effect caused by the interaction of the CMB photons with the hot gas associated with clusters of galaxies [203]. Active sources of non-Gaussianity include topological defects such as cosmic strings, domain walls (see for a general review [204]) or primordial bubble relics of a first order phase transition during the inflationary era [205, 206]. For these classes of models analytical formula of the higher order correlation functions have been calculated in a number of papers [191, 192, 208]. As far as the non-Gaussianity arising from secondary source of anisotropies is concerned, an analytical estimate of the three point correlation function has been obtained in the case of the Rees-Sciama effect [207], while the value of the bispectrum produced by the S-Z effect and extragalactic radio sources has been obtained in [209], whilst the case of the Vishniac effect has been considered in [210]. In what follows we determine the spectrum and the bispectrum for the case of a distribution of localized anisotropies in the CMB sky, using a formalism introduced in [208].

Power Spectrum

Let us consider a nearly circular spot on the sky and perform the spherical harmonic decomposition in the frame where the z-axis coincides with the center of the spot. The brightness of the temperature fluctuation of the spot is b, and $f(\theta)$ is its angular profile. In this frame, we can write the temperature fluctuation as $\Delta_s(\theta) = b \cdot f(\theta)$, expanding it in spherical harmonics we find [208]:

$$\tilde{a}_{lm} = 2\pi b \sqrt{\frac{2l+1}{4\pi}} \mathscr{I}_l \cdot \delta_{m0} + \epsilon_{ml}, \tag{7.19}$$

with

$$\mathscr{I}_l = \int_{-1}^{1} d(\cos\theta) f(\theta) P_l(cos\theta), \tag{7.20}$$

where $P_l(cos\theta)$ is the Legendre polynomial and ϵ_{lm} is a perturbation induced by the irregularity of the spot. As a first approximation it can be neglected, as the CMB measurements do not have the enough resolution to resolve its ϕ-angular structure. For a distribution of N spots, performing a rotation to a general frame where the n-th spot is at the angle

$\hat{\gamma}_n = (\theta_n, \phi_n)$ and summing over all the spots we obtain:

$$a_{lm} = \sum_n b_n \mathscr{I}_n^l Y_l^{m*}(\hat{\gamma}_n), \tag{7.21}$$

where b_n is the brightness of the n-th spot and

$$\mathscr{I}_n^l = 2\pi \int d(\cos\theta) f_n(\theta) P_l(cos\theta) \tag{7.22}$$

is the Legendre transform of its temperature profile. We can now calculate the power spectrum,

$$\begin{aligned} C_l &= \frac{1}{2l+1} \sum_m |a_{lm}|^2 \\ &= \sum_n \sum_{n'} b_n b_{n'} \mathscr{I}_n^l \mathscr{I}_{n'}^l C_{nn'} \cdot \sum_m \frac{Y_l^{m*}(\hat{\gamma}_n) Y_l^{m*}(\hat{\gamma}_{n'})}{2l+1} \\ &= \sum_n \sum_{n'} b_n b_{n'} \mathscr{I}_n^l \mathscr{I}_{n'}^l C_{nn'} \cdot \frac{P_l(\hat{\gamma}_n \hat{\gamma}_{n'})}{4\pi}, \end{aligned} \tag{7.23}$$

where we have used the completeness relation of the spherical harmonics and $C_{nn'} = \delta_{nn'} + w_{nn'}$, with $w_{nn'}$ taking into account the possibility that the spots are uncorrelated ($\delta_{nn'}$), as for a Poisson distribution, or that are correlated two by two ($w_{nn'}$). Therefore by expanding the sums we finally obtain:

$$C_l = \frac{1}{4\pi} \left[\sum_n b_n^2 (\mathscr{I}_n)^2 + \frac{1}{2} \sum_{n \neq n'} b_n b_{n'} w_{nn'} \mathscr{I}_n^l \mathscr{I}_{n'}^l P_l(\hat{\gamma}_n \hat{\gamma}_{n'}) \right]. \tag{7.24}$$

We assume now that the spots have about the same brightness and the same temperature profile: $b = \langle b_n \rangle$ and $f = \langle f_n \rangle$ where the average is taken over the ensemble of spots. Because the number of spots in a circular ring centered on a single spot is proportional to the angular extension of the ring we can substitute the sums over the number of spots with an integral over the whole sky. Hence we can substitute the discrete correlation coefficient $w_{nn'}$ with the two-point angular correlation of the spots, $w(\alpha)$. If the spots correspond to radio sources or clusters of galaxies $w(\alpha)$ would be the angular correlation function estimated from large scale structure observations. The mean value over the spot distribution of Eq. (7.24) becomes:

$$\langle C_l \rangle = N b^2 \left[\mathscr{I}_l^2 + \mathscr{I}_l \cdot \mathscr{G}_l \right], \tag{7.25}$$

where N is a normalization constant and

$$\mathscr{G}_l = \int_{-1}^{1} d(\cos\alpha) \mathscr{I}_l(\alpha) w(\alpha) P_l(\cos\alpha), \tag{7.26}$$

with

$$\mathscr{I}_l(\alpha) = \int_{-1}^{1} d(\cos\theta) f(\theta+\alpha) P_l(\cos\theta). \tag{7.27}$$

From Eq. (7.25) we may note that the contribution to the anisotropy power spectrum from a localized distribution of spots increases with the brightness b. If the spots are uncorrelated the second term $\mathscr{I}_l \cdot \mathscr{G}_l$ drops from the equation and the only contribution is due to the projection of the spot's signal in the multipole space $\mathscr{I}_l$. In particular the largest contribution will occur in the range of multipoles that correspond to the effective angular size of the spots. If the spots are correlated, the overall contribution to the power spectrum will depend on the sign of $\mathscr{I}_l \cdot \mathscr{G}_l$.

Bispectrum

Following the same procedure as just described we calculate the angular bispectrum. Substituting Eq. (7.21) in Eq. (7.7) we have:

$$\begin{aligned} B_{l_1 l_2 l_3} &= \sum_{m_1,m_2,m_3} \begin{pmatrix} \ell_1 & \ell_2 & \ell_3 \\ m_1 & m_2 & m_3 \end{pmatrix} a_{l_1}^{m_1} a_{l_2}^{m_2} a_{l_3}^{m_3} \\ &= \sum_{n_1,n_2,n_3} b_{n1} b_{n_2} b_{n_3} \mathscr{I}_{n_1}^{l_1} \mathscr{I}_{n_2}^{l_2} \mathscr{I}_{n_3}^{l_3} C_{n_1 n_2 n_3} \\ &\quad \times \sum_{m_1,m_2,m_3} \begin{pmatrix} \ell_1 & \ell_2 & \ell_3 \\ m_1 & m_2 & m_3 \end{pmatrix} Y_{l_1}^{m_1 *}(\hat{\gamma}_{n_1}) Y_{l_2}^{m_2 *}(\hat{\gamma}_{n_2}) Y_{l_3}^{m_3 *}(\hat{\gamma}_{n_3}), \end{aligned} \tag{7.28}$$

where $C_{n_1 n_2 n_3}$ takes into account all the possible correlations between the spots up to third order,

$$C_{n_1 n_2 n_3} = \delta_{n_1 n_2}\delta_{n_2 n_3} + w_{n_1 n_2}\delta_{n_3 n_3} + w_{n_1 n_3}\delta_{n_2 n_2} + w_{n_2 n_3}\delta_{n_1 n_1} + w_{n_1 n_2 n_3}, \tag{7.29}$$

with $w_{n_1 n_2 n_3}$ the correlation between three different spots. Using the definition of the Wigner 3J symbols in terms of an angular integral of three spherical harmonics and the completeness relation of the spherical harmonics Eq. (7.28) becomes:

$$\begin{aligned} B_{l_1 l_2 l_3} = \mathscr{M}_{l_1 l_2 l_3} \Bigg[& \sum_{n_1} b_{n_1}^3 \mathscr{I}_{n_1}^{l_1} \mathscr{I}_{n_1}^{l_2} \mathscr{I}_{n_1}^{l_3} \cdot \mathscr{R}_{\hat{\gamma}_{n_1}}^{l_1 l_2 l_3} + \frac{3}{2} \sum_{n_1 \neq n_2} b_{n_1}^2 b_{n_2} \mathscr{I}_{n_1}^{l_1} \mathscr{I}_{n_1}^{l_2} \mathscr{I}_{n_2}^{l_3} w_{n_1 n_2} \cdot \mathscr{R}_{\hat{\gamma}_{n_1}\hat{\gamma}_{n_2}}^{l_1 l_2 l_3} \\ & + \frac{1}{3} \sum_{n_1 \neq n_2 \neq n_3} \mathscr{I}_{n_1}^{l_1} \mathscr{I}_{n_3}^{l_2} \mathscr{I}_{n_3}^{l_3} w_{n_1 n_2 n_3} \cdot \mathscr{R}_{\hat{\gamma}_{n_1}\hat{\gamma}_{n_2}\hat{\gamma}_{n_3}}^{l_1 l_2 l_3} \Bigg], \end{aligned} \tag{7.30}$$

where

$$\mathscr{M}_{l_1 l_2 l_3} = \frac{(4\pi)^{3/2}}{\sqrt{(2l_1+1)(2l_2+1)(2l_3+1)}} \begin{pmatrix} \ell_1 & \ell_2 & \ell_3 \\ 0 & 0 & 0 \end{pmatrix}^{-1}, \tag{7.31}$$

$$\mathscr{R}^{l_1 l_2 l_3}_{\hat{\gamma}_{n_1}} = \int d\Omega_\gamma P_{l_1}(\hat{\gamma}\cdot\hat{\gamma}_{n_1}) P_{l_2}(\hat{\gamma}\cdot\hat{\gamma}_{n_1}) P_{l_3}(\hat{\gamma}\cdot\hat{\gamma}_{n_1}), \tag{7.32}$$

$$\mathscr{R}^{l_1 l_2 l_3}_{\hat{\gamma}_{n_1}\hat{\gamma}_{n_2}} = \int d\Omega_\gamma P_{l_1}(\hat{\gamma}\cdot\hat{\gamma_{n_1}}) P_{l_2}(\hat{\gamma}\cdot\hat{\gamma}_{n_1}) P_{l_3}(\hat{\gamma}\cdot\hat{\gamma}_{n_2}), \tag{7.33}$$

$$\mathscr{R}^{l_1 l_2 l_3}_{\hat{\gamma}_{n_1}\hat{\gamma}_{n_2}\hat{\gamma}_{n_3}} = \int d\Omega_\gamma P_{l_1}(\hat{\gamma}\cdot\hat{\gamma_{n_1}}) P_{l_2}(\hat{\gamma}\cdot\hat{\gamma_{n_2}}) P_{l_3}(\hat{\gamma}\cdot\hat{\gamma_{n_3}}). \tag{7.34}$$

Due to the background isotropy of the space, we are free to choose $\hat{\gamma} = \hat{\gamma}_{n_1}$. As consequence the integrals Eq. (7.32-7.34) become:

$$\mathscr{R}^{l_1 l_2 l_3}_{\hat{\gamma}_{n_1}} = 4\pi, \tag{7.35}$$

$$\mathscr{R}^{l_1 l_2 l_3}_{\hat{\gamma}_{n_1}\hat{\gamma}_{n_2}} = \int d\Omega_{\gamma_{n_1}} P_{l_3}(\hat{\gamma}\cdot\hat{\gamma_{n_2}}), \tag{7.36}$$

$$\mathscr{R}^{l_1 l_2 l_3}_{\hat{\gamma}_{n_1}\hat{\gamma}_{n_2}\hat{\gamma}_{n_3}} = \int d\Omega_{\gamma_{n_1}} P_{l_2}(\hat{\gamma}\cdot\hat{\gamma}_{n_2}) P_{l_3}(\hat{\gamma}\cdot\hat{\gamma}_{n_3}). \tag{7.37}$$

As for the power spectrum, we can average over the ensemble of all the spots and substitute the sums over the spots with integrals over the whole sky. In this case the discrete correlation coefficient $w_{n_i n_j}$ and $w_{n_i n_j n_k}$ are replaced with the corresponding angular correlation function $w(\alpha)$ and $w(\alpha,\beta)$. After tedious calculations we obtain:

$$\langle B_{l_1 l_2 l_3}\rangle = 4\pi^2 \mathscr{M}_{l_1 l_2 l_3} b^3 \left[\mathscr{B}^{(0)} + \frac{3}{2}\mathscr{B}^{(1)} + \frac{1}{3}\mathscr{B}^{(3)}\right], \tag{7.38}$$

where

$$\mathscr{B}^{(0)} = \mathscr{I}_{l_1}\mathscr{I}_{l_2}\mathscr{I}_{l_3}, \tag{7.39}$$

$$\mathscr{B}^{(1)} = \mathscr{I}_{l_1}\mathscr{I}_{l_2}\mathscr{G}_{l_3}, \tag{7.40}$$

$$\mathscr{B}^{(2)} = \mathscr{I}_{l_1}\int_{-1}^{1} d(\cos\alpha)\int_{-1}^{1} d(\cos\beta)\mathscr{I}_{l_2}(\alpha)\mathscr{I}_{l_3}(\beta) w(\alpha,\beta) P_{l_2}(\cos\alpha) P_{l_3}(\cos\beta), \tag{7.41}$$

with $\mathscr{I}_l$ and $\mathscr{G}_{l_3}$ defined by Eq. (7.22) and Eq. (7.26) respectively and $\mathscr{I}_l(\alpha)$ defined by Eq. (7.27). As we can see from Eq. (7.38) for a Poisson distribution $\mathscr{B}^{(1)}$ and $\mathscr{B}^{(2)}$ vanish, but the bispectrum remains non-vanishing due to the term $\mathscr{B}^{(0)}$ that account for the localized structure of the anisotropies.

7.4 Discussion

In the previous section we presented a general formalism to calculate the contribution to the power spectrum and the bispectrum of a distribution of spots in the CMB sky. The formulae Eq. (7.25) and Eq. (7.38) have to be considered as a starting point for further investigation. They take into account several effects, for instance the brightness and the

angular size of the signals contribute at zeroth order to the spectrum and the bispectrum. On the other hand the presence of internal correlations in the spot distribution, which are described by the angular correlation functions $w(\alpha)$ and $w(\alpha, \beta)$, contribute as first and second order effects respectively. As a specific application, Eq. (7.25) and Eq. (7.38) can be computed in the case of a distribution of spots caused by the SZ effect of a cluster of galaxies. Approximating the shape of this signal with a Gaussian profile characterized by a given width, it will be possible to numerically compute the integrals Eq. (7.22). Moreover without loss of generality the angular correlation function $w(\alpha)$ can be assumed to be a power law. In such a case the integrals Eq. (7.26) can also be numerically computed. The resulting power spectrum can be compared with the prediction of numerical simulations. This will allow us to test how crucial is the assumption that $b = \langle b_n \rangle$ and $f = \langle f_n \rangle$. The next generation of CMB measurements will measure the bispectrum at very high multipoles, therefore using Eq. (7.38) in a specific case such as the SZ effect offers an alternative way of inferring cosmological information.

Conclusion and prospects

In this thesis we have discussed various aspects of dark energy dominated cosmologies. In Chapter 1 we have reviewed the observational evidence of the dark energy. We have seen that different cosmological measurements are consistent only if the dark energy accounts for most of the matter content of the Universe. In Chapter 2 we have discussed some of the proposed dark energy candidates and we have focused on the quintessence scenario. In spite of the theoretical difficulties of a viable quintessence model building, this scenario has a number of interesting features that can be tested with cosmological measurements. In particular in Chapter 3 we reviewed the dynamics of scalar field perturbations for two different class of minimally coupled quintessence models. We have learnt that quintessence perturbations have no active role during the structure formation. However their presence can lead to time integrated effects in the evolution of the gravitational potential. Therefore they can leave a characteristic imprint in the Cosmic Microwave Background anisotropy power spectrum through the Integrated Sachs-Wolfe effect. In Chapter 4 we have constrained with Sn Ia data and the position of the CMB peaks a parameterized quintessence potential that accounts for a large class of quintessence models. Using the properties of the tracker regime we have been able to put upper limits on the present value of the quintessence equation of state. We have found that by the present time the scalar field is evolving in flat region or close to a minimum of its potential. However the results of this analysis clearly indicate that the possibility the quintessence equation of state was largely different from its present value cannot be excluded. In this direction a lot of effort has been made to detect time variation of the quintessence with cosmological distance measurements. In Chapter 5 we reviewed some of the proposed methods and we pointed out a number of potential problems. In particular the use of a constant equation of state to parameterize the dark energy leads to misleading conclusions. Using a very general

argument we showed that if the dark energy is time varying the constraints on a constant equation of state will be pushed towards large negative values. Therefore all the results obtained using this approach have to be carefully interpreted. In particular the fact that several data analysis found the equation of state best fit value to be $w \lesssim -1$ can be just a bias effect. On the contrary we have proposed a time parameterization of the dark energy equation of state in terms of physical parameters. This accounts for most of the proposed dark energy models and moreover is valid at all the redshifts. Hence this approach allows us to take into account in a model independent way not only the effects dark energy has had on the expansion rate of the Universe but also on the structure formation. In Chapter 5 we have applied this parameterization to study the dark energy effects in the CMB power spectrum. As conjectured in Chapter 3 we have found that the dark energy leaves a characteristic imprint through the ISW effect. The amplitude of this signature selects the class of models which are distinguishable from the cosmological constant scenario. In particular we have shown that using ideal CMB data, only models characterized by a rapid transition of the equation of state can be distinguished from the Λ case. In Chapter 7 we have introduced an alternative cosmological test using higher order statistics of the CMB anisotropies. We have computed the spectrum and the bispectrum for a distribution of localized non-Gaussian anisotropies. These can be applied to specific cases such as the SZ effect to constrain cosmological parameters through the non-gaussianity produced by the imprint of cluster of galaxies. We can find a number of directions where the work so far reviewed can be further extended. Under some general assumptions it would be interesting to test the formulae developed in Chapter 7 with the predictions of the SZ effect from numerical simulations of cluster galaxies [211]. A complete likelihood analysis of the parameterized dark energy equation of state is currently in progress. We make use of the full cosmological data so far available. We intend to extend this analysis to the quasar clustering, that is a good candidate for testing the dark energy [212]. An interesting issue arises from the recent WMAP data. In fact it has been found that the quadrupole and octupole are suppressed in contrast with the prediction of ΛCDM cosmologies [32]. The possibility that this is caused by a cancellation mechanism between the SW and ISW effects due to clustering properties of the dark energy needs further investigation [35]. At moment there are no final conclusions about the nature of the dark energy, luckily the upcoming and future cosmological data will provide a new insight of the dark energy phenomenology. It has to be hoped that such measurements will help us to formulate

the new paradigm of Cosmology that will allows us to correctly address the dark energy problem. The history of science shows that no scientific activity is possible in subjects where no paradigms have been found. Therefore we should ask ourself what direction will the cosmological investigation take if the dark energy problem remains unsolved.

Bibliography

[1] T.S. Kuhn, *The Structure of Scientific Revolutions*, Chicago Univ. Press, (1962).

[2] S. Weinberg, *The cosmological constant problem*, Rev. Mod. Phys. **61**, 1 (1989).

[3] S. M. Carroll, W. H. Press and E. L. Turner, *The cosmological constant* , Ann. Rev. Astron. Astrophys. **30**, 499 (1992).

[4] V. Sahni and A. Starobinsky, *The Case for a Positive Cosmological Lambda-term* , Int. J. Mod. Phys. D**30**, 373 (2000), astro-ph/9904398.

[5] S. M. Carroll, *The cosmological constant*, Living Rev.Rel. **4**, 1 (2001), astro-ph/0004075.

[6] N. Straumann, *On the Cosmological Constant Problems and the Astronomical Evidence for a Homogeneus Energy Density with Negative Preassure*, astro-ph/0203330.

[7] A. D. Dolgov, *Mystery of vacuum energy or rise and fall of cosmological constant*, hep-ph/0203245.

[8] A. Einstein, *Cosmological Considerations in the General Theory of Relativity*, Sitzungsber. Preuss. Akad. Wiss. Berlin (Math. Phys.), 142 (1917)

[9] W. de Sitter, Proc. Acad. Sci. **19**, 1217 (1917); and **20**, 229 (1917).

[10] A. Friedmann, Z. Phys. **10**, 377 (1922).

[11] A. Friedmann, Z. Phys. **21**, 326 (1924).

[12] E. Hubble, Proc. N.A.S. **15**, 168 (1929).

[13] V. Petrosian, E. Salpter and P. Szekeres, Astrophys. J. **147**, 1222 (1967).

[14] J. Shklovsky, Astrophys. J. Lett. **150**, L1 (1967).

[15] N. Kardashev, Astrophys. J. Lett. **150**, L135 (1967).

[16] T. Padmanabham, *Cosmological constant - The weight of the vacuum*, hep-th/0212290.

[17] R.A. Sunyaev and Ya. B. Zeldovich, Astrophysics and Space Science 7, 3-19 (1970).

[18] P.J.E. Peebles and J.T. Yu, *Primeval Adiabatic Perturbation in an Expanding Universe*, Astrophys. J. **162**, 815 (1970).

[19] P. De Bernardis et al. (Boomerang Collaboration), *A Flat Universe from High-Resolution Maps of the Cosmic Microwave Background Radiation*, Nature **404**, 955 (2000), astro-ph/0004404.

[20] A.E. Lange et al., *First Estimations of Cosmological Parameters from BOOMERANG*, Phys. Rev. D**63**, 042001 (2001), astro-ph/0005004.

[21] C.B. Netterfield et al., *A measurement by BOOMERANG of multiple peaks in the angular power spectrum of the cosmic microwave background*, Astrophys.J. **571**, 604 (2002), astro-ph/0104460.

[22] J.E. Ruhl et al., *Improved Measurement of the Angular Power Spectrum of Temperature Anisotropy in the CMB from Two New Analyses of BOOMERANG Observations*, astro-ph/0212229.

[23] A. Balbi et al., *Constraints on Cosmological Parameters from MAXIMA-1*, Astrophys. J. **558**, L145 (2001), astro-ph/0005124.

[24] C. Pryke et al., *Cosmological Parameter Extraction from the First Season of Observations with DASI*, Astrophys.J. **568**, 46 (2002), astro-ph/0104490.

[25] J.L. Sievers et al., *Cosmological Parameters from Cosmic Background Imager Observations and Comparisons with BOOMERANG, DASI, and MAXIMA*, astro-ph/0205387.

[26] A. Benoit et al., *Cosmological constraints from Archeops*, astro-ph/0210306.

[27] K. Grainge et al., *The CMB power spectrum out to l=1400 measured by the VSA*, astro-ph/0212495.

[28] J.H. Goldstein et al., *Estimates of Cosmological Parameters Using the CMB Angular Power Spectrum of ACBAR*, astro-ph/0212517.

[29] W.L. Freedman et al., *Final Results from the Hubble Space Telescope Key Project to Measure the Hubble Constant* Astrophys. J. **553**, 47 (2001), astro-ph/0012376.

[30] C.L. Bennett et al., *First Year Wilkinson Microwave Anisotropy Probe (WMAP) Observations: Preliminary Maps and Basic Results*, astro-ph/0302207.

[31] L. Page et al., *Interpretation of the TT and TE Angular Power Spectrum Peaks*, astro-ph/0302220.

[32] D.N. Spergel et al., *First Year Wilkinson Microwave Anisotropy Probe (*WMAP*) Observations: Determination of Cosmological Parameters*, astro-ph/0302209.

[33] A. Kogut et al., *Wilkinson Microwave Anisotropy Probe (WMAP) First Year Observations: TE Polarization*, astro-ph/0302213.

[34] X. Fan et al., *Evolution of the Ionizing Background and the Epoch of Reionization from the Spectra of z 6 Quasars*, Astrophys. J. **123**, 1247 (2002), astro-ph/0111184.

[35] C. Contaldi, M. Peloso, L. Kofman and A. Linde, *Suppressing the lower Multipoles in the CMB Anisotropies*, astro-ph/0303636.

[36] G. Efstathiou, *Is the Low CMB Quadrupole a Signature of Spatial Curvature?*, astro-ph/0303127.

[37] W.J. Percival et al., *The 2dF Galaxy Redshift Survey: the power spectrum and the matter content of the Universe*, Mon. Not. Roy. Astron. Soc. **327**, 1297 (2001), astro-ph/0105252.

[38] S. Dodelson et al., *The 3D power spectrum from angular clustering of galaxies in early SDSS data* Astrophys. J. **572**, 140 (2001), astro-ph/0107421.

[39] G. Efstathiou et al., *Evidence for a non-zero Lambda and a low matter density from a combined analysis of the 2dF Galaxy Redshift Survey and Cosmic Microwave Background Anisotropies*, astro-ph/0109152.

[40] L. Silberman, A. Dekel, A. Eldar and I. Zehavi, *Cosmological density and power spectrum from peculiar velocities: non linear corrections and PCA*, Astrophys. J. **557**, 102 (2001), astro-ph/0101361.

[41] S.W. Allen, R.W. Schmidt, A.C. Fabian and H. Ebeling, *Cosmological constraints from the local X-ray luminosity function of the most X-ray luminous galaxy clusters*, astro-ph/0208394.

[42] P.T.P. Viana et al., *The power spectrum amplitude from clusters revisited: σ_8 using simulations with preheating and cooling*, astro-ph/0211090.

[43] A. Vikhlinin et al., *Cosmological constraints from evolution of cluster baryon mass function at $z \sim 0.5$*, astro-ph/0212075.

[44] J.J. Mohr, B. Mathiesen and A.E. Evrard, *Properties of the Intracluster Medium in an Ensemble of Nearly Galaxy Clusters*, Astrophys. J. **517**, 627 (1999).

[45] S.W. Allen, R.W. Schmidt and A.C. Fabian, *Cosmological constraints from the X-ray gas mass fraction in relaxed lensing clusters observed by Chandra*, Mon. Not. Roy. Astron. Soc. **334**, L11 (2002), astro-ph/0205007.

[46] K.H. Chae et al., *Constraints on Cosmological Parameters from the Analysis of the Cosmic Lens All Sky Survey Radio-Selected Gravitational Lens Statistics*, Phys. Rev. Lett **89**, 151301 2002.

[47] B. Chaboyer, P. Demarque, P. J. Kernan and L. M. Krauss, *The Age of Globular Clusters in Light of Hipparcos: Resolving the Age Problem?*, Astrophys. J. **494**, 96 (1998).

[48] J. S. Alcaniz and J. A. S. Lima, *New limits on Ω_Λ and Ω_m from old galaxies at high redshift*, Astrophys. J. **521**, L87 (1999), astro-ph/9902298.

[49] W. Hillebrandt and J.C. Niemeyer, *Type Ia Supernova Explosion Models*, Ann. Rev. Astron. Astrophys. **38**, 191 (2000), astro-ph/0006305.

[50] B. Leibundgut, *Type Ia Supernovae*, Astron. Astrophys. Rev. **39**, 67 (2001), astro-ph/0003326.

[51] S.J. Perlmutter at al., *Discovery of a Supernova Explosion at Half the Age of the Universe and its Cosmological Implications*, Nature **391**, 51 (1998), astro-ph/9712212.

[52] A.G. Riess et al., *Observational Evidence from Supernovae for an Accelerating Universe and a Cosmological Constant*, Astron. J. **116**, 1009 (1998), astro-ph/9805201.

[53] S.J. Perlmutter at al., *Measurements of Omega and Lambda from 42 High-Redshift Supernovae*, Astrophys. J. **517**, 565 (1999), astro-ph/9805201.

[54] A.G. Riess et al., *The Farthest Known Supernova: Support for an Accelerating Universe and a Glimpse of the Epoch of Deceleration*, Astrophys.J. **560**, 49 (2001), astro-ph/0104455.

[55] M. Sullivan et al., *The Hubble Diagram of Type Ia Supernovae as a Function of Host Galaxy Morphology*, Mont. Not. Roy. Astron. Soc. **340**, 1057, astro-ph/0211444.

[56] N.A. Bahcall, J.P. Ostriker, S. Perlmutter and P.J. Steinhardt, *The Cosmic Triangle: Assessing the State of the Universe*, Science **284**, 1481 (1999), astro-ph/9906463.

[57] M. Tegmark, D.J. Eisenstein, W. Hu and R. Kron, *Cosmic complementarity: probing the acceleration of the Universe*, astro-ph/9805117.

[58] X. Wang, M. Tegmark, M. Zaldarriaga, *Is cosmology consistent?*, Phys. Rev. D**65**, 123001 (2002), astro-ph/0105091.

[59] Ya. B. Zeldovich, *The cosmological constant and the theory of elementary particles*, Soviet Physics Uspekhi **11**, 381 (1968).

[60] E. Witten, *The Cosmological Constant from the Viewpoint of String Theory*, hep-th/0002297.

[61] J. Garriga and A. Vilenkin, *Solutions to the cosmological constant problems*, Phys. Rev. D**64**, 023517 (2001), hep-th/0011262.

[62] P.C.W. Davies and S. Unwin, Proc. R. Soc. London **377**, 147 (1981).

[63] J.D. Barrow and F.J. Tipler, *The Anthropic Cosmological Principle*, Claredon, Oxford (1986).

[64] S. Weinberg, *Anthropic Bound on the Cosmological Constant*, Phys. Rev. Lett **59**, 2607 (1987).

[65] A. Vilenkin, *Predictions from Quantum Cosmology*, Phys. Rev. Lett **74**, 846 (1995), gr-qc/9507018.

[66] G. Efsthathiou, *An anthropic argument for a cosmological constant*, Mont. Not. Roy. Astron. Soc. **274**, L73 (1995).

[67] H. Martel, P.R. Shapiro and S. Weinberg, *Likely Values of the Cosmological Constant*, Astrophys. J. **492**, 29 (1998), astro-ph/9701099.

[68] R. Bousso and J. Polchinski, *Quantization of Four-form Fluxes and Dynamical Neutralization of the Cosmological Constant*, J. High Energy Phys. **06**, 006 (2000), hep-th/0004134.

[69] M.S. Turner and M.J. White, *CDM models with a smooth component*, Phys. Rev. D**56**, 4439 (1997), astro-ph/9701138.

[70] T. Chiba, N. Sugiyama and T. Nakamura, *Cosmology with X-matter*, Mon. Not. Roy. Astron. Soc. *289*, L5 (1997), astro-ph/9704199.

[71] T. Chiba, N. Sugiyama and T. Nakamura, *Observational tests of X-matter models*, Mon. Not. Roy. Astron. Soc. *301*, 72 (1998), astro-ph/9806332.

[72] C. Wetterich, *Cosmology and the fate of dilatation symmetry*, Nucl. Phys. B **302**, 668 (1988).

[73] B. Ratra and P.J.E. Peebles, *Cosmological consequences of a rolling homogeneus scalar field*, Phys. Rev. D**37**, 3406 (1988).

[74] J.A. Frieman, C.T. Hill, A. Stebbins and I. Waga, *Cosmology with ultralight pseudo Nambu-Goldstone bosons*, Phys. Rev. Lett. **75**, 2077 (1995), astro-ph/9505060.

[75] K. Coble, S. Dodelson and J.A. Frieman, *Dynamical Lambda models of structure formation*, Phys. Rev. D **55** (1997), astro-ph/9608122.

[76] R.R. Caldwell, R. Dave and P.J. Steinhardt, *Cosmological Imprint of an Energy Component with General Equation of State* Phys. Rev. Lett. **80**, 1582 (1998), astro-ph/9708069.

[77] P.G. Ferreira and M. Joyce, *Cosmology with a Primordial Scaling Field*, Phys. Rev. D**58**, 023503 (1998), astro-ph/9711102.

[78] C. Wetterich, *The Cosmon Model for an Asymptotically Vanishing Time-Dependent Cosmological "Constant"*, Astron. & Astrophys. **361**, 321 (1995), hep-th/9408025.

[79] I. Zlatev, L. Wang and P.J. Steinhardt, *Quintessence, Cosmic Coincidence, and the Cosmological Constant*, Phys. Rev. Lett. **82**, 896 (1999), astro-ph/9807002.

[80] P.J. Steinhardt, L. Wang and I. Zlatev, *Cosmological Tracking Solutions*, Phys. Rev. D**59**, 12350 (1999), astro-ph/9812313.

[81] C. Kolda and D.H. Lyth, *Quintessential Difficulties*, Phys. Lett. B**458**, 197 (1999), hep-ph/9811375.

[82] L. Amendola, *Coupled Quintessence*, Phys. Rev. D**62**, 043511 (2000), astro-ph/9908023.

[83] D.J. Holden and D. Wands, *Self-similar cosmological solutions with a non-minimally coupled scalar field*, Phys. Rev. D**61**, 043506 (2000), gr-qc/9908026.

[84] L. Amendola and D. Tocchini-Valentini, *Stationary dark energy: the present universe as a global attractor*, Phys. Rev. D**64**, 043509 (2001), astro-ph/0011243.

[85] R. Bean and J. Magueijo, *Dilaton-derived quintessence scenario leading naturally to the late-time acceleration of the Universe*, Phys. Lett. B**517**, 177 (2001), astro-ph/0007199.

[86] L. Amendola, *Acceleration at $z > 1$?*, astro-ph/0209494.

[87] P. Binetruy, *Models of dynamical supersymmetry breaking and quintessence*, Phys. Rev. D**60**, 063502 (1999), hep-ph/9810553.

[88] A. Masiero, M. Pietroni and F. Rosati, *SUSY QCD and Quintessence*, Phys. Rev. D**61**, 023504 (2000), hep-ph/9905346.

[89] M. Gasperini, *Dilatonic Interpratation of the Quintessence*, Phys. Rev. D**64**, 043510 (2001), gr-qc/010582.

[90] M. Gasperini, F. Piazza and G. Veneziano, *Quintessence as a run-away Dilaton*, Phys. Rev. D**65**, 023508 (2001), hep-ph/0108016.

[91] E. Witten, *Some Properties of O(32) Superstrings*, Phys. Lett. B**149**, 351 (1984).

[92] T. Damour, F. Piazza and G. Veneziano, *Violations of the Equivalence Principle in a Dilaton-Runaway Scenario*, Phys. Rev. D**66**, 046007 (2002), hep-th/0205111.

[93] C. Wetterich, *Crossover quintessence and cosmological history of fundamental "constants"*, hep-ph/0301261.

[94] N. Bartolo and M. Pietroni, *Scalar-Tensor Gravity and Quintessence*, Phys. Rev. D**61**, 023518 (2000), hep-ph/9908521.

[95] M. Pietroni, *Brane Worlds and the Cosmic Coincidence Problem*, hep-ph/0203085.

[96] P. Brax and J. Martin, *Quintessence and Supergravity*, Phys. Lett. B**468**, 40 (1999), astro-ph/9905040.

[97] P. Brax and J. Martin, *The Robustness of Quintessence*, Phys. Rev. D**61**, 103502 (2000), astro-ph/9912046.

[98] P. Brax, J. Martin and A. Riazuelo, *Quintessence with two energy scales*, Phys. Rev. D**64**, 083505 (2001), hep-ph/0104240.

[99] K. Choi, *String or M theory axion as a quintessence*, Phys. Rev. D**62**, 043509 (2000), hep-ph/9902292.

[100] T. Barreiro, E.J. Copeland and N.J. Nunes, *Quintessence arising from exponential potentials*, Phys. Rev. D/textbf61, 127301 (2001), astro-ph/9910214.

[101] E.J. Copeland, N.J. Nunes and F. Rosati, *Quintessence models in Supergravity*, Phys. Rev. D**62**, 123503 (2002), hep-ph/0005222.

[102] J.M. Cline, *Quintessence, Cosmological Horizons, and Self-Tuning*, JHEP **0108**, 035 (2001), hep-ph/0105251.

[103] R. Bean, S.H. Hansen and A. Melchiorri, *Early-universe constraints on a Primordial Scaling Field*, Phys. Rev. D**64**, 103508 (2001), astro-ph/0104162.

[104] R.R. Caldwell, M. Doran, C.M. Mueller, G. Schaefer and C. Wetterich, *Early Quintessence in Light of WMAP*, astro-ph/0302505.

[105] F. Perrotta and C. Baccigalupi, *Early time perturbations behaviour in scalar field cosmologies* Phys. Rev. D**59**, 123508 (1999), astro-ph/9811156.

[106] P. Brax, J. Martin and A. Riazuelo, *Exhaustive Study of Cosmic Microwave Background Anisotropies in Quintessential Scenarios* Phys. Rev. D**62**, 103505 (2000), astro-ph/0005428.

[107] P.T.P Viana and A.R. Liddle, *Perturbation evolution in cosmologies with a decaying cosmological constant*, Phys. Rev. D**57**, 674 (1998), astro-ph/9708247.

[108] L.R. Abramo and F. Finelli, *Attractors and Isocurvature Perturbations in Quintessence Models*, Phys. Rev. D**64**, 083513 (2001), astro-ph/0101014.

[109] M. Malquarti and A.R. Liddle, *Evolution of large-scale perturbations in quintessence models* Phys. Rev. D**66**, 123506 (2002), astro-ph/0208562.

[110] P.S. Corasaniti and E.J. Copeland, *Constraining the quintessence equation of state with SnIa data and CMB peaks*, Phys. Rev. D**65**, 043004 (2002), astro-ph/0107378.

[111] A. Vilenkin, *String-Dominated Universe*, Phys. Rev. Lett. **53**, 1016 (1984).

[112] P. Garnavich at al., *Supernova Limits on the Cosmic Equation of State*, Astrophys. J.**509**, 74 (1998), astro-ph/9806396.

[113] S. Perlmutter, M.S. Turner and M. White, *Constraining dark energy with SNe Ia and large-scale structure*, Phys. Rev. Lett. **83**, 670 (1999), astro-ph/9901052.

[114] G. Efstathiou, *Constraining the equation of state of the Universe from Distant Type Ia Supernovae and Cosmic Microwave Background Anisotropies*, Mont. Not. Roy. Astron. Soc. **342**, 810 (2000), astro-ph/9904356.

[115] T.D. Saini, S. Raychaudhury, V. Sahni and A.A. Starobinsky, *Reconstructing the Cosmic Equation of State from Supernova distances*, Phys. Rev. Lett. **85**, 1162 (2000), astro-ph/9910231.

[116] I. Waga and J.A. Frieman, *New Constraints from High Redshift Supernovae and Lensing Statistics upon Scalar Field Cosmologies*, Phys. Rev. D**62**, 043521 (2000), astro-ph/0001354.

[117] J.R. Bond et al., *The Quintessential CMB, Past & Future*, astro-ph/0011379.

[118] A. Albrecht and C. Skordis, *Phenomenology of a realistic accelerating universe using only Planck-scale physics*, Phys. Rev. Lett.**84**, 2076 (2000), astro-ph/9908085.

[119] A. Riazuelo and J.P. Uzan, *Cosmological observations in scalar-tensor quintessence*, Phys. Rev. D**66**, 023525 (2002) astro-ph/0107386.

[120] D. Huterer and M.S. Turner, *Probing the dark energy: methods and strategies*, Phys. Rev. D**64**, 123527 (2001), astro-ph/0012510.

[121] W. Hu, *Concepts in CMB Anisotropy Formation*, Lect. Notes Phys. **470**, 207 (1996), astro-ph/9511130.

[122] W. Hu and M. White, *Measuring the Curvature of the Universe*, astro-ph/9606140.

[123] M. Doran and M. Lilley, *The Location of CMB Peaks in a Universe with Dark Energy*, Mon. Not. Roy. Astron. Soc. **330**, 965 (2002), astro-ph/0104486.

[124] M. Doran, M. Lilley, J. Schwindt and C. Wetterich, *Quintessence and the Separation of CMB Peaks*, Astrophys. J. **559**, 501 (2001), astro-ph/0012139.

[125] M. Doran, M. Lilley and C. Wetterich, *Constraining Quintessence with the New CMB Data*, Phys. Lett. B**528**, 175 (2002), astro-ph/0105457.

[126] W. Hu, N. Sugiyama and J. Silk, *The Physics of Microwave Background Anisotropies*, Nature **386**, 37 (1997), astro-ph/9604166.

[127] F. Perrotta, C. Baccigalupi and S. Matarrese, *Extended Quintessence*, Phys. Rev. D**61**, 023507 (2000), astro-ph/9906066.

[128] C. Baccigalupi, S. Matarrese and F. Perrotta, *Tracking Extended Quintessence*, Phys. Rev. D**62**, 123510 (2000), astro-ph/0005543.

[129] P. Brax, J. Martin and A. Riazuelo, *Exhaustive Study of Cosmic Microwave Background Anisotropies in Quintessential Scenarios*, Phys. Rev. D*62*, 103505 (2000), astro-ph/0005428.

[130] G. Efstathiou et al., *Constraints on Omega$_\Lambda$ and Omega$_m$ from Distant Type 1a Supernovae and Cosmic Microwave Background Anisotropies*, Mon. Not. Roy. Astron. Soc. **303**, L47 (1999), astro-ph/9812226.

[131] De Bernardis et al., *Multiple Peaks in the Angular Power Spectrum of the Cosmic Microwave Background: Significance and Consequences for Cosmology*, Astrophys. J. **564**, 559 (2002), astro-ph/0105296.

[132] R. Durrer, B. Novosyadlyj and S. Apunevych, *Acoustic peaks and dips in the CMB power spectrum: observational data and cosmological constraints*, Astrophys. J. **583**, 33 (2003), astro-ph/0111594.

[133] C. Baccigalupi, A. Balbi, S. Matarrese, F. Perrotta and N. Vittorio, *Constraints on flat cosmologies with tracking Quintessence from Cosmic Microwave Background observations*, Phys. Rev. D*65*, 063520 (2002), astro-ph/0109097.

[134] R. Bean and A. Melchiorri, *Current constraints on the dark energy equation of state*, Phys. Rev. D**65**, 041302 (2002), astro-ph/0110472.

[135] B.A. Bassett, M. Kunz, J. Silk and C. Ungarelli, *A late-time transition in the cosmic dark energy?*, Mon. Not. Roy. Astron. Soc. **336**, 1217 (2002), astro-ph/0203383.

[136] M. Doran, J.M. Schwindt and C. Wetterich, *Structure Formation and the Time Dependence of Quintessence*, Phys. Rev. D64, 123520 (2001), astro-ph/0107525.

[137] P.S. Corasaniti and E.J. Copeland, *A Model Independent Approach to the Dark Energy Equation of State*, Phys. Rev. D**65**, 043004 (2002), astro-ph/0107378.

[138] V. Sahni and L. Wang, *A New Cosmological Model of Quintessence and Dark Matter*, Phys. Rev. D**62**, 103517 (2000), astro-ph/9910097.

[139] S. Dodelson, M. Kaplinghat and E. Stewart, *Solving the Coincidence Problem: Tracking Oscillating Energy*, Phys. Rev. Lett. **85**, 5276 (2000), astro-ph/0002360.

[140] Supernova Acceleration Probe, http://snap.lbl.gov.

[141] I. Maor, R. Brustein and P.J. Steinhardt, *Limitations in using luminosity distance to determine the equation of state of the universe*, Phys. Rev. Lett. **86**, 6 (2001); Erratum-ibid. **87**, 049901 (2001), astro-ph/0007297.

[142] I. Maor, R. Brustein, J. McMahon and P.J. Steinhardt, *Measuring the Equation-of-state of the Universe: Pitfalls and Prospects*, Phys. Rev. D**65**, 123003 (2002), astro-ph/0112526.

[143] S. Hannestad and E. Mortsell, *Probing the dark side: Constraints on the dark energy equation of state from CMB large scale structure and Type Ia supernovae*, Phys. Rev. D**66**, 063508 (2002), astro-ph/0205096.

[144] A. Melchiorri, L. Mersini, C.J. Odman and M. Trodden, *The State of the Dark Energy Equation of State*, astro-ph/0211522.

[145] J. Weller and A. Albrecht, *Opportunities for future supernova studies of cosmic acceleration*, Phys. Rev. Lett. **86**, 1939 (2001), astro-ph/0008314.

[146] B.F. Gerke and G. Efstathiou, *Probing quintessence: reconstruction and parameter estimation from supernovae*, Mon. Not. Roy. Astron. Soc. *335*, 33 (2002), astro-ph/0201336.

[147] D. Huterer and M. Turner, *Prospects for probing the dark energy via supernova distance measurements*, Phys. Rev. D**60**, 081301 (1999), astro-ph/9808133.

[148] G. Efstathiou, *Constraining the equation of state of the Universe from Distant Type Ia Supernovae and Cosmic Microwave Background Anisotropies*, Mont. Not. Roy. Astron. Soc. **342**, 810 (2000), astro-ph/9904356.

[149] T. Chiba and T. Nakamura, *Feasibility of Reconstructing the Quintessential Potential Using SNIa Data*, Phys. Rev. D**62**, 121301 (2000), astro-ph/0008175.

[150] T. Nakamura and T. Chiba, *Determining the Equation of State of the Expanding Universe Using a New Independent Variable*, Astrophys. J. **550**, 1 (2001), astro-ph/0011157.

[151] P. Astier, *Can luminosity distance measurements probe the equation of state of dark energy*, Phys. Lett. B **500**, 8 (2001), astro-ph/0008306.

[152] M. Goliath, M. et al., *Supernovae and the Nature of the Dark Energy*, astro-ph/0104009.

[153] J. Weller and A. Albrecht, *Future Supernovae observations as a probe of dark energy*, Phys. Rev. D**65**, 103512 (2002), astro-ph/0106079.

[154] V. Sahni, T.D. Saini, A.A. Starobinsky and U. Alam, *Statefinder – a new geometrical diagnostic of dark energy*, JETP Lett. **77**, 201 (2003), astro-ph/0201498.

[155] U. Alam, V. Sahni, T.D. Saini and A.A. Starobinsky, *Exploring the Expanding Universe and Dark Energy using the Statefinder Diagnostic*, astro-ph/0303009.

[156] D. Huterer and G. Starkman, *Parameterization of Dark-Energy Properties: a Principal-Component Approach*, Phys. Rev. Lett. **90**, 031301 (2003), astro-ph/0207517.

[157] C. Armendariz-Picon, V. Mukhanov and P.J. Steinhardt, *A Dynamical Solution to the Problem of a Small Cosmological Constant and Late-time Cosmic Acceleration*, Phys. Rev. Lett. **85**, 4438 (2000), astro-ph/0004134.

[158] L. Parker and A. Raval, *Vacuum effects of ultra-low mass particle account for Recent Acceleration of Universe*, Phys. Rev. D**60**, 123502 (1999), gr-qc/9908013.

[159] M. Yahiro et al., *Constraints on Cosmic Quintessence and Quintessential Inflation*, Phys. Rev. D**65**, 063502 (2002), astro-ph/0106349.

[160] R. Dave, R.R. Caldwell, P.J. Steinhardt, *Sensitivity of the Cosmic Microwave Background Anisotropy to Initial Conditions in Quintessence Cosmology* Phys. Rev. D*66*, 023516 (2002), astro-ph/0206372.

[161] P.S. Corasaniti, B.A. Bassett, C. Ungarelli and E.J. Copeland, *Model-independent dark energy differentiation with the ISW effect*, Phys. Rev. Lett. **90**, 091303 (2003), astro-ph/0210209.

[162] P.S. Corasaniti, *Dark energy effects in the Cosmic Microwave Background Radiation*, Proceedings of the XVIII IAP Colloquium 'On the nature of dark energy', Paris, 1-5 July 2002, astro-ph/0210257.

[163] G. Smoot et al., *Preliminary results from the COBE differential microwave radiometers - Large angular scale isotropy of the cosmic microwave background* Astrophys. J. Lett. **371**, L1 (1991).

[164] A. Liddle and D. Lyth, *Cosmological Inflation and Large Scale Structure*, Cambridge University Press, (2000).

[165] M.L. Wilson, *On the anisotropy of the cosmological background matter and radiation distribution. II - The radiation anisotropy in models with negative spatial curvature*, Astrophys. J. **273**, 2 (1983).

[166] N. Gouda, N. Sugiyama and M. Sasaki, *Large Angle Anisotropy of the Cosmic Microwave Background in an Open Universe*, Prog. Theor. Phys. **85**, 1023 (1991).

[167] W. Hu and N. Sugiyama, *Anisotropies in the Cosmic Microwave Background: an analytic approach*, Astrophys. J. **444**, 489 (1995), astro-ph/9407093.

[168] R.K. Sachs and A.M. Wolfe, *Perturbations of a Cosmological Model and Angular Variations of the Microwave Backgroud*, Astrophys. J. **147**, 73 (1967).

[169] W. Hu and N. Sugiyama, *Toward understanding CMB anisotropies and their implications* Phys. Rev. D**51**, 2599 (1995).

[170] M.J. Rees and D.W. Sciama, Nature **217**, 511 (1968).

[171] J. Silk, *Cosmic Black-Body Radiation and Galaxy Formation*, Astrophys. J. **151**, 459 (1968).

[172] R.G. Crittenden and N. Turok, *Looking for a Cosmological Constant with the Rees-Sciama Effec*, Phys. Rev. Lett. **76**, 575 (1996), astro-ph/9510072.

[173] C.P. Ma, R.R. Caldwell, P. Bode and L. Wang, *The Mass Power Spectrum in Quintessence Cosmological Models*, Astrophys. J. **521**, L1-L4 (1999), astro-ph/9906174.

[174] W. Hu, *Structure Formation with Generalized Dark Matter*, Astrophys. J **506**, 485 (1998), stro-ph/9801234.

[175] L. Parker and A. Raval, *Non-perturbative effects of vacuum energy on the recent expansion of the universe*, Phys. Rev. D**60**, 123502 (1999), gr-qc/9905031.

[176] C.T. Hill and A.K. Leibovich, *Natural Theories of Ultra-Low Mass PNGB's: Axions and Quintessence*, Phys. Rev. D**66**, 075010 (2002), hep-ph/0205237.

[177] C. Wetterich, *Can Structure Formation Influence the Cosmological Evolution?*, Phys. Rev. D*67*, 043513 (2003), astro-ph/0111166.

[178] U. Seljak and M. Zaldarriaga, *A line of sight approach to Cosmic Microwave Background anisotropies*, Astrophys. J. **469**, 437 (1996), astro-ph/9603033.

[179] W. Hu, M. Fukugita, M. Zaldarriaga and M. Tegmark, *CMB Observables and Their Cosmological Implications*, Astrophys. J. **549**, 699 (2001), astro-ph/0006436.

[180] J.K. Erickson, R.R. Caldwell, P.J. Steinhardt, C. Armendariz-Picon and V. Mukhanov, *Measuring the Speed of Sound of Quintessence*, Phys. Rev. Lett. **88**, 121301 (2002), astro-ph/0112438.

[181] W. Hu, *Dark Synergy: Gravitational Lensing and the CMB*, Phys. Rev. D**65**, 023003 (2002), astro-ph/0108090.

[182] A. Cooray, *The integrated Sachs-Wolfe Effect – Large Scale Structure Correlation*, Phys. Rev. D**65**, 103510 (2002), astro-ph/0112408.

[183] S.P. Boughn, R.G. Crittenden, *Cross-Correlation of the Cosmic Microwave Background with Radio Sources: Constraints on an Accelerating Universe*, astro-ph/0111281.

[184] I. Wasserman, *On the Degeneracy Inherent in Observational Determination of the Dark Energy Equation of State*, Phys. Rev. D**66**, 123511 (2002), astro-ph/0203137.

[185] J.A. Frieman, D. Huterer, E.V. Linder and M.S. Turner, *Probing Dark Energy with Supernovae: Exploiting Complementarity with the Cosmic Microwave Background*, Phys. Rev. D**67**, 083505 (2003), astro-ph/0208100.

[186] A. Guth and Y.S. Pi, Phys. Rev. Lett. **49**, 1110 (1982).

[187] J.M. Bardeen, P.J. Steinhardt and M.S. Turner, Phys. Rev. D**28**, 670 (1983).

[188] A. Kogut et al., *Tests for Non-Gaussian Statistics in the DMR Four-Year Sky Maps*, Astrophys. J. L**29**, 439 (1996), astro-ph/9601062.

[189] A. Gaungui, F. Lucchin, S. Matarrese and S. Mollerach, *The Three–Point Correlation Function of the Cosmic Microwave Background in Inflationary Models*, Astrophys. J. **430**, 447 (1994), astro-ph/9312033.

[190] A. Gangui and S. Mollerach. *Cosmic Microwave Background non-Gaussian signatures from analytical texture models*, Phys. Rev. D**54**, 4750 (1996), astro-ph/9601069.

[191] A. Gangui, *Textures and Cosmic Microwave Background non-Gaussian Signatures*, Helv. Phys. Acta **69**, 215 (1996), astro-ph/9711343.

[192] P.S. Corasaniti, L. Amendola and F. Occhionero, *Present Limits to Cosmic Bubbles from COBE-DMR Three Point Correlation Function*, Mon. Not. Roy. Astron. Soc. **323**, 677 (2001), astro-ph/0005575.

[193] E. Gaztanaga, J. Wagg, T. Multamaki, A. Montana and D.H. Hughes, *2-point anisotropies in WMAP and the Cosmic Quadrupole*, astro-ph/0304178.

[194] J. Magueijo, *Cosmic Confusion* Phys. Lett. B**342**, 32 (1995).

[195] P. Ferreira, J. Magueijo and K.M. Gorski, *Evidence for non-Gaussianity in the COBE DMR Four Year Sky Maps*, Astrophys. J. **503**, L1 (1998), astro-ph/9803256.

[196] J. Magueijo, P. Ferreira and K.M Gorski, *Evidence for non-Gaussianity in the CMB*, astro-ph/981041.

[197] A.J. Banday, S. Zaroubi and K.M. Gorski, *On the Non-Gaussianity Observed in the COBE-DMR Sky Maps* Astrophys. J. **533**, 575 (1999), astro-ph/9908070.

[198] E. Komatsu et al., *Measurement of the cosmic microwave background bispectrum on the COBE DMR sky maps*, Astrophys. J. **566**, 19 (2002), astro-ph/0107605.

[199] N.G. Phillips and A. Kogut, *Statistical Power, the Bispectrum and the Search for Non-Gaussianity in the CMB Anisotropy*, Astrophys. J. **548**, 540 (2001), astro-ph/0010333.

[200] E. Komatsu et al., *First Year Wilkinson Microwave Anisotropy Probe (WMAP) Observations: Tests of Gaussianity*, astro-ph/0302223.

[201] C.R. Contaldi and J. Magueijo, *Generating non-Gaussian maps with a given power spectrum and bispectrum*, astro-ph/0101512.

[202] M. Kendall, A. Stuart and J.K. Ord, *Advanced Theory of Statistics* Oxford University Press, New York, Vol. 1, (1979).

[203] Ya.B. Zeldovich and R.A. Sunyaev, Astrophys. Space. Sci. **4**, 301 (1969).

[204] A. Vilenkin and E.P.S. Shellard, *Cosmic Strings and Other Topological Defects*, Cambridge University Press, (1995).

[205] F. Occhionero and L. Amendola, *Primordial Bubbles from Quadratic Gravity*, Phys. Rev. D**50**, 4846 (1994).

[206] C. Baccigalupi, L. Amendola and F. Occhionero, *Imprints of Primordial Voids on the CMB*, Mont. Not. Roy. Astron. Soc. **288**, 387 (1997), astro-ph/9611038.

[207] S Mollerach, A. Gangui, F. Lucchin and S. Matarrese, *Contribution to the Three–Point Function of the Cosmic Microwave Background from the Rees–Sciama Effect*, Astrophys. J. **453**, 1 (1995), astro-ph/9503115.

[208] J. Magueijo, *Analytical modeling of large-angle CMBR anisotropies from textures*, Phys. Rev. D**52**, 4361 (1995), astro-ph/9504042.

[209] D.M. Goldberg and D.N. Spergel, *The Microwave Background Bispectrum, Paper II: A Probe of the Low Redshift Universe*, Phys. Rev. D**59**, 103002 (1999), astro-ph/9811251.

[210] P.G. Castro, *The Bispectrum and the Trispectrum of the Ostriker and Vishniac Effect*, astro-ph/0212500.

[211] A.C. da Silva, D. Barbosa, A.R. Liddle and P.A. Thomas, *Hydrodynamical simulations of the Sunyaev–Zel'dovich effect*, astro-ph/9907224.

[212] M.O. Calvao, J.R.T. de Mello Neto and I. Waga, *Probing the dark energy with quasar clustering*, Phys. Rev. Lett. **88**, 091302 (2002), astro-ph/0107029.